Alma Mater Studiorum Università di Bologna

Dipartimento di Ingegneria dell'Energia Elettrica e dell'Informazione

Scuola di Dottorato in Automatica e Ricerca Operativa
XXVII CYCLE

Settore Concorsuale : Area 09/G1
Settore Scientifico Disciplinare : Automatica (ING-INF/04)

Design and Control of Robotic Hands

Coordinatore Dottorato:
Prof. Daniele Vigo

Supervisore:
Prof. Claudio Melchiorri

Autore:
Umberto Scarcia

Tesi conforme ai requisiti
per il rilascio del titolo di Doctor Europaeus

in

Automatica e Ricerca Operativa

March 2015

Alma Mater Studiorum
University of Bologna

Department of Electrical, Electronic and Information Engineering (DEI) "Gulglielmo Marconi"

Doctoral School of Automation and Operative Research
XXVII CYCLE

Design and Control of Robotic Hands

Ph.D. Coordinator:
Prof. Daniele Vigo

Supervisor:
Prof. Claudio Melchiorri

Author:
Umberto Scarcia

A thesis submitted in fulfilment of the requirements for the degree of Doctor Europaeus of Philosophy

in

Automation and Operative Research

March 2015

Declaration of Authorship

I, Umberto Scarcia, declare that this thesis titled, 'Design and Control of Robotic Hands' and the work presented in it are my own. I confirm that:

- This work was done wholly or mainly while in candidature for a research degree at this University.
- Where any part of this thesis has previously been submitted for a degree or any other qualification at this University or any other institution, this has been clearly stated.
- Where I have consulted the published work of others, this is always clearly attributed.
- Where I have quoted from the work of others, the source is always given. With the exception of such quotations, this thesis is entirely my own work.
- I have acknowledged all main sources of help.
- Where the thesis is based on work done by myself jointly with others, I have made clear exactly what was done by others and what I have contributed myself.

Signed: _____

Date: _____

"Life is one big road with lots of signs. So when you riding through the ruts, don't complicate your mind. Flee from hate, mischief and jealousy. Don't bury your thoughts, put your vision to reality. Wake Up and Live!"

Bob Marley

ALMA MATER STUDIORUM
UNIVERSITY OF BOLOGNA

Abstract

School of Engineering and Architecture
Department of Electrical, Electronic and Information Engineering (DEI) "Gulglielmo Marconi"

Doctor Europaeus of Philosophy

Design and Control of Robotic Hands

by Umberto Scarcia

The application of dexterous robotic hands out of research laboratories has been limited by the intrinsic complexity that these devices present. This is directly reflected as an economically unreasonable cost and a low overall reliability. Within the research reported in this thesis it is shown how the problem of complexity in the design of robotic hands can be tackled, taking advantage of modern technologies (i.e. rapid prototyping), leading to innovative concepts for the design of the mechanical structure, the actuation and sensory systems. The solutions adopted drastically reduce the prototyping and production costs and increase the reliability, reducing the number of parts required and averaging their single reliability factors.

In order to get guidelines for the design process, the problem of robotic grasp and manipulation by a dual arm/hand system has been reviewed. In this way, the requirements that should be fulfilled at hardware level to guarantee successful execution of the task has been highlighted.

The contribution of this research from the manipulation planning side focuses on the redundancy resolution that arise in the execution of the task in a dexterous arm/hand system. In literature the problem of coordination of arm and hand during manipulation of an object has been widely analyzed in theory but often experimentally demonstrated in simplified robotic setup. Our aim is to cover the lack in the study of this topic and experimentally evaluate it in a complex system as a anthropomorphic arm hand system.

Acknowledgements

I sincerely would like to thank all the people that believed in me and made possible this period of professional and personal growth. First of all my parents and my sister, that supported my choice to continue the studies with the Ph.D. program and have been always close to me during difficulties. Even if they do not have a clear idea of what I am actually doing, they were always excited to share with me satisfactions and great results. My tutor, professor Melchiorri that left me the freedom to find my research way and warmly supported me with invaluable advices. He has been and will be an extraordinary example for my future carrier. I want to thank my co-tutor, Gianluca Palli for all the interesting discussions about Robotics and life in general. He thought me how to remain modest and to share the knowledge with passion and generosity. A great thank goes also to professor Vassura that at the beginning of my research period opened me the doors to prototyping, of thinking in function of the realization. I had the chance to collaborate with him as an assistant for his course and it was extremely formative. A huge hug goes to my colleagues of the LAR: Gildo, Lorenzo, Leonardo, Alberto and Daniele that made me growing the belief that we are not just unstable employes of the University but the main wheels of the entire system and that we can reach every goal with the right amount of passion and sacrifice. I hope that this wonderful friendship, in and outside the lab, will last forever. I want to thank also the University of Bologna, and in particular, the School of Engineering and Architecture, that offers an extremely high level of teaching and that brings willing people to a successful carrier. I am infinitely grateful with the research group of the DLR that welcomed me in my period abroad and naturally shared the knowledge.

Lastly I want to thank everyone that appreciated or criticized my work. The process of research need your support to go ahead and to get always new incitement.

Contents

List of Figures

Dedicated to me

Chapter 1

Introduction

1.1 Motivation

Since ancient times, engineers have been attempting to develop machines which could substitute humans performing, being telemanipulated or autonomously, alienating and dangerous actions. However, before the so called "Third Industrial Revolution", in the second half of XX century, with the introduction of first models of programmable electronic logic, it was not possible to conceive devices able to execute a broad range of preset motion paths. Around the Seventies, robotic manipulators have been firstly introduced in the mass production lines to carry out heavy jobs, like soldering and pick and place of products. The capabilities of moving heavy loads with fast and accurate dynamics and the programming flexibility were satisfactory since early stages They presented limits, instead, to be adapted to different type of tasks, due to the inflexibility of terminal organs, that had to be designed for the particular application to accomplish. With the grow of computational capacity and the miniaturizing of electronic components it became possible to foresee the development of general purpose end effectors with the shape of robotic hands. These devices would allow to grasp and manipulate objects and tools just as humans do. Complexity involved in the design of such devices is relevant, since obtaining dexterity means having an high number of degrees of freedom (articulations) in a very compact space. Moreover, if we look at human hands as a model for the sketch of specifications that robotic hands have to fulfill, it is easy to notice that such devices need to exert high forces and, at the same time, be delicate. It implies the necessity to integrate within the hand a great number of suitable actuators and sensors in order to be able to feedback the state of the hand and then calculate and actuate the control action, accordingly to the the task being executed. Robotic hands, with anthropomorphic shape and capabilities, together with anthropomorphic arms, also let

us consider the possibility to develop humanoid machines that can work out of the industrial environment and cooperate with humans, helping us in everyday tasks.
Researchers have been prototyping over the years an impressive amount of robotic hands. Although many challenges have been already overcame, at the moment there is not any solution ready to be brought to the mass market. The main problems of robotic hands are the cost and the reliability, both caused by their intrinsic complexity above mentioned.
Within the research reported in this thesis we reviewed the state of art of robotic hands development together with the ultimate techniques to plan and control task of grasp and manipulation by means of a dexterous robotic systems. Our aim is to get inspiration and guidelines for the design of innovative devices that could drastically reduce the complexity and therefore fill the gap between the use of robots in industrial environments and the use of future robots in everyday human and unstructured environments.
We show the results obtained in the conception and prototyping of several robotic hands, in particular anthropomorphic hands and multi fingered grippers for marine applications. The research also cover the set up of a robotic system for the execution of grasp and manipulation tasks. It consists of an anthropomorphic arm and hand, and a vision system. Innovative solutions to retrieve visual information in the manipulation scene have been investigated trying to maximize the ratio between reliability and cost.
From the plan and control point of view, the problem of redundancy resolution of the system with regard the object manipulation has been studied. The main contribution is based on a novel approach to explore the internal manipulation reachable space given a grasp configuration.

This research have been partially carried out within projects founded by the European Commission and the Italian government which will be briefly introduced in the next section.

The thesis is organized as follow:

- in Chapter 2 the state of art and a exhaustive classification of Robotic Hands developed over the years is presented, highlighting qualities and weakness of different design solutions. A particular focus has been deployed in the presentation of the UB Hand project, the University of Bologna Hand, which started in the late Eighties and that has set some of the breakthrough innovations in the topic;
- in Chapter 3 the problem of robotic grasp and manipulation is described, and the state of art of the technics used to control the dexterous robotic system are

presented. In this chapter are also summarized which are, in our perspective, the aspects that should guide the designer during the development of an innovative robotic hand, aiming to simplify the planning phase and maximize the rate of success of task executions;

- in Chapter 4 the solutions adopted in the design of UBHand IV, an anthropomorphic tendon based robotic hand, are shown. The performances are illustrated through experiments;
- in Chapter 5 the solutions adopted in the design of a multi-fingered gripper suitable for marine applications are shown;
- in Chapter 6 is discussed the advantages that come by considering the arm/hand system as a unique redundant manipulator. It is presented a reactive algorithm for the planning; of manipulation tasks in which the arm and the hand are involved in a coordinate way in the motion of the object. The performances are illustrated by means of experiments on a dual arm/hand system;
- in the last Chapter we summarize the results of the research and we draw the path for future works.

1.1.1 The Dexmart Project

The recent trend of European Commission is to push the research community towards integration in order to aggregate solutions that single groups all over the continent are achieving. Dexmart, that stands for "DEXterous and autonomous dual-arm/hand robotic manipulation with sMART sensory-motor skills", has been a large scale integrating project, funded under the European Community's 7th Framework Program. Its ambition has been to put together the most advanced technologies and techniques in the field of humanoid robotics and therefore fill the gap between the use of robots in industrial environments and the use of future robots in everyday human and unstructured environments.
The research group of Bologna have been involved mainly in the design and development of new sensors and actuators, as well as new mechanical structures and materials, able to overcome the limitations of current manipulation devices.

1.1.2 The Trident and Maris projects

Underwater activities represent a field of application in which dexterous robotics can play a crucial role. A typical scenario is represented by off-shore industries, where

transportation of construction materials, maintenance and monitoring of plants have to take place in deep oceans.
Trident and Maris projects, funded respectively by the European Community and the Italian Ministry of Research, have the objective of studying, developing and integrating, technologies and methodologies enabling the development of underwater robotic systems for autonomous exploration, manipulation and transportation activities. Within both projects the research group of Bologna has been involved in the design and prototyping of multi-fingered and dexterous gripper, and as well in the sensory and control aspects, suitable for marine application up to 100 meters of depth.

Chapter 2

Classification of Robotic Hands

Several authors in literature have attempted to give an exhaustive classification of robotic hands (Bicchi 2000 [1]) and (Vassura et al. 2004 [2]) in order to draw guidelines for future developments. In the following sections the main aspects that characterizes robotic hands will be analyzed, giving references to devices developed over the year within research groups all over the world.

2.1 Range of application

One of the main aspect in the conception of a robotic hand is to define clearly from the early stage of the design process what kind of application it will be used for, since its definition will condition substantially further decisions. The main fields in which a robotic hand can be involved are:

- prosthetic, to replace, completely or partially, the hand or fingers of amputees;
- tele-manipulation, in which the hand is mounted as end effector of a robotic arm, being controlled by some kind of joystick, and executes tasks inaccessible and dangerous for humans;
- industrial, for the execution of autonomous grasp and manipulation tasks;
- service and care, in humanoid robots that help humans in everyday tasks.

2.1.1 Prosthetic Hands

Before the Nighties prothesis have been conceived as strictly passive mechanisms, able to replace the amputated limb and serve as statical support. In the field of hand prothesis,

(a) Bebionic (b) Ottobock (c) Touch Bionics

FIGURE 2.1: State of the art prosthetic hands

nowadays, there are few companies (Bebionic, Touch Bionics, Ottobock) that are selling devices capable of some degrees of freedom, being controlled typically with impulses generated by muscles activities. The design of such hands needs to comply to precise requirements. In order to produce a comfortable feeling to the patients, they need to mimic as much as possible the human hand in terms of weight, size and shape.
Typically prosthetic hands have more articulations (DoF) than the variables that can be directly affected with the control (DoCs). The choice of having only few independent degrees of freedom is pushed by the following considerations:

- the human machine interface available is rather poor, since it is limited to the coordination of muscle activations registered by electromyographic sensors (EMG);
- the housing space available for the actuators is extremely narrow;
- power saving is crucial in order to guarantee longer charge-to-charge time.

Several prosthetic devices have been developed in the recent past, including the SPRING Hand [3], the Cyberhand [4], the DLR/HIT prosthetic hand [5], the MLR Hand [6] and the work of Dalley et al. [7].

2.1.2 Hands for Telemanipulation

Another application of a dexterous robotic system is to replace the intervention of humans in hazardous and dangerous circumstances by means of a tele-manipulation link. Currently, several research groups are involved in the development of such systems, trying to evaluate what are the best control strategies and tradeoff of autonomy that should be implemented. In figure 2.2, as an example, it is shown the tele-manipulation system built by the German Aerospace Research Center (DLR), conceived to support

astronauts during maintenance operations in the Space Station [8].

The master (see figure 2.2(a)) is equipped with two anthropomorphic arms that can be

(a) Master: HUG (b) Slave: SpaceJustin (c) Hands: DLR-HIT HAND II

FIGURE 2.2: State of art dexterous tele-manipulation robotic system

plugged to the wrists of the operator. An input device for the hands control is mounted to the flanges of the two arms. The operator can wear a mask with a binocular screen to fell immersed in the augmented reality. The slave (see figure 2.2(b)) consists of two torque controlled anthropomorphic arm/hand systems and a motorized head . The head has two degrees of freedom and is equipped with a stereo vision system that streams in realtime to the operator. The tele manipulation behavior is realized by means of a cascade of an admittance and an impedance controller block [8].

The common approach for the tele manipulation of a dexterous robotic hand is to use an input device such as a data glove (see figure 2.3) in order to acquire the desired motion of the user hand and convert it to the motion of the robotic hand. However, the imprecise compensation of different user and robotic hand kinematics often leads to a counterintuitive experience.

With the term autonomy we refer to the capability of the robotic system to take decisions based on the built-in feedback apparatus. As an example we can think to the capability to autonomously avoid collision with the environment and the robot body itself or automatically plan the grasp configuration once located and recognized the object.

In a tele manipulated robotic system, a sort of shared autonomy appears to be conve-

FIGURE 2.3: 3D hand motion capture: CyberGlove

nient, as it lightens the effort required to the operator [9]. In the case of the execution of a grasp task, the user could, for example, simply manifest the intention to grasp an object, while the system autonomously plan the grasp configuration of the hand. This can be done based on the actual relative pose of the arm with respect to the object, the object shape and the hand kinematic. The implementation of such technique becomes feasible if a reactive and accurate vision system, to retrieve objects and obstacles informations, is available. In a similar way, in the case of an internal manipulation task, the desired motion of the object can be commanded through a joystick, instead of controlling each finger joint velocities or torques separately.
In this particular application the robot is conceived to deal with a large number of tools, preferably the same that the human operator does use. Hence, the robot hand has to mimic as much as possible the human hand in terms of strength, workspace and dexterity (see figure 2.2(c)). The anthropomorphism also simplify the conversion of the user commands, when they are generated with a data glove.
Another typical application of tele manipulated robotic systems is represented by assisted surgery. In figure 2.4 it is shown the Da Vinci robot developed by the Intuitive Surgical company. The surgeon safely and precisely controls the surgical tools by means of two haptic joysticks plugged to the thumb and the index of both hands (see figure 2.4(c)). The system also provides to the user an immersive 3D view of the scene where the tools are operating.
In this case the requirements for the design are completely different. It does not make sense to reproduce the shape and the size of the human hand, rather it is more convenient to have a compact and light gripper with few degrees of freedom (see figure 2.4(b)).

2.1.3 Hands for autonomous tasks execution

The third scenario in which a robotic hand can be exploited is in a robotic system intended to execute grasp and manipulation tasks autonomously. Such systems find application in industries, typically in assembly and packaging operations. As we can see in figure 2.5, different typologies of hands can be found, depending on the level of flexibility required.

2.1.4 Service robotics

The actual trend of robotics seems to be strongly projected toward the development of domestic appliances whit the shape of humanoid robots. Such devices would substantially upgrade the state of the art of what a domestic machine can do. Instead of

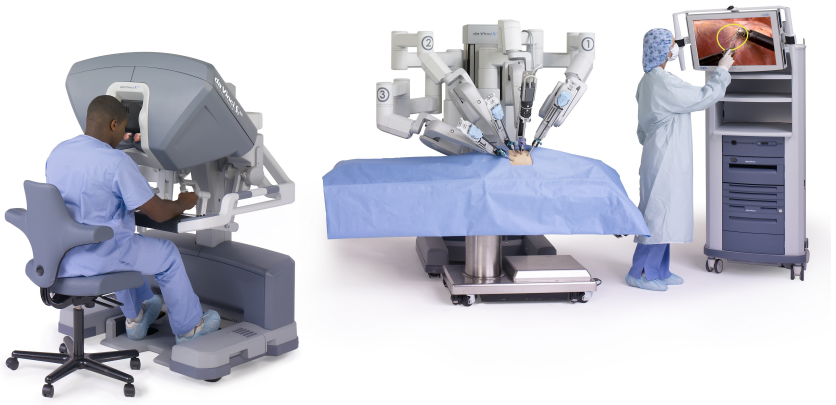

(a) Da Vinci Robot

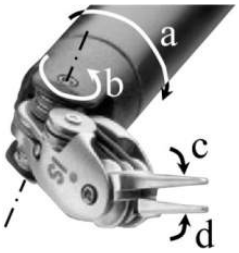

(b) Hand

(c) HMI

FIGURE 2.4: State of art telesurgery robotic system

(a) Two fingers gripper

(b) Three fingers gripper

(c) Anthropomorphic gripper

FIGURE 2.5: State of art arm hand robotic systems for industrial application

being conceived for a single or a set of tasks, a service robot is supposed to be able to execute a broad range of actions and possibly to learn always more, being properly programmed. In this perspective, we can foresee robotic helpers, that can cook and take care of the laundry as well as cradling babies or lifting elderlies. To this end, it is reasonable to imagine that this kind of machines will be very anthropomorphic. First of all, anthropomorphism means dexterity and flexibility, second compactness and third friendly appearance and safety. Very important will be the level of performance reachable by the robotic hands of service robots. In figure 2.6 we show three service robot

prototype at the state of art. In figure 2.6(a) is shown TORO, Torque Controlled Humanoid Robot, developed by the German Aerospace Center (DLR) [10]. It has 27 DoF for the arms, the legs, the torso and the head. At the actual stage of the project only two prosthetic hands have been integrate (the one seen in figure 2.1(a)) , since the current main problem is enhancing the balance control while walking and moving the arms. In figure 2.6(b) the PR2 produced and commercialized by Willow Garage is shown. It is intended as a flexible platform that researchers can use to study and implement innovative methods for service robotics. Finally in figure 2.6(c) the humanoid robot Asimo developed by Honda is reported. In this case we have an high level of integration of the hands, since they consist in two dexterous anthropomorphic hands which it has been shown to be able to perform both power grasp and fine internal manipulation.

(a) Toro (DLR) (b) PR2 (WILLOW GARAGE) (c) Asimo (HONDA)

FIGURE 2.6: Humanoid robots

2.2 Key features of Robotic Hands

In this section we summarize what are the key features that characterize a robotic hand, highlighting how they influence the overall complexity and therefore the cost and the reliability.

2.2.1 Level of anthropomorphism

The human hand is considered the result of a millenary biological adaptation process to primary needs of beings. Then it comes natural to use it as a source of observation and inspiration for the design of a robotic gripper. With the term “anthropomorphism”

we relate to the capability of a robotic hand to mimic the human hand under a number of aspects, such as the size, weight, number of fingers, number of degrees of freedom (DoF) per finger, number of degrees of freedom controllable (DoC), size and shape of the workspace, range of joints speeds and torques.
Although an high level of anthropomorphism would guarantee an high dexterity of the robotic hand, at the same time it also means an increased complexity of the mechanical project. Satisfy at the same time all the aspects above mentioned is more than a challenging problem. In figure 2.7 are reported the distribution of the weight in human body. The average weight of the hand is about 0.6 Kg and the forearm 1.5 Kg. The average size, in terms of palm width and hand length (see figure 2.8), is reported by several anthropometric studies to be around 180mm x 105mm. The number of fingers is 5 and 22 total DoFs actuated by a complex network of muscles and tendons. The thumb mobility allow an high space of opposability with all the upper fingers. As a measure of the strength of the hand, maximal forces applicable with different type of grip are shown in figure 2.9. For short action the hand is able to exert, in average, up to 250 N for power configuration (all fingers involved) and 60 N for finger-thumb configurations. For longer actions the performance are scaled of 60%. The maximum angular velocitiy achievable by the finger joints is approximately 4 rad/sec.

Percentages of Total Body Weight

Segment	Males	Females	Average
Head	8.26	8.2	8.23
Whole Trunk	55.1	53.2	54.15
Thorax	20.1	17.02	18.56
Abdomen	13.06	12.24	12.65
Pelvis	13.66	15.96	14.81
Total Arm	5.7	4.97	5.335
Upper Arm	3.25	2.9	3.075
Forearm	1.87	1.57	1.72
Hand	0.65	0.5	0.575
Forearm & Hand	2.52	2.07	2.295
Total Leg	16.68	18.43	17.555
Thigh	10.5	11.75	11.125
Leg	4.75	5.35	5.05
Foot	1.43	1.33	1.38
Leg & Foot	6.18	6.68	6.43

Plagenhoef et al., 1983

Percentages of Total Body Weight

Segment	Males	Females	Average
Head & Neck	6.94	6.68	6.81
Trunk	43.46	42.58	43.02
Upper Arm	2.71	2.55	2.63
Forearm	1.62	1.38	1.5
Hand	0.61	0.56	0.585
Thigh	14.16	14.78	14.47
Shank	4.33	4.81	4.57
Foot	1.37	1.29	1.33

de Leva, 1996

FIGURE 2.7: Average distribution of human weight

2.2.2 Hand Kinematics

With the term hand kinematics we refer to the geometrical model that describes the motion of the points of the given mechanical structure. The kinematics of a gripper is rather an important feature, as it gives roughly an upper bound of the set of objects

Hand anthropometry of non-disabled individuals.
(Sources: DTI, 2002; Ergonomics for Schools, 2008; RoyMech, 2008)

Dimension	Gender	5th percentile (mm)	50th percentile (mm)	95th percentile (mm)
Hand length	Male	173-175	178-189	205-209
	Female	159-160	167-174	189-191
Palm length	Male	98	107	116
	Female	89	97	105
Thumb length	Male	44	51	58
	Female	40	47	53
Thumb breadth	Male	11-12	23	26-27
	Female	10-14	20-21	24
Index finger length	Male	64	72	79
	Female	60	67	74
Hand breadth	Male	78	87	95
	Female	69	76	83-85

(a) Average distribution of human hand size

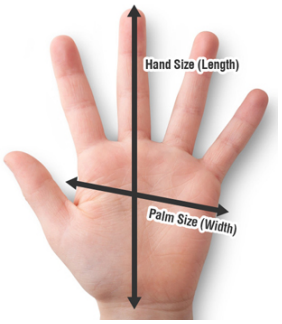

(b) Hand dimensions

FIGURE 2.8: Hand size

Hand and thumb-finger strength (N)

	Hand grip		Thumb-finger grip {Palmer}	Thumb-finger grip {tips}
	L	R		
Momentary hold	250	260	60	60
Sustained hold	145	155	35	35

Note:
* Elbow angle shown in radians
** L=Left; R=Right

FIGURE 2.9: Hand strength

that the robot might be able to manipulate. Basic condition to have a feasible grasp is the existence of a non null intersection of the hand kinematics and the object surface. Grippers kinematics can be divided in two main categories: anthropomorphic and non anthropomorphic (see figures 2.10(a) and 2.10(b))
An anthropomorphic kinematics tries to simulate human hand kinematics under the following aspects:

- similar arrangement of the joints (compare figures 2.10(a) and 2.10(c));
- similar length and proportion of the links of the fingers;
- clear distinction of the thumb and the upper fingers: the thumb have a workspace such that can reach and touch all the upper fingers;
- existence of an hand configuration in which the palm and the fingers lies in a flat surface.

An anthropomorphic kinematics is strongly asymmetric, which makes more complex the research of modularity, that might simplify the assembly and maintenance of the resulting device.

From an analytical point of view, the kinematic problem of robotic grippers, has been extensively studied. It has been demonstrated that to perform basic prehension a minimum of 3 DoF are required under the assumption of an hand with rigid, hard finger, non-rolling and non-sliding contacts. To achieve dexterous manipulation, instead, a minimum of 9 DoC are needed, how first postulated by Salisbury [11].

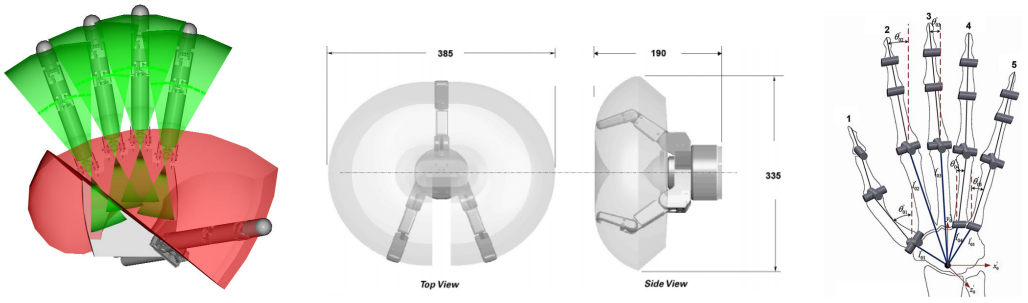

(a) Anthropomorphic Kinematics (b) Non-anthropomorphic Kinematics (c) Human Hand Kinematics

FIGURE 2.10: Difference between Anthropomorphic and non Anthropomorphic Kinematics

2.2.3 Level of actuation

Independently from the number of fingers and the number of joints per finger, different level of actuation can be pursued. We can distinguish two case:

- fully actuated robotic hands, in which every joint is independently controllable ($DoF = DoC$);
- under actuated hands, in which some of the joints are coupled mechanically in such a way their motion can be realized with a fixed ratio, that can be eventually dynamically variated under the effect of external forces ($DoF > DoC$).

The reasons that push designer towards under actuation are numerous. Mechanically coupling DoFs means primarily a reduction of the number of actuators needed, affecting directly the size, the weight and the complexity of the device. Several mechanical solutions have been investigated to realize the coupling of multiple DoFs, ranging from classical rigid coupling (gears) to mechanism based on compliant and flexible linkage (cables, springs).
From a control perspective, under actuation leads to a reduction of the dimension of the state space of the robotic system and then a simplification of the control strategies. Guidelines for evaluating where and how the coupling should occur in a given mechanism are possible through statistical observation of the state during the execution of a set of

operations: synergic approach [12].
A relevant number of under actuated robotic hands prototypes have been developed by the research community[13–15].

2.2.4 Type of actuation

Another key feature in the design of robotic hands is the type of actuators and transmission used. Among the principles of actuation found in the known robotic hand projects, the following can be listed:

- electric motors;
- pneumatic actuators;
- hydraulic actuators;
- shape memory alloys (SMA).

Proprieties class	Power density ρ[W/Kg]	σ_{max} [MPa]	ε_{max}	E [GPa]	Efficiency
DC motors	100	0.1	0.4	*	0.6–0.8
Pneumatic	400	0.5–0.9	1	5–9 $\times$ 10^{-4}	0.4–0.5
Hydraulic	2,000	20–70	1	2–3	0.9–0.98
SMA	1,000	100–700	0.07	30–90	0.01–0.02
Human muscle	500	0.1–0.4	0.3–0.7	0.005–0.09	0.2–0.25

FIGURE 2.11: Actuator Performance Indices: Power density ρ = Power per unit of weight, σ_{max}= Maximum force exerted by the actuators per area, ϵ_{max}= Maximum run per length, E Actuator stiffness. Maximum stress and strain are indexes specifically designed for linear actuators. Units are expressed as follow: W Watt, Kg kilogram, MPa Mega Pascal, GPa Giga Pascal.
*Depending on the gearhead

In figure 2.11 indices for different mechanical actuators [16] are given. It is interesting to note that, despite the electric motors represent the choice with smallest power density, i.e. the power available per unit of weight, it is the most common solution adopted in the development of robotic hands. The low power to weight ratio is compensated by the flexibility and simplicity of the control. Moreover, the wide availability of batteries to store the energy required plays a crucial role to address the choice.
The pneumatic actuators have the advantage to have rather high power density, but low stiffness, that introduces several issues in the control. The energy required has to be stored in tank (big volumes) or need to be connected directly to a compressor, which make the choice of this solution inconvenient for prosthetics. A famous example of robotic hand actuated by pneumatic energy is given by the Shadow Hand (in figure 2.12(b) only a finger module is shown), in which the McKibben actuators (see

figure 2.12(a)) are integrated. These devices are constituted of a flexible chamber in which the change of internal pressure results in a contraction or an extension, simulating the behavior of human muscles. The main advantages are the low weight and cost, at the expense of a variable volume required and a complex control due to the non-linearity of the system.

Hydraulic actuators have very high performance indices, but are often discarded for the

(a) McKibben actuators (b) Shadow Hand finger set-up

FIGURE 2.12: Pneumatic actuators for robotic hands

same storage difficulties of pneumatic actuators and because they need to work with high pressure to guarantee the right amount of output power at the joint level. Recently this principle has been used to design fingers with a continuos degree of flexion resembling the behavior of octopus limbs. In figure 2.13 it is shown a finger prototype realized as an asymmetric plastic tube that exploit the change of pressure to realize the flexion. The concept has been successfully applied to the design of a non-anthropomorphic robotic hand (see 2.13(b)) [17].

SMA have been utilized in several projects with promising results [18], but the technology seems to be not mature yet.

(a) Hydraulic actuator under different pressure conditions (0 0.5 0.6 0.7) Mpa (b) TUM Hand

FIGURE 2.13: Hydraulic actuation

2.2.5 Type of transmission

Different approaches can be followed to transmit the motor power to the joints:

- tendons and pulleys or sheath (steal wires, synthetic strings, plastic strips);
- rigid connection (gears, articulated mechanism).

Using a flexible mean (tendons) to transmit the power to the joint shaft make easier to place remotely the actuators. The use of tendon transmission also reduce the number of parts required for the linkage. Depending on the elasticity of the tendon, the transmission becomes compliant, that represents a positive aspect with regard to the safety but introduces non linearities in the control. For a given mechanism, there exist infinite configuration of tendons networks that can control it. The research of an optimized tendon network is an open problem, as it has to take into account many design aspects. Analytically, has been proved that for a mechanism with n DoFs, $n+1$ is the minimum number of tendons required to fully control it [19]. Usually the tendons are routed by means of pulleys [20, 21] or slide inside sheaths [22–24]. A great number of projects aimed to the development of tendon driven robotic hands has been found in literature. For instance, the UTAH/MIT Hand [25], in which two antagonistic tendons are used for each joint, or the JPL/Stanford Hand [26], in which an N+1 tendon network is adopted to minimize the number of actuators. In the UB Hand III [22] sheath-guided tendons are adopted and recently DLR has developed the tendon-driven DLR Hand-Arm system [27, 28] focusing on the robustness of the device as a primary target introducing elements able to absorb and store the energy during impacts. It is also worth mentioning the only commercially available tendon driven device, the Shadow Hand [29].
The use of classical geared coupling mechanisms introduces weight to the device but offer better performance in terms of friction. It is a good solution especially when the actuators have to be integrated in the palm or in the fingers for application requirements. In this case, being the space available limited, custom miniaturized gears and parts have to be designed with evident consequences on the time and cost for prototyping. Different types of transmission mechanisms have been adopted: harmonic drive [30], spur and worm gears [31, 32], flexible shafts [33] or leverages [34].

2.2.6 Level of sensing

The observation of the humans reveals an incredibly spontaneity and rapidity in the plan and execution of grasp and manipulation operations. The fusion of the information coming from the sensors (tactile, visual) is made fluently and, accordingly with the

intention, the motion is planned and executed reactively.
The skin of the human body is covered with a continuos network of tactile sensors offering, within a threshold (see figure 2.14), feedback about the amount of force applied and about the region of the body interested in the contact. In figure 2.14 the average human accuracy estimating the actual contact points is shown. The curve represents the minimum distances between contact points that the human is able to distinguish, in relation with the region of the body stimulated. This distance is about 5mm for the palm and around 2mm for the fingers. As a matter of fact, the hand is the region of the human body with the highest tactile performance.

When the hand grasps an object, changes in skin temperature can assist in identifying

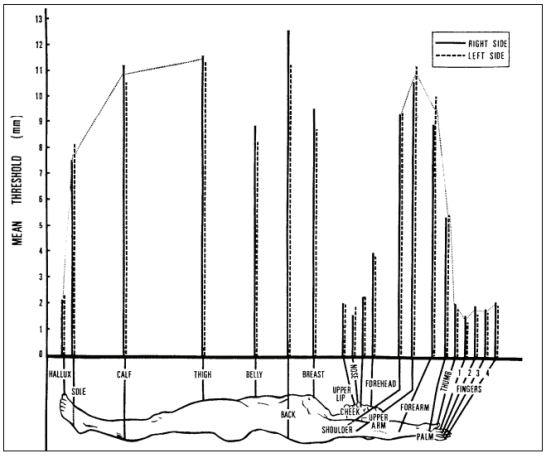

FIGURE 2.14: Two-point discrimination thresholds for females for different areas of the body (source: Weinstein, 1968)

the object especially when there is not visual feedback (searching an object in the dark). The type of feeling is differential, that means that is relative to the difference between the actual temperature of the skin and of the object. Therefore it is possible to discriminate object that are cooler or warmer than us. With this information the human usually generates hypothesis about the material (metal, wooden, plastic) of the objects. The thermal sensory system is extremely sensitive to very small changes in temperature such that people can perceive a difference of 0.02-0.07 °C.
With regard to the visual sensing capabilities, human eyes allow:

- a rapid and precise segmentation of the scene, clustering objects and obstacles;
- the estimation of the relative distances of recognized objects;
- the tracking of moving objects through the coordinated motion of the eyes and the head.

Visual feedback is essential in the execution of grasp because, both the object and desired contact regions of the hand, are tracked and evaluated in the same image space.

In a robotic system is not possible to faithfully reproduce the level of sensing of humans in terms of tactile and visual feedback, however different tradeoffs can be pursued. In the following, a list of known sensory equipments suitable for the design of robotic hands are shown:

- motor position sensors;
- finger joints position sensors;
- motor torque sensors;
- joint torque sensors;
- tactile sensors;
- temperature sensors;
- in hand camera.

More desirable controller for robotic hands are based on position and torque feedback, therefore sensors need to be integrated in the mechanical structure. In literature, we can find solutions in which the position and torque sensors are coupled with the joint mechanisms, and therefore give a direct measurement, or in which the sensors are located at the motor side, and therefore the measures have to be reconstructed taking into account the transmission. This last approach has the advantage to avoid complex cabling along the fingers, but introduce side effects due to the non-ideality of the transmission (mechanical play, not modeled elasticities, not modeled friction). The principle of position sensors can be various: magnetic, resistive, capacitive, inductive, optical. Typical torque sensors are based on strain gauges and optical components. In figure 2.15 are shown typical mechanical structures that integrate strain gauges, obtaining single, double and six dimensional force torque sensors.

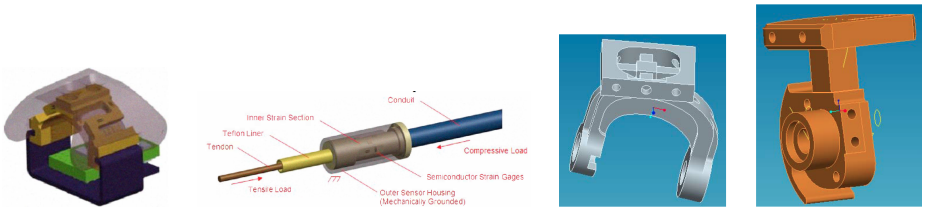

(a) Force/Torque sensor [35] (b) Tendon tension sensor [35] (c) Single axis joint sensor [36] (d) Double axis joint sensor [36]

FIGURE 2.15: Force/Torque integrated sensors

Tactile feedback offers important cues for the control, such as the shape of the contact and the distribution of the pressure. In literature can be founded a great number of concepts for tactile sensors. The main problem is technological and lies in the high miniaturization required and the need to be produced as a flexible layer to be adapted to the surface of the hand. The resulting devices are often poorly integrable and can cover only small regions of the hand. In figure 2.16 some prototypes found in literature are shown.

Temperature sensors have been seldom taken into account in the project of robotic

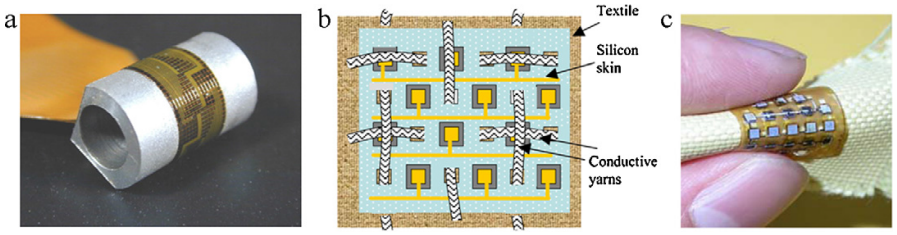

(a) Strain gauges tactile sensor [37]

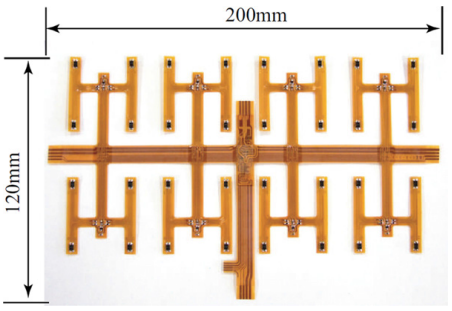

(b) Led based tactile sensor [38]

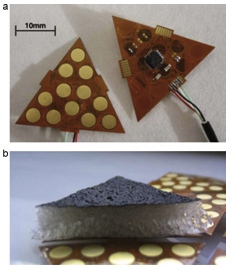

(c) Capacitive tactile sensor [39]

FIGURE 2.16: Tactile sensors

hands, probably due to the low control benefits compared to the integration complexity. In robotics, vision systems are typically mounted in a fixed position to the ground or to the body of the robot. Sometimes they are flanged to an articulated mechanism that allows to dynamically change the point of view. As emphasized by a recent patent (see figure 2.17) submitted by Barrett Technology company, the trend seems to go towards the integration of cameras right on the palm and fingers of robotic hands. By putting sensors in the palm it is possible to have a wide view when far away and high resolution when close up, with the freedom to actively avoid occlusions.

2.2.7 Type of contact surface

The dynamical model that describes the contact substantially changes with the type of surface involved. Although the surface of the object can not being known a priori (can

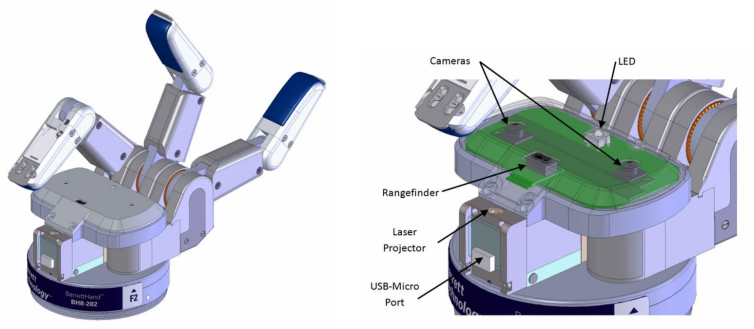

(a) Barrett Hand (b) In Hand Cam Integration

FIGURE 2.17: Patented Hand-Eye integration [32]

be both rigid or soft), the surface that covers the hand represents an important degree of freedom in the design. In general the surfaces of a robotic grippers can be rigid or soft. The choice of having a rigid surface is justified when the type of grasp expected by the application is a firm and power grip or if the expected objects to handle are soft. In other cases, providing at least zones of the fingers covered with soft layers, is preferable. The attempt to reproduce biological skin is a very challenging task. Berselli et al. in [40] carried out an interesting study on the design of fluid-filled soft covers for robotic hands and some prototypes are shown in figure 2.18.

The use of soft layers that continuously covers the surface of the hand is quite rare to

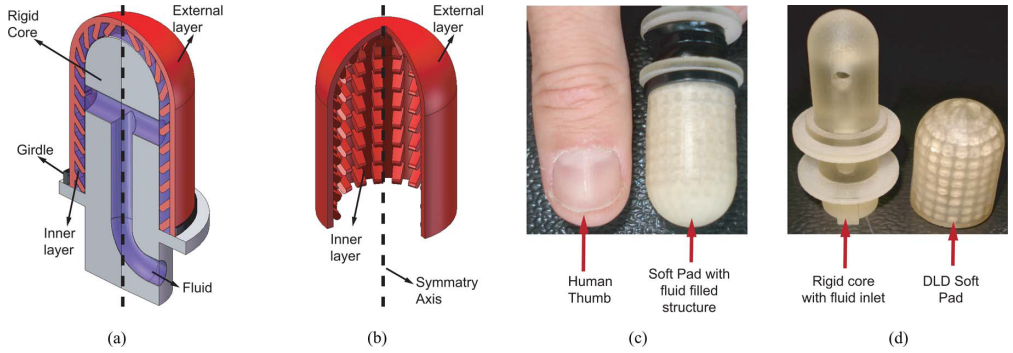

FIGURE 2.18: Fluid-filled soft-pad concept and prototype. (a) 3-D model. (b) Longitudinal cross section. (c) Prototype comparison with human-thumb dimensions. (d) Rigid core with fluid inlet and soft pad.

see in robotic gripper projects. The main development issues are legated to the design of a flexible cover that does not affect the motion of the articulations. Several are also the attempts to integrate tactile sensors right inside the soft covers, as we can see in figure 2.19 in the ACT Hand [41] .

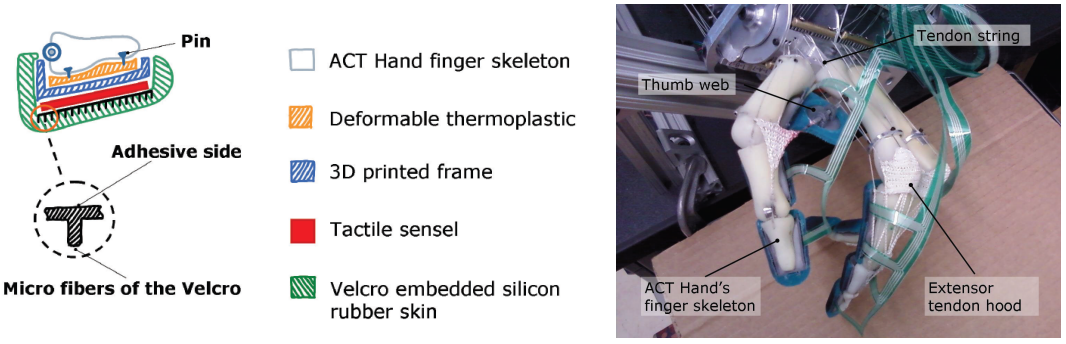

(a) Sensorized artificial skin concept

(b) Integration of the skin within the robotic hand

FIGURE 2.19: Artificial skin with integrated tactile sensors

2.3 The UB Hand project

Since the end of the Eighties, researchers of the Laboratory of Automation and Robotics (LAR) have been involved in the design and development of dexterous hands for industrial applications. So far, four generations of UB Hands, University of Bologna Hands, can be counted.

The first prototype (UB Hand I)(figure 2.20(a)) was released in the 1988 and it consisted of a device with two parallel fingers, an opposable thumb and a palm. The device was also provided with a wrist articulation with only one DoF. The actuation was realized by means of iron wires routed along pulleys and sheaths. The tendons were driven by DC motors controlled by custom electronics. Strain gauges based force sensors were mounted within the fingertips to feedback the contact.

Considering the technology available at that time the results of the project represented a milestone for the research in this area.

Soon, the researchers of Bologna started a new iteration of the hardware design process

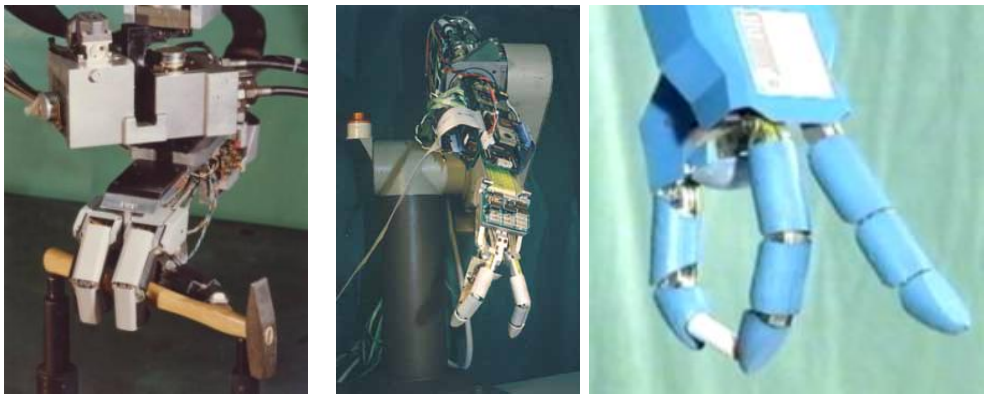

(a) UB Hand I

(b) UB Hand II

FIGURE 2.20: First two UB Hand prototypes

(UB Hand II), with the intention to solve some of the weakness that affected the first prototype (figure 2.20(b))[42]. The kinematic structure was basically confirmed, with the introduction of a second DoF in the wrist articulation. The entire actuation system was embedded in the forearm. Synthetic wires were used to transmit the power from the motors to the finger joints, without the employment of sheaths for the routing. The phalanxes were equipped with force/torque sensors rigidly connected to the pulps. Such it was possible to measure directly the contact forces acting all over the surface of the finger covers. The contact forces were also used, in combination with a precise knowledge of the covers 3D shape, to estimate the actual location of contact points [43]. The hand was mounted substituting the last three links of a 6 DoF industrial robot (PUMA 560). The research of integration of the hardware gave great advantages also from the control side. This allowed the engineers to conceive control strategies in which the hand and the arm can be controlled uniformly in real time, with a common update time.
With the third stage of the project (UB Hand III) (figure 2.21(a)), the research group started to investigate novel concepts for the hand mechanism which can safely interact with the environment and the humans. Several prototypes of compliant joints were analyzed and evaluated, taking advantage of rapid prototyping technology. The research of simplification, both of the mechanical structure and of the control strategy, was stressed.
A new wave of innovation in the UB Hand project (DEXMART Hand, UB Hand IV)

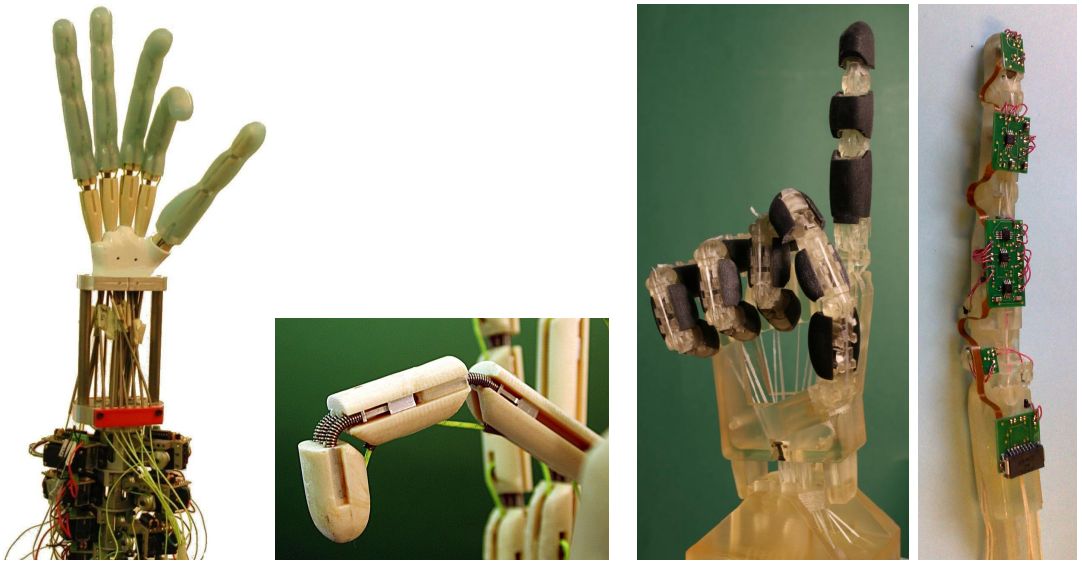

(a) UB Hand III (b) UB Hand IV

FIGURE 2.21: Last two UB Hand prototypes

comes from the participation of the LAR group to the DEXMART project, mentioned in Section 1 (figure 2.21(b)). The researchers were challenged to design a robotic hand supposed to drastically reduce the complexity and the cost, enhancing the usability and the reliability. As a result, innovative technologies for the actuation and sensors have

been investigated. Particularly interesting is the original adoption of twisted string actuators in an anthropomorphic robotic hand. The idea behind the actuator is to control the length of a loop of wire twisting quickly one of its extremities with a small rotational motor. In this way a simple transformation of the motor torque to the tension of the tendon is realized. The ratio of the transmission is very high (low torque/high linear force) and the connection obtained presents intrinsic compliance. The sensing apparatus was provided with tactile, angular and force sensors, exploiting the combination of rapid prototyping techniques and extremely cheap and simple optical components. More details are reported in Chapter 4.

2.4 Resulting Guidelines

As we have seen in the previous sections, many are the factors to take into account in the design of a robotic hand. In literature, the amount of works that investigate all the mentioned research directions, is huge. The community, now more than ever, is interested in finding solutions that can really deliver to the market a device with comparable capabilities of an human hand. It would open the frontiers of a new technological age. Although many single technological aspects have been already solved, there are still some points that limits the introduction of such device in mass market:

- the price of a dexterous hand is too high to represent a convenient investment for a private user. On the market, there are several products (especially for research purpose), with a price that is around 80K-100K euro;
- the robustness of such devices is still not acceptable. Usually these devices are delicate with regard to collisions and usually need periodic intervention of experts;
- the user interface needs to be clear even from a totally ignorant user in the field of robotics;
- solutions found all over the world in robotic hand projects need to be aggregated.

In this thesis we deal with the problem of conceiving new approaches in order to reduce the gap between the use of robotic hands in research laboratories and their employment as human helpers of the next future.
After a deep analysis of the state of art, these are the guidelines that will prompt us in the design process:

- investigate alternative manufacturing approaches that reduce the time and cost of prototyping (exploiting as much as possible rapid prototyping);

- reduce the number of the parts conceiving non-conventional mechanical solutions that avoid at most screws and ball bearings;
- stress the modularity in order ease the design, manufacturing, assembly and repairing time ;
- try to average the reliability of the hand subsystems and avoid bottlenecks

Chapter 3

Robotic Grasp and Manipulation

Robotic grasp and manipulation is still an open problem among the research community. Many are the aspects that need to be considered for the plan and execution of the task and different level of complexity, flexibility and autonomy can be pursued. We can roughly divide the problems related to robotic manipulation into the following classes:

- grasp planning, establishment and control;
- plan and control of the manipulation motion;
- control of the interaction of the object with external forces.

In the next sections we will review the state of art of techniques used in industries and research studies to deal with these problems.

3.1 Grasp Planning

With the term grasp we refer to the action of immobilizing an object under the effect of contact forces between the surfaces of the object and the gripper. Although humans are able to plan a grasp instinctively, for a robotic system selecting a feasible and "optimal" solution represents a complex problem. From a mathematical perspective it consists of finding a relative configuration of the gripper and the object in which all the degrees of freedom of the object are constrained by the contacts with the fingers and palm bodies. A finite set of external forces can be resisted. Typically the external forces are the weight of the object that acts in the direction of gravity, and forces that arise from the interaction with other objects or with the environment. Of course the complexity involved in the computation of a suitable grasp configuration scales with the complexity

of the shape of the object and with the number of degrees of freedom of the gripper. As an example we can give two extreme cases, the first in which a simple geometric object with strong symmetry such as a box has to be grasped with a two-fingered parallel gripper and the second in which an anthropomorphic hand has to grasp a non-geometric object such an animal toy (see figure 3.1). In the first case the research of a suitable

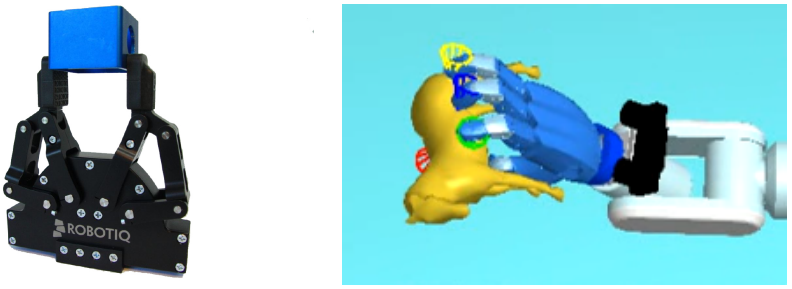

(a) Grasp of a box with a two-fingered parallel gripper

(b) Grasp of an horse statuette with an anthropomorphic robot hand

FIGURE 3.1: Grasp examples

solution is straightforward because it can be easily found exploiting the symmetry of the object and the geometry of the gripper. Considering the object to have uniform distribution of the weight, the grasp will take place in two contact points located in two opposite faces of the object, lying on the longitudinal symmetry plane. The amount of force needed will be simply related to the weight, the external forces applied to the box, and the relative friction coefficient of the contact between fingers and object. The solution can be parametrized with regard of the size and weight of the box, and the dimension of the gripper.
In the second case, the problem is much more complex:

- the surfaces do not have any particular shape and weight symmetry, therefore the center of mass can not be deducted by simple geometric considerations;
- the distribution of the normals is not uniform and need to be evaluated with a discrete representation of the object (mesh, voxmap points shell);
- the hand does not have a favorite grasp approach direction and it needs to be selected accordingly with the contact points and the obstacle-free space.

The solution is not unique, rather, in general there exist infinite. A criterion to select an optimal solution has to be formulated. Different aspects can be optimized with the cost function, such as the distance of finger joints from the limits, the amount of force needed to have a stable grasp, or the biggest wrench that the grasp configuration can resist.

3.1.1 Grasp analysis

In literature can be found several studies that attempt to define meaningful grasp quality indices that can be used to compare grasp configurations [44].
The research community concords that a grasp configuration to be effective, at least in theory, needs to comply with force or form closure tests. In literature a wide number of methodologies and algorithms to implement the tests are proposed [45, 46]. We can describe the difference between force and form closure properties of a grasp configuration analyzing figure 3.2. In figure 3.2(a) a schematic example of a 2D form closure grasp is depicted. The contacts are represented with rigid pins that inhibit the motion of the object only in the direction of penetration. The (partial) form closure property of a grasp is related with ability to (partially) constraint the object motion, only relying on unilateral and frictionless contacts constraints [47]. In contrast, force closure consider the existence of friction in the contact and therefore, the forces applicable are not only in the direction of the normal with the object surface in the contact point, but lie in a cone with the axis aligned with the normal and with an opening angle proportional to the friction coefficient (see figure 3.2(c)). A force closure grasp is able to resist completely of partially an external wrench suitably modulating the amplitude of the contact forces arising in the contact points [47]. In a force closure grasp, if we ideally consider infinite torques available at the finger joints, infinite wrench could be resisted. The limits of the real robotic device bound the subset of external forces and momentum that can be resisted. Establishing whether a grasp is force closure involves:

- approximating the contact friction cones as a convex sum of a finite number of force vectors around the boundary of the cone;
- computing the associated object wrench for each force vector;
- finding the convex hull of this set of wrenches.

If the origin of object system reference (typically the center of mass) is contained within the convex hull computed, the grasp have force-closure, otherwise, there exists some set of disturbance wrenches that cannot be resisted by the grasp [48].

An important tool in the analysis of grasp is the grasp matrix $\mathbf{G}$. It describes analytically the relation between the twist and wrench acting on the object and the velocities and forces at the contact points. In [47] Bicchi shows how it is possible to extract information on force and form closure relying on the geometric analysis of the matrix (rank, null-space). If the contact points expressed in the object system reference are called $\boldsymbol{c_i}$ the

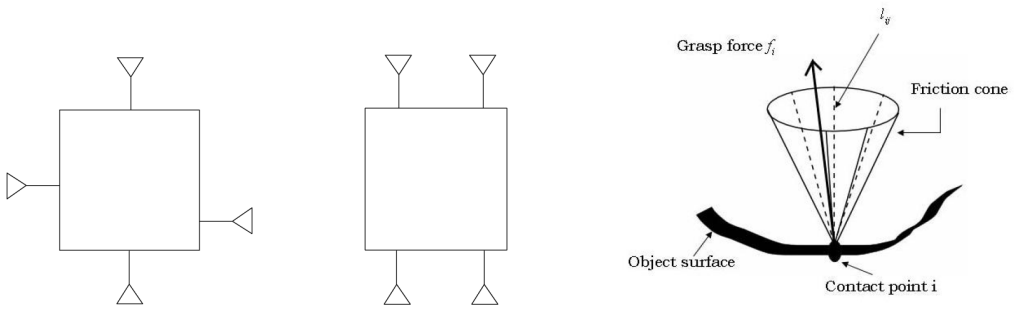

(a) Form closure grasp (b) Force closure grasp (c) Friction cone and a possible contact force

FIGURE 3.2: Difference between form and force closure grasps

grasp matrix can be written as follow:

$$\mathbf{G} = \begin{pmatrix} \boldsymbol{I_3} & \cdots & \boldsymbol{I_3} \\ \boldsymbol{S(c_1)} & \cdots & \boldsymbol{S(c_n)} \end{pmatrix} \tag{3.1}$$

where $\boldsymbol{S(C_i)}$ is cross-product matrix of $\boldsymbol{c_i}$ and $\boldsymbol{G} \in \mathbb{R}^6 \times \mathbb{R}^{3n}$.

3.1.2 Contact Forces computation

An essential aspect to face during the planning of the grasp is the computation of contact forces that should be applied to the object in order to resist the external forces. As already mentioned in the previous section the complexity involved in this calculation can vary substantially depending on the the type of gripper considered. In a two-fingered parallel gripper the amount of force needed in the two contact points can be easily calculated once known the weight, the relative positions of the contact points with respect to the object center of mass, and the friction coefficient that describe the contact between the fingers and the object surfaces. When a dexterous hand is used to grasp an object the problem is rather more complex and a solution can be computed considering it as a non-linear programming problem in which the contact forces has to be computed and optimized. In literature different approaches can be found. Particularly interesting is the adaptation of ray-shooting algorithm to the research of optimal contact forces [49, 50]. The method is applied to the convex hull generated with the primitive contact wrenches and the vector in the wrench space that represents the direction of action of the external forces. Using the linearized friction model and the duality principle, the ray-shooting problem is casted as a 6-dimensional linear programming problem and solved with the simplex algorithm. [51]. This approach is efficient when the number of primitive contact wrenches is small. However, using fewer primitive contact wrenches reduces the solution accuracy and it may also result in a discontinuous solution. There have been

attempts to solve the ray-shooting problem in 6D wrench space without linearizing the friction model [52, 53], but the computation times can be considerably high.

3.2 Grasp Control

Once the grasp is planned, a proper method to control the robotic system during the execution need to be selected.
The type of control laws implementable on real systems strictly rely on the sensors and actuators available and at which level of the mechanism they are integrated. As we have seen in Chapter 2, the sensors can be found both at the joint and motor level. Merely from the control point of view, both position and force sensors would be desirable to act at the joint level in order to avoid the introduction of transmission uncertainties and non linearities in the measures.
When there are not force sensors available, the grasp control can only be kinematic, and the hand is basically controlled in position. In this case it is important to have an intrinsic compliant mechanism to avoid damage of the object and the overload of the fingers due to uncertainties.
If force sensors are present, the contact forces computed can be actively controlled. The most common approaches that can be found in literature to this end are hybrid position/force [54] and impedance controllers [55].
In hybrid controllers, the position is the main variable to control, while the force is supplied by parallel controllers. The position control can be defined in joint or Cartesian space and its robustness is guaranteed. The parallel force control is based upon the requirements for the particular task and usually is activated when the contact between the object and the finger is detected. An effective observer of the state of contact is crucial to maintain the stability of the force loop, which could easily diverge if a false positive contact is considered.
Impedance controllers overcome the stability problems intrinsic in force control loops exploiting the passivity coming from considering the robot as mass-damper mechanism with user customizable parameters. Therefore, impedance controllers have the advantage that stability is given independently from the contact state since they converge to an equilibrium state that is the desired position in case of free motion, and that is a stable equilibrium position in case of interaction with a passive environment. With regard to the control of the fingers of a robotic hand, an impedance behavior can be implemented both at joint or Cartesian level. In order to establish and maintain the desired grasp configuration, virtual linear springs are created (torsional springs are not considered when the contact model is restricted to a point with friction) with origin in the contact point, directed as the normal to the object surface in contact point. The

amount of compression of the virtual springs, and therefore the force applied to the object is typically computed by means of an admittance block with the same parameters as the impedance block, that input the contact forces given from the grasp planner and output the displacement desired. In [55, 56] Wimboeck and Stramigioli present a simpler implementation of virtual springs, in which the elastic elements connect the contact points defined on the real object and dummy contact points lying on the surface of a virtual object scaled in dimension with respect to the real one figure 3.3.

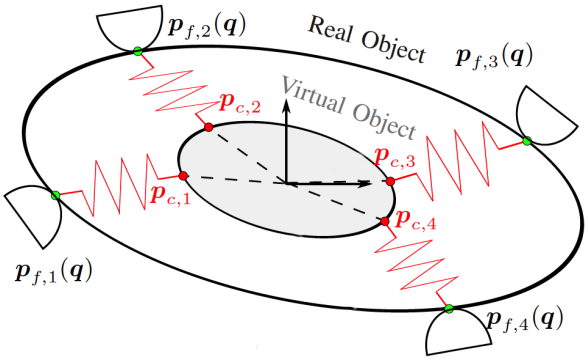

FIGURE 3.3: Definition of contact forces through virtual springs and object

3.3 Manipulation Planning

The term manipulation is related to the motion and the interaction with the environment of a grasped object by means of an articulated arm/hand system. Planning a manipulation task therefore consists of selecting a feasible evolution of the state of the dexterous robotic system such that the operation can be successfully controlled and fulfilled. The planners can be divided in two broad branches: offline and online. The offline planners are more suited when the task require a relevant optimization. The task and the information on the obstacles have to be known and modeled a priori and the solution can be hardly adapted to the feedback of sensors during the execution. Online planners, at expense of optimization, allows to implement reactive behaviors and therefore, the solution can be adapted with regard to variations of the goal and of the location of obstacles at runtime.

Manipulation planners usually attempt to take into account the constraints given by the joint limits, kinematic singularities, and the avoidance of obstacles present in the working area.

It is widely accepted among researchers to have an object centric approach for manipulation planning. It means that the task is basically defined in the object space, defining a desired trajectory that the object has to describe over the time and the forces that we want to apply to other objects. In order to transform the object references to the robot

joint space the solution can be found working backwards from the object to the robot, considering the kinematics and the dynamics of the overall object/manipulator system. Given the redundancy of the arm hand chain with respect to the object manipulation, during the planning, a policy to divide the task between the two subsystems can be considered. For those operations in which the hand is able to perform at least a part of the required motion, it might be convenient to prioritize the use of the hand, when possible, during the execution of the task. It reduces the moving inertias saving power, and increasing the accuracy [57, 58]. Another positive aspect gained comes from the point of view of safety, as it allows to plan trajectory in which the arm, usually quite stiff and heavy, is used just when it is needed, reducing the risk of collision with the environment and human users. Moreover, depending on the actual grasp configuration, the resulting workspace reachable by the object combining the use of the the two subsystems is increased, especially in rotations. In Chapter 6 is presented a novel approach to implement the coordination policy during the plan of a manipulation task for a dexterous robotic system.

Another aspect that can be considered during the planning is the possibility to divide the task in sub-actions, including moves such as the exchange of the object between two hands, the place and re-grasp or the rearrangement of contact points locations [59, 60]. In figure 3.4 are shown some screenshots of an offline manipulation planner based on contact-invariant optimization [61], that outputs the motion of a robotic system given a desired operation defined on the object. Results are very promising and a wide range of tasks including grasping and picking up objects, or advanced manipulation as spinning or drawing are possible through the method.

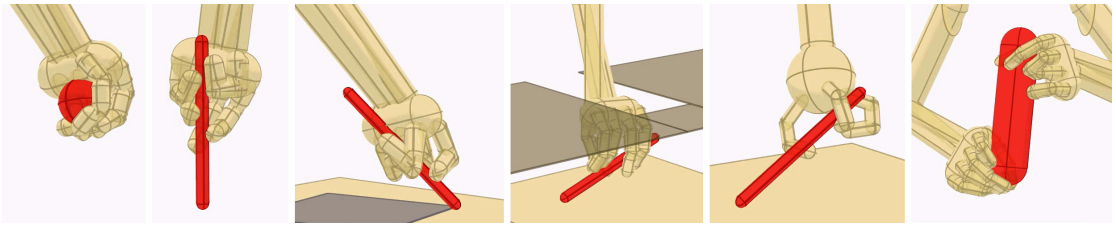

FIGURE 3.4: Manipulation planning screenshots

3.4 Manipulation Control

The control of a dexterous robotic system during the execution of manipulation tasks involves different levels of abstraction. At the two extremities there are the object control, that considers the physical interaction of the grasped object with the environment, and the joint space control, that directly interfaces with the hardware of the manipulator. In the middle there is the operational space control of the robots, in particular of the

hand and of the arm. For the arm, operational space control means regulating twist and wrenches of the end effector directly in the Cartesian space, thanks to the kinematic mapping and the feedback of position and force sensors. For the hand, that can be considered as an aggregation of n serial chains (fingers), the middle level can be dived into two sub-levels. The lower is equivalent to the one described for the arm, replicated n times, and the higher takes into account the coordinate motion of the desired contact points of the fingers to perform the grasp. In order to control the pose of the end effectors, position controller, based on inverse kinematic, or impedance controllers, based on the definition of virtual spring-dumper constraints, can be implemented. Despite position control loops guarantee an accurate execution of the planned trajectories, do not allow the regulation of compliance during interaction with the environment. This issues is partially solved using impedance based algorithm that are able to regulate the stiffness at expense of the tracking precision.
In literature can be found an extensive investigation about how it is possible to transform the information and references all along the chain, from the object to the joint space and vice versa [57, 62]. Figure 3.5 shows how the motion and force relationships between object and hand space can be linearly mapped by means of the hand and grasp Jacobians. In the table, the notation of θ, x_f, x_p, and x_b are the displacements in the joint space, in the Cartesian space at the contact points on the fingers and on the object, and the object reference frame. With x_{tr} are denoted the transmitted components. The δ prefix denotes infinitesimal changes in the named coordinates. The forces with corresponding subscripts are referenced to the corresponding coordinates as those of the displacement described above.

Motion	$\mathbf{J}_\theta \quad \delta\boldsymbol{\theta} \quad = \delta \boldsymbol{x}_\mathrm{f}$		$\mathbf{H} \quad \delta \boldsymbol{x}_\mathrm{f} \quad = \delta \boldsymbol{x}_\mathrm{tr} \quad = \mathbf{H} \quad \delta \boldsymbol{x}_\mathrm{p}$		$\mathbf{J}_\mathrm{c} \quad \delta \boldsymbol{x}_\mathrm{b} \quad = \delta \boldsymbol{x}_\mathrm{p}$	
	$(6\times\boldsymbol{m})(\boldsymbol{m}\times 1) \quad (6\times 1)$		$(\boldsymbol{n}\times 6)(6\times 1) \quad (\boldsymbol{n}\times 1) \quad (\boldsymbol{n}\times 6)(6\times 1)$		$(6\times 6)(6\times 1) \quad (6\times 1)$	
	Joints	$\rightleftharpoons$	**Contact**	$\rightleftharpoons$	**Object**	
Force	$\mathbf{J}_\theta^\mathsf{T} \quad \boldsymbol{f}_\mathrm{f} \quad = \boldsymbol{\tau}$		$\boldsymbol{f}_\mathrm{f} \quad = \mathbf{H}^\mathsf{T} \quad \boldsymbol{f}_\mathrm{tr} \quad = \boldsymbol{f}_\mathrm{p}$		$\mathbf{J}_\mathrm{c}^\mathsf{T} \quad \boldsymbol{f}_\mathrm{p} \quad = \boldsymbol{f}_\mathrm{b}$	
	$(\boldsymbol{m}\times 6) \; (6\times 1) \quad (\boldsymbol{m}\times 1)$		$(6\times 1) \quad (6\times \boldsymbol{n}) \; (\boldsymbol{n}\times 1) \quad (6\times 1)$		$(6\times 6) \; (6\times 1) \quad (6\times 1)$	

FIGURE 3.5: The role of hand and grasp Jacobians

3.5 Synergic approach

Recent studies on neurosciences and robotics have shown that imitating human prehension is a promising way to simplify and improve grasp planning and control issues related to high multiple DOF devices such as anthropomorphic robotic hands. In Santello et al. [63], the authors measure a set of static human hand postures by recording 15 joint angles and, by means of PCA, they show that the first two principal components account for >80% of the hand postures. Thus, the use of the principal components, also called

postural synergies, holds great potential for robotic hand control, implying a substantial reduction in the dimension of the grasp synthesis problem. Transferring human hand motion to a robotic hand is quite a challenging problem due to the complexity and variety of hand kinematics and the dissimilarity with the robotic hand. Indeed, in order to obtain a thorough estimation of human hand posture, a reliable kinematic hand model and highly accurate motion tracking instrumentation are required. A synergy mapping from the human hand to the robotic hand has been addressed by Gioioso et al. [64]. The proposed mapping strategy between the synergies of a paradigmatic human hand and a robotic hand is carried out in the task space and is based on the use of a virtual sphere. This approach has the advantages to be independent of the robotic hand and depends only on the specific operation, and thus it can be used for robotic hands with very dissimilar kinematics. Three synergies have been extracted from data on human grasping experiments and mapped to a robotic hand by Geng et al. [65]. Recently, Kinect technology is increasingly used for hand tracking, since it interprets 3D scenes thanks to the depth sensor, consisting of an infrared laser projector, combined with an RGB camera. In Oikonomidis et al. [66] a model-based method for recovering and tracking the 3D position, the orientation and the full articulation of a human hand has been proposed from marker-less visual observations. In Frati and Prattichizzo [67] a heuristic hand tracker has been developed for animating a hand avatar in virtual reality and for implementing force rendering in wearable haptics. In Ficuciello et al. [68] and Villani et al. [69] a set of 36 human hand grasp configurations was selected and adopted for experiments carried out on the UB Hand IV [24, 70]. In Ficuciello et al. [71], neural networks have been integrated to allow synergy-based grasp planning relying only on geometric features of objects and task requirements.

Chapter 4

The design of the UB Hand IV

4.1 Introduction

In this chapter the development of an innovative anthropomorphic robotic hand, called the DEXMART Hand, is presented. The main goal of this research is to face the problems that affect current robotic hands by introducing suitable design solutions aimed at achieving simplification and cost reduction while possibly enhancing robustness and performance.
Particular emphasis has been placed on the kinematics of the fingers and of the thumb, the wrist architecture, the dimensioning of the actuation system, and the final implementation of the position, force and tactile sensors. It is also shown how these solutions have been integrated into the mechanical structure of this innovative robotic hand to enable precise force and displacement control of the whole system.

The simplification of the robotic hand mechanism has been achieved through the introduction of novel design solutions, reducing the number of components and avoiding the use of any conventional mechanical parts such as bearings, pins, bushings and screws. Moreover, an innovative actuation system called the *twisted string* principle [72] has been purposely developed for actuating the robotic hand. The actuators are placed in the forearm and the forces are transmitted to the hand by means of tendons, obtaining in this way an integrated hand-forearm system. Since no commercial solutions exist that fit with the requirements of miniaturization of both the sensing elements and the electronics, the adoption of non-conventional design choices implies the development of suitable sensors, purposely designed to be integrated into the hand-forearm structure. Moreover, due to the number of sensors, their conditioning electronics should also be as simple as possible, and a common interface that limits the number of wires for communicating with the control system is needed.

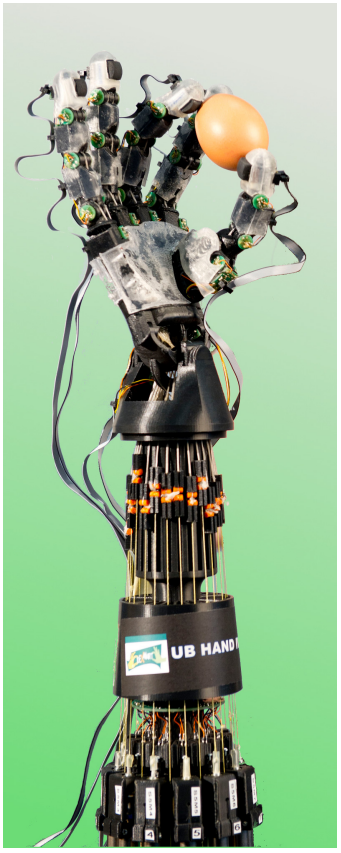

FIGURE 4.1: The DEXMART Hand.

The adoption of suitable control strategies for compensating the side effects given by these design choices must be also considered. This fact is a direct consequence of the needs in terms of increased reliability and reduced costs, which shift the complexity of the system from the time-consuming mechanical design to the easy-reprogrammable device control strategies.

In previous publications the DEXMART Hand has been presented in detail with reagard of the design structure [24, 70], the design of finger joints [73], the tendon transmission [74, 75], the actuation system [72, 76], the force, joint angle and tactile sensors[77–79] and the soft hand covers [80, 81].

4.2 The Design of the DEXMART Hand

The majority o robotic gripper projects known so far have been constrained to the adoption of metallic or hard plastic materials combined with classical manufacturing process such as CNC milling. In the last decade a fast grown of new technologies and materials have been observed. Such technologies include plastic molding (such as Shape Deposition Manufacturing (SDM)), Selective Laser Sintering (SLS), Fused Deposition

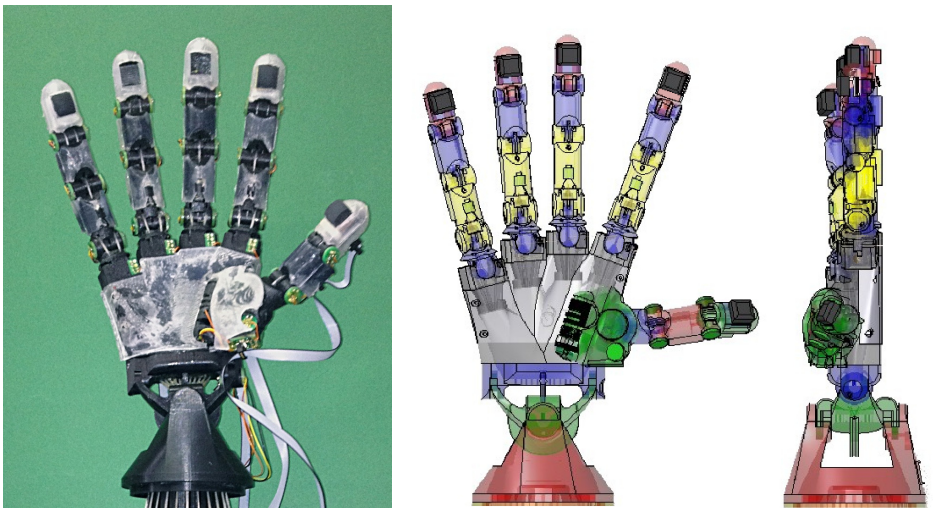

FIGURE 4.2: DEXMART Hand: Detailed view of the hand design.

Modeling (FDM), Stereo-Lithography (SLA) and Electron Beam Melting (EBM) and they are commonly identified with the term "rapid prototyping". In parallel, important advances in plastic materials technology have been carried out with the synthesis of polymers optimized for the rapid prototyping processes that show mechanical properties suitable for robotic applications. For these reasons, and also to allow a fast evaluation of different design solutions, all parts constituting the mechanical structure of the DEXMART Hand have been produced by means of FDM in ABS plastic. It is also important to say that the DEXMART Hand has not been conceived for mass production, but it is a test-bench for the evaluation and the integration of innovative solutions for robotic hands. Then, further steps are necessary for the industrialization of the system since some of the adopted solutions are not optimized from the point of view of the lifecycle. This is true also for the mechanical parts, and in particular for the adopted manufacturing process. The DEXMART Hand design is, however, compatible with alternative production processes, such as injection molding adopting high-performance plastic materials. Indeed, the mechanical parts manufactured by means of rapid prototyping can be used for creating molds for large scale production.

The design of the robotic hand is based on an endoskeletal structure articulated by means of non-conventional joints and actuated through a tendon-based transmission system by actuators that are remotely located in the forearm. The tendons are routed from the forearm through the wrist, the palm and the fingers by means of sliding paths (*sliding tendons*). To exhibit a proper compliance, the contact surface of the hand has been covered by a purposely designed soft cover mimicking the human dermal-epidermal layers [80, 81]. A general view of the present DEXMART Hand prototype is shown in Fig. 4.1, whereas in Fig. 4.2 it is possible to see the mechanical structure of the robotic hand in detail and in particular to appreciate the limited number of mechanical parts

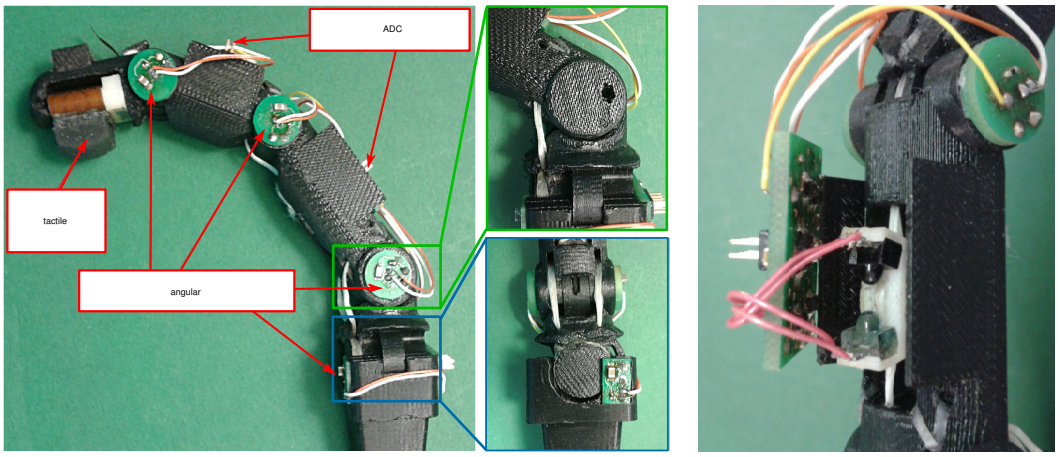

(a) Details of the tactile and position sensors.

(b) Detail of the tendon force sensor on the finger back side.

FIGURE 4.3: Detailed view of the DEXMART Hand finger.

(only 29) that compose the hand itself. The DEXMART Hand can be assembled very fast and simply without the need of any screw or other fixing parts. This result has been achieved by means of a design approach oriented to a systematic integration of the mechanical parts and by exploiting the potentialities of FDM. This approach allows a reduction of the production time, of the weight and the cost of the overall hand system, increasing its "affordability."

4.2.1 Finger Design

In Fig. 4.3 a prototype of the DEXMART Hand finger is shown. In particular, Fig. 4.3(a) shows the location of the position and tactile sensors, while the location of the tendon force sensor inside the finger is detailed in Fig. 4.3(b). The design of the finger is oriented to the maximum achievable integration between the mechanical structure, the sensors, the electronics, the actuation and the soft pads and in light of structural simplification, allowing one-step monolithic manufacturing of each finger link and consequent reduction of the assembly complexity. With reference to Fig. 4.4(a), the fingers are composed of the distal, the medial and the proximal phalanges, connected by distal interphalangeal (DIP) and proximal interphalangeal (PIP) joints and by a base whose function is twofold: it implements the 2-DOF metacarpal (MC) joint and allows an easy connection of the finger to the palm. The structure of the thumb is quite different with respect to the other fingers, as can be seen in Fig. 4.4(b). It is shorter and stronger than the other fingers (as in the human hand) and is composed of 3 links, the distal phalanx, the proximal phalanx and the metacarpal, connected by the interphalangeal (IP) and the metacarpophalangeal (MP) joint, and by a base that implements, together with the palm itself, the 2-DOF

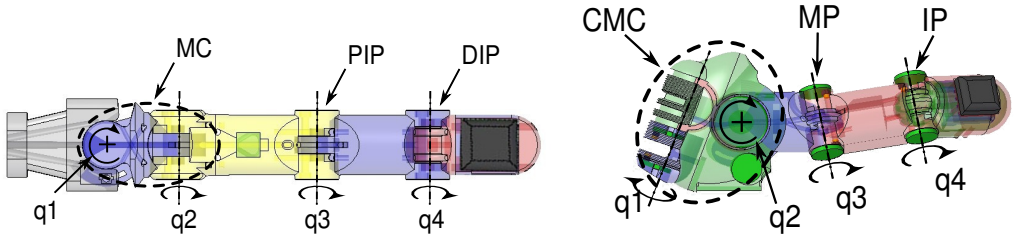

(a) Detail of the finger. (b) Detail of the thumb.

FIGURE 4.4: Details of the DEXMART Hand finger and thumb design.

carpometacarpal (CMC) joint. In particular, the implementation of the MC, the MP and the CMC joints represents a technical solution that aims both at replicating the functionality of the biological counterpart and at simplifying the manufacturing and the assembly of the overall robotic hand. As a fundamental component of the whole robotic system, particular attention has been paid to simplify the design of the finger joints, avoiding the use of mechanical parts such as bearings or other similar hardware that may cause problems in the integration of the sensors and the tendon network in the proximity of the joint itself. After evaluating several alternatives including compliant joints [73], pin joints with sliding profiles integrated into the phalanx body - simply consisting of a plastic shaft that maintains the joint assembled and by a circular profile which slides on a cylindrical surface (Integrated Pin Joints, IPJs) - have been selected for the implementation of the joints that connect the phalanges of both the fingers and the thumb. Due to the different requirements in terms of strength of the finger base and to allow the dislocation of the finger in case of overload or impact, thus avoiding damages to the mechanical structure of the hand, a sightly different implementation of the same concept has been adopted for both the MC and the CMC joints. The assembly pin has been removed and the joint simply comprises two sliding profiles that are maintained in contact by the tendon tension, and a minimum tendon tension is ensured by the actuator controller. Figure 4.5 reports a detail of the MC finger joints where both of these solutions are used: in particular, Figure 4.5(a) shows the disassembled joints, whereas in Fig. 4.5(b) the final assembly of the MC joint is shown. As stated before, the selected implementation of the finger joints targets simplification of both the design and assembly and at increasing the robustness of the mechanical structure in case of finger overload. However, it introduces a non negligible friction at the joint level. This issue has been investigated deeply in previous work [82] with the aim of mitigating its effects by means of the hand control system.

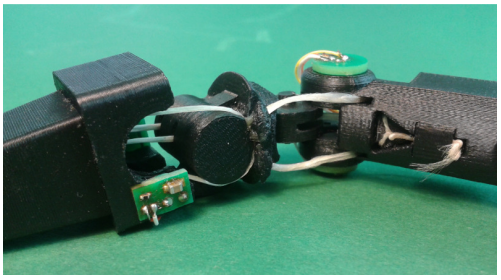

(a) Disassembled joints.

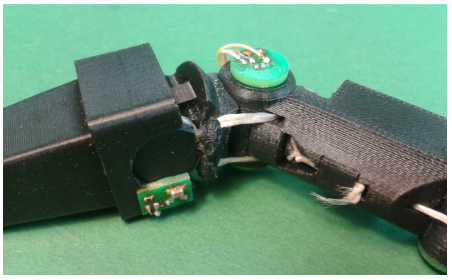

(b) Assembled joints.

FIGURE 4.5: Detail of the base and the proximal joints.

4.2.2 Hand Kinematics

It is well known that large differences exist in the dimensions and the joint mobility of the human hand among different subjects without significantly affecting grasping and manipulation capabilities [83]. As a consequence, it is not possible to define an optimal kinematics for a robotic hand [84], so the design of robotic hand kinematics must be focused on replicating the main functional aspects of the human hand, which have been analyzed in Subsection 2.2.2.

The main difference between anthropomorphic and non-anthropomorphic gripper kinematics lies in the presence of the thumb. This finger has a wide workspace that allows to touch all the other fingers and, in general, to execute force closure grasps on a large set of objects of different shapes and sizes. The kinematic reproduction of the thumb function can be achieved by a suitable misalignment between the rotational axes of the thumb joints. To maximize the opposability also a suitable inward rotation of the base of both the little and the ring fingers has been introduced. It is worth mentioning that the hamatometacarpal (HMC) joint of the little finger, which allows the motion of the little finger metacarpal toward the thumb, has not been implemented in the DEXMART Hand because of its limited range of motion and to achieve the maximum design simplification. Moreover, the 2-DOF CMC joint of the thumb has been implemented in a particular way compared to the 2-DOF MC joints of the other fingers:

- it is stronger to support the larger force that the thumb provides;
- the two rotational axes are combined in a different way compared to the other fingers, see Fig. 4.4;
- it provides a larger movement range than the MC joint to increase thumb mobility.

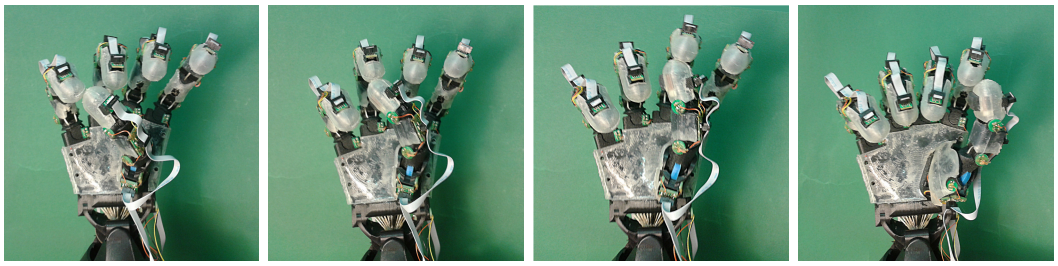

FIGURE 4.6: Opposition between the thumb and the fingers.

TABLE 4.1: Denavit-Hartenberg parameters of the DEXMART Hand fingers.

Link (Thumb)	d [mm]	θ	a [mm]	α [deg]
1	7.53	$\theta_1 + 85$	19.64	-110
2	-42.5	$\theta_2 - 80$	18	-90
3	-1.65	$\theta_3 + 10.62$	24.57	70.32
4	4.89	$\theta_4 - 3.61$	30	0
5	0	θ_4	30	0
Link(Index)	d [mm]	θ	a [mm]	α [deg]
1	40.75	θ_1	82	-95
2	-2.91	$\theta_2 - 20$	18	90
3	0	θ_3	38	0
4	0	θ_4	28	0
5	0	θ_4	28.5	0
Link (Middle)	d [mm]	θ	a [mm]	α [deg]
1	14.34	θ_1	86	-86
2	-4.91	θ_2	18	90
3	0	θ_3	40	0
4	0	θ_4	28	0
5	0	θ_4	28.5	0
Link (Ring)	d [mm]	θ	a [mm]	α [deg]
1	-11.16	θ_1	82	-80
2	-1.93	$\theta_2 - 5$	18	90
3	0	θ_3	38	0
4	0	θ_4	28	0
5	0	θ_4	28.5	0
Link (Little)	d[mm]	θ	a [mm]	α [deg]
1	-36.1	θ_1	68	-75
2	4.24	$\theta_2 + 15$	18	90
3	0	θ_3	35	0
4	0	θ_4	28	0
5	0	θ_4	28.5	0

In Tab. 4.1 the Denavit-Hartenberg parameters of the DEXMART Hand are reported, showing the particular arrangement of the finger joints that allows this result to be achieved.

4.2.3 Implementation of the Wrist Mechanism

As for the other parts of the system, also the wrist has been conceived to achieve the maximum manufacturing and assembly simplification. As shown in Fig. 4.7, it is composed of only three parts (manufactured by means of FDM), and no bearings,

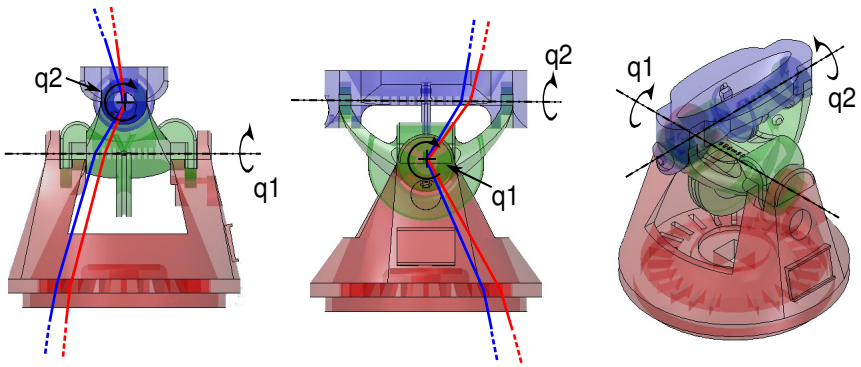

FIGURE 4.7: Details of the DEXMART Hand wrist design.

screws or other hardware are necessary for its assembly. It implements 2 DOF, the flexion/extension and the adduction/abduction movements (the pronation/supination movement has not been implemented since, in robotic hands with integrated forearm, it usually occurs at elbow level), and also in this case the joints are composed of sliding profiles that can be eventually dislocated in case of overload to prevent damage to the mechanical structure of the hand. Since the tendons go from the forearm, where the actuators are placed, to the fingers passing through the wrist, particular attention has been paid to achieve decoupling between the wrist and the tendon movements. Several technical solutions that allow decoupling of the wrist and the finger movements can be found in literature, but in our case this goal has been achieved by introducing a certain distance (20 mm) between the two orthogonal axes of the wrist (this distance is about 5 mm in humans [85]) to allow the tendons to pass through both rotational axes. Figure 4.7 shows the routing of the tendons through the wrist. With the aim of reducing the friction acting on the tendons, during the wrist design particular attention has also been given to avoid any contact between the different tendons and to minimize the tendon curvature [75]. Not only the fingers, but also the wrist, is driven by means of tendons, and its actuators are located in the forearm. Considering also the larger force required, two antagonistic actuators have been used for each DOF, resulting in a total of 4 actuators used to drive the wrist.

4.3 The DEXMART Hand Actuation

Despite the continuous evolution of actuator technology, the current state of the art in this field does not allow arranging twenty or more actuators in a robotic hand with dimensions similar to those of a human hand and with suitable requirements in terms of speed and forces. The tendon-based transmission system partially solves this problem allowing the allocation of the actuators within the forearm, where the most powerful

muscles are located in the biological model and more space is available for the motors. This actuator arrangement simplifies the hand construction, frees up space in the fingers for the integration of the sensors and achieves a more anthropomorphic weight distribution. Consequently, the tendon-based transmission system represents the most promising solution for dexterous anthropomorphic robotic hands.

The DEXMART Hand is actuated by means of four tendons for each finger, plus four additional tendons for the wrist actuation, resulting in a requirement of 24 independent actuators. In the following, the tendon-based transmission system of the device is detailed and the twisted string actuators are described.

4.3.1 The Tendon Network

The way the tendons are routed from the motors to the joints is a fundamental design problem in tendon-based actuation. Usually, tendons are routed by means of pulleys, sheaths or sliding surfaces: pulleys have been widely used for the implementation of tendon-driven robots, and in particular for robotic hands, since they minimize the friction forces acting along the tendon. The drawback of this approach consists in a more complicated mechanical design due to the presence of bearings and similar hardware, which partially reduce the advantages introduced by the use of tendons. The use of sheaths is a convenient solution due to its simplicity, but it introduces distributed friction along the tendon, and therefore hysteresis and dead-zones in the transmission system characteristic [75, 86]. In the DEXMART Hand, the routing of the tendons from the actuators in the forearm to the fingers is implemented by a series of sliding paths enclosed directly within the finger structure. A complete analysis of the tendon transmission modeling, control and material selection is reported in [75]. As for sheath routing, also in this case the stiction and the dynamic friction acting on the tendons affect the performance of both the position and the force control of the finger. To limit this undesired effect, a suitable low-level control strategy able to minimize the internal tendon forces (the tendon forces that do not contribute to the overall joint torques) has been adopted, see Borghesan et al. [74] for additional details.

Instead of directly imitating the biological model, many different simplified solutions have been proposed in the literature to replicate the functionality of the quite complicated human tendon network. Whereas in the biological model the tendons slide around the bones, for the optimization of the transmission system in terms of reducing both the friction and the coupling among the hand movements, the structure of the hand has been designed to allow the tendon to pass through the endoskeleton by means of suitable channels. In this way, the tendons can be routed through the center of rotation

of the joints when needed, obtaining a complete decoupling between the movements of consecutive joints.

Different studies confirm that the total amount of friction acting along the tendon depends only on the friction coefficient and on the total curvature of the tendon path from the motor to the joint [75, 86]. In the DEXMART Hand, this non-trivial design problem has been faced by minimizing the tendon path curvature, by making the path of each tendon as straight as possible and by a suitable selection of the tendon materials in addition to the use of tendon lubrication. Usually, very thin steel cables are used allowing a linear force-elongation behavior of the tendon to be obtained but introducing some design and assembly constraints due to the limited curvature radius of steel cables. In the last years, polymeric fibers have largely been adopted to improve the design flexibility of tendon transmissions, and in particular a Dyneema-based fiber called Fast-flight has been used for the tendons of the DEXMART Hand. It is also worth mentioning that the nature of the mechanical part surfaces obtained (in ABS plastic) by means of FDM imposes that:

- the diameter of the tendons cannot be too small (less than 1 mm from our experience) to avoid that the tendon may "cut" the plastic parts in case the tendon applies a load along the material deposition plane;
- the surface of the tendon must be smooth to reduce the friction coefficient and the wear of the sliding surfaces.

These are among the main motivations that brought us to the selection of the Fast-Flight cables for the tendon network of the DEXMART Hand. This cable is characterized by a very smooth and continuous surface (it does not have any external cover for protecting the fibers) that allows achieving a very reliable transmission system avoiding the use of pulleys or other additional elements for the sliding surfaces. Indeed, by adopting these design expedients, no failure in the sliding surface of the tendons has occurred. Moreover, it is also important to note that these issues imposed the use of different materials for the implementation of the twisted string actuation (whose cables do not slide over any surface) and the tendon network of the hand itself. In [75, 87], the tendon-based transmission system of the hand has been studied in detail, and suitable control strategies for the compensation of the friction acting on the tendons have been proposed and experimentally tested.

The fingers of the DEXMART Hand are actuated by means of an N+1 tendon network, whereas a 2N approach has been used for the wrist actuation due to the higher requirements in terms of amplitude and "symmetry" of the actuation force. In Fig. 4.8,

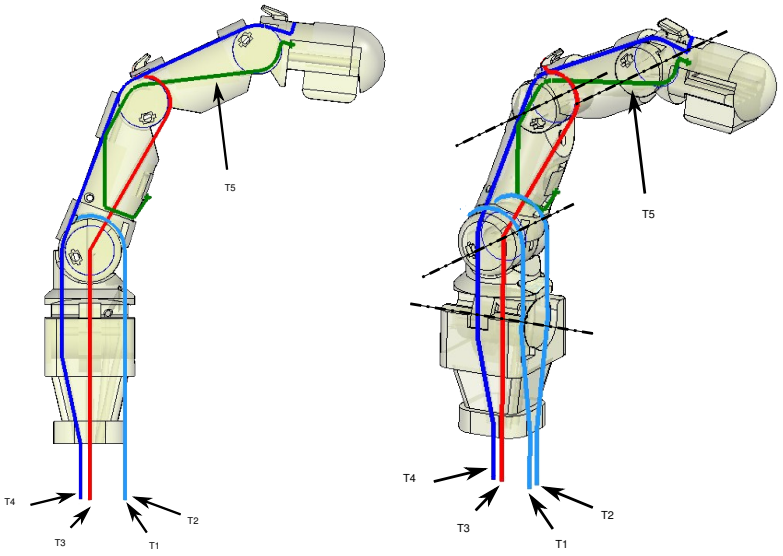

FIGURE 4.8: Details of the tendon network inside the finger.

a detailed view of the tendon path inside the finger and the DEXMART Hand is shown. With reference to Fig. 4.8 where the tendon path inside the finger is reported, the tendons that actuate the MC joint (T1 and T2) are connected directly to the proximal phalanx, whereas the antagonistic tendon (T4) slides over the joints on the back of the finger. The tendon that actuates the PIP joint (T3) is routed very closely to the center of the rotational axes of the MC joint to limit as much as possible the coupling between the movements of this joint and the others. The path of the tendon (T5) that connects the PIP to the DIP joint inside the medial phalanx is straight so as to limit the friction acting on the tendon. This tendon is not driven by any actuator but it is only used to couple the motion of the DIP and the PIP joints in the same way they are coupled in the human hand. By neglecting the tendon elasticity (thanks to the very high modulus of the tendon material [75]), the relationship between the tendon displacements and the finger joint positions can be expressed by the following relations:

$$l = H\,\theta, \qquad \text{with} \qquad H = \begin{bmatrix} r_{11} & r_{21} & 0 & 0 \\ -r_{12} & r_{22} & 0 & 0 \\ 0 & 0 & r_{33} & 0 \\ 0 & -r_{24} & -r_{34} & -r_{44} \\ 0 & 0 & -r_{35} & r_{45} \end{bmatrix}, \tag{4.1}$$

$$v = \dot{l} = H\dot{\theta}, \tag{4.2}$$

where $l = \begin{bmatrix} l_1 & l_2 & l_3 & l_4 & l_5 \end{bmatrix}^T$ is the vector of the tendon displacements with respect to the zero position, i.e. with the finger in the straight configuration, v is the tendon velocity vector, $\theta = \begin{bmatrix} \theta_1 & \theta_2 & \theta_3 & \theta_4 \end{bmatrix}^T$ is the vector of the finger joint angles and r_{ij} is the distance of the j-th tendon with respect to the i-th joint rotation axis. The

numerical values of r_{ij} are reported in Tab. 4.2. Note that, thanks to the DEXMART Hand design, the value of r_{ij} is constant, and in particular it does not depend on the joint configurations. The coupling given by the introduction of the coupling tendon T5 results in a kinematic constraint that can be expressed as:

$$\theta_4 = \frac{r_{35}}{r_{45}}\theta_3. \tag{4.3}$$

Due to the virtual work principle, the relation between the tendon force f and the finger joint torques $\tau = \begin{bmatrix}\tau_1 & \tau_2 & \tau_3 & \tau_4\end{bmatrix}^T$ can be computed as:

$$\tau = H^T f. \tag{4.4}$$

Since the dimensions of the tendons and the joint space are different, i.e., 5 and 4 respectively, in order to compute the actuation forces f given the desired joint torques τ, the pseudo-inverse H^{T^+} of the matrix H must be used:

$$\hat{f} = H^{T^+}\tau \tag{4.5}$$

$$f = \hat{f} + \lambda f_k \tag{4.6}$$

where $\hat{f}$ is the minimum module force vector so that $\tau = H^T\hat{f}$, f_k is a base of the null space of H^T, and $\lambda \in \mathbb{R}$ is chosen in order to impose the tendon tensions above a certain threshold f_0

$$\lambda = \max_{i\in\{1,\cdots,5\}} \frac{f_{0_i} - \hat{f}_i}{f_{k_i}} \tag{4.7}$$

where i denotes the element index of each vector. The force computed in (4.5) is then a five elements vector, including the force applied to the passive tendon. The forces to be applied by the actuators consist then in the first four elements of f, whereas the passive tendon tension f_5 will be univocally determined by the forces applied by the actuators on the other tendons. Then, the low-level controller of the twisted actuation system applies the desired force to each tendon ensuring also the minimum desired tension in the passive tendon, as described in detail in Palli et al. [72]. Together with the kinematic parameters reported in Tab. 4.1, eq. (4.1)-(4.5) allow computing the relation between the fingertip, the joints and the tendon motion.

r_{11}	r_{12}	r_{21}	r_{22}	r_{33}	r_{24}	r_{34}	r_{44}	r_{35}	r_{45}
8.2	8.2	7.8	7.8	6.3	5.3	5.3	5.3	3.5	5.0

TABLE 4.2: Values of r_{ij} (in mm).

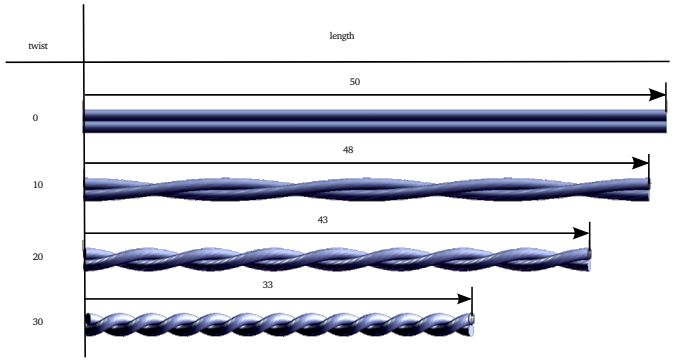

FIGURE 4.9: Basic concept of the twisted string actuation system.

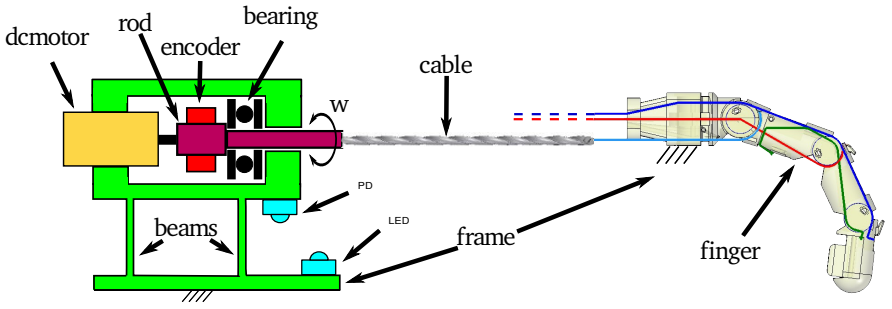

FIGURE 4.10: Schematic representation of the DEXMART Hand actuation system structure.

4.3.2 The Twisted String Actuation System

The actuation of the robotic hands developed so far are based essentially on rotative electric motors [7, 31, 88] or linear pneumatic actuators [29], usually McKibben motors [89]. The use of pneumatic actuators, besides the higher power density compared to electric motors, presents some difficulties from the control point of view and also conflicts with the integration requirements, since the valves and the compressor cannot be included into the hand structure due to their dimensions and weight.

Although the actuation solutions adopted in robotic hands developed so far have their own benefits and shortcomings, the so-called twisted string actuation system has been developed for the DEXMART Hand, aiming at fitting with its design requirements. Compared to conventional solutions, the main advantages of this actuation system consist in the direct connection between the motor and the tendon without any intermediate mechanisms such as gearboxes, pulleys or ballscrews, in the direct transformation from rotative to linear motion, in the extremely reduced friction (only an axial bearing is needed), in the very high reduction ratio, in its intrinsic compliance and in the use of very small high-speed motors. The basic idea of this quite simple actuation system is illustrated schematically in Fig. 4.9: two or more strands are connected in parallel on one end to a rotative electrical motor and on the other end to the load to be actuated.

Twisting the strands at the one end by means of the motor reduces the length of the transmission, resulting in a linear motion of the other end.

The basic principle of this actuation concept has already been used for different applications [90–93], and the growing interest in this actuation concept, in particular for robotic hand development, is shown by several recent publications [94–96]. In contrast with previous designs reported in the literature, the twisted string actuation system adopts very thin and long strings twisted around themselves allowing the use of very small high-speed motors without a speed-reducer, reducing the costs of the motors and simplifying the mechanical design. As a specification for the actuation system design, a 10 N load applied perpendicularly to the tip of an outstretched finger has been considered. Taking into consideration the finger kinematics and the tendon routing, this requirement translates into a maximum force of 80 N and a displacement corresponding to full closure of the hand of 25 mm maximum for each tendon. The twisted string actuators of the DEXMART Hand have been organized in two levels, characterized by different lengths of the strands, 0.21 m (Actuation Level 1, AL1) and 0.28 m (Actuation Level 2, AL2), respectively, to reduce the overall dimension of the actuation system.

The twisted string actuators are composed of 2 strands each, and each strand has a diameter of 0.14 mm. Since each strand can support a maximum load of 160 N, this element represents the weak point in the force transmission chain from the motors to the joints, allowing the use of the strand as a mechanical fuse, also thanks to its extremely low cost, in case of actuation system overloading. Suitable research has been carried out to select a proper fixing mechanism of the strands to both the motor and the linear guide on the tendon side to increase the lifetime of the strands and allow an easy and fast substitution of this element in case of damage. The solution for fixing the strands adopted in the DEXMART Hand allows the twisted string actuators to resist more than 10000 working cycles [72]. For implementing the twisted string actuators, the coreless DC motors A12C-12S from C.I. Kasei Co. have been selected. They are characterized by an outer diameter of 12.4 mm, a length of 30.8 mm, a stall torque of 21.3 Nmm and a maximum rotating speed of 21600 rpm. According to the kinetostatic model of the twisted string actuation system presented by Palli et al. [72], the relationship between the motor angle φ and the length of the actuator p can be easily derived from the geometry of the helix formed by the strands:

$$L = \sqrt{\varphi^2 r^2 + p^2}, \tag{4.8}$$

$$\sin\alpha = \frac{\varphi r}{L}, \quad \cos\alpha = \frac{p}{L}, \quad \tan\alpha = \frac{\varphi r}{p}, \tag{4.9}$$

where α is the helix slope and L is the strand length. From eqs. (4.8) and (4.9) it follows that:

$$\dot{L} = \dot{p}\cos\alpha + \dot{\varphi}\, r \sin\alpha. \tag{4.10}$$

From this last equation, the maximum speed of the actuation can be computed neglecting the finite stiffness of the strands or, in other words, in case of small load (free hand motion), which implies a constant length of the strand, i.e.:

$$\dot{L} = 0 \implies \dot{p} = \dot{\varphi}\, r\, \tan\alpha = \dot{\varphi}\,\frac{\varphi\, r^2}{p} = \dot{\varphi}/h. \tag{4.11}$$

Note that eq. (4.11) defines the configuration dependent generalized reduction ratio $h = p/(\varphi\, r^2)$ of the twisted string actuator since it also converts rotative to linear quantities. The equilibrium between the motor torque τ_m and the force acting in each strand F_i (along the strand direction) is:

$$\tau_m = 2\, r\, F_i\, \sin\alpha. \tag{4.12}$$

The resulting actuation force F_z is then:

$$F_z = 2\, F_i \cos\alpha \quad \Rightarrow \quad \tau_m = F_z\, r\, \tan\alpha = F_z \frac{\varphi\, r^2}{p} = F_z/h. \tag{4.13}$$

Since the model (4.8) is singular with respect to the configuration $\varphi = 0$, the twisted string actuation of the DEXMART Hand has been designed to present a minimum actuator contraction of 5 mm to prevent control singularities [72]. While considering a maximum tendon displacement of 25 mm, the maximum needed actuator contraction is 30 mm. From eq. (4.13) follows that the reduction rate of AL1 ranges from $2.4{\times}10^4\,\mathrm{m}^{-1}$ to $6.6{\times}10^4\,\mathrm{m}^{-1}$, while the one of AL2 ranges from $3.2{\times}10^4\,\mathrm{m}^{-1}$ to $7.4{\times}10^4\,\mathrm{m}^{-1}$. The actuators have been designed to satisfy the actuation requirements for both AL1 and AL2 with a suitable margin for preventing performance degradation due to undesired effects like motor friction. Then, the maximum force requirements must be tested against the minimum reduction ratio of AL1, while the speed requirements need to be verified against the maximum reduction ratio of AL2. From eq. (4.11) and considering that the motors present the maximum output power at about 10000 rpm, it follows that the maximum contraction velocity of AL2, in the worst conditions, is about 0.014 m/s, while the minimum force of AL1, in the worst conditions and neglecting friction, is about 288 N. Moreover, the maximum time required by the actuators to accomplish a complete contraction movement is about 0.84 s. The actuation force is then limited by the actuator's low-level control system to a maximum value of 80 N to prevent both damage to the transmission system and motor overheating.

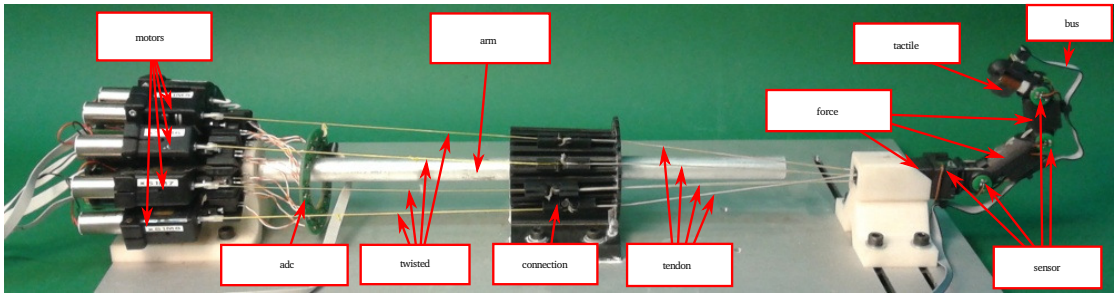

FIGURE 4.11: Detailed view of the finger actuation module and sensory equipment.

It is worth remarking that the force applied by the twisted string system can be efficiently controlled using only force feedback, while neither measurement of the motor angular placement and velocity or of the load position and velocity, nor an accurate knowledge of the system parameters (e.g. string or actuation length, string radius, motor or string preload angle, load parameters) are required. Moreover, due to the finite stiffness of the strings and to the particular implementation, a non-negligible configuration-dependent compliance of the proposed transmission systems was observed during the early experimentation. This phenomenon has been exploited to improve the robustness of the device and for safety purposes [97]. Another important feature of this transmission system is the fact that, due the high reduction ratio, the twisted string transmission system is (practically) non-backdrivable, a fact that together with its inherent compliance, allows maintaining also large gripping forces without needing to continuously supply power to the motors, and thus allowing a significant reduction of the overall control action requirements and power consumption.

With the aim of providing an effective description of the actuation system of the DEXMART Hand, a schematic representation of the actuation system is reported in Fig. 4.10 and a picture of a preliminary prototype of the actuation system for the finger is reported in Fig. 4.11. This module allows the detailed view of all of its basic components: from left to right, the system is comprised of the motor modules (see also Fig. 4.12), the acquisition electronics of the motor force sensors, the twisted string, the linear guides for the connection of the twisted strings with the finger tendons and the finger. As can also be seen in Fig. 4.1, the actuators are placed around the supporting structure of the forearm, allowing easy access to each actuation module for rapid repair and assembly. A detailed view of the motor module is reported in Fig. 4.12. Also the body of this part is manufactured in ABS plastic by means of FDM and is characterized by a mounting rail for rapid mechanical connection with the forearm structure, which eases assembly and repair of the system. A pair of flexible beams give the structure a certain compliance as well as facilitate implementing the force sensor (whose working principle will be detailed in the next section). Lateral barriers prevent cross coupling between the sensors of adjacent modules, while a case hosts the DC motor. As shown in Fig. 4.12, also the motor

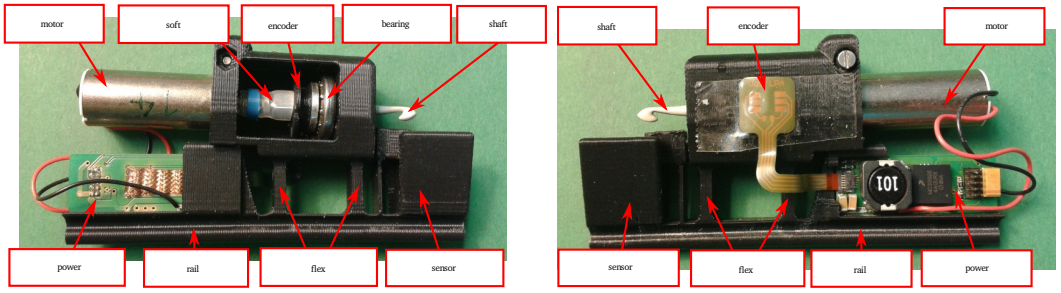

FIGURE 4.12: Detail of the motor module.

power electronics is arranged in the motor module, whereas the connection between the motor shaft and the transmission shaft has been implemented by means of a silicon tube in such a way as to introduce suitable flexibility for compensating any misalignment between the rotational axes of the motor and that of the transmission shaft (where the twisted string is attached). The particular structure of the motor module allows the transmission force to be entirely supported by the output shaft through a combined bearing, whereas the motor is only used to transmit the necessary torque for driving the twisted string actuation to the output shaft.

4.4 The sensory system

The DEXMART Hand is equipped with angular position sensors for the measurement of both the joints and the actuator configurations, with force sensors to measure the actuation force and with force/tactile sensors in the fingertips to reconstruct the pressure map as well as the contact area during the contact. Optoelectronic components have been implemented in all the sensors to achieve a fundamental simplification of the conditioning and acquisition electronics, thanks to their inherently high immunity to electromagnetic disturbances and with limited requirements in terms of amplification. As a consequence, the same conditioning circuit can be adopted for all of the sensors, and no amplifiers are needed for the resulting signal. The schematic illustrating the very simple acquisition electronics adopted in the DEXMART Hand for all of the sensors is shown in Fig. 4.13; the data collected from the sensors are, in this way, directly digitalized and transmitted through a digital SPI bus to the hand control system. A crucial aspect in the use of this type of optoelectronic sensor is the stability of the LED current. In our experience, the use of a stabilized power supply is sufficient to avoid any appreciable current fluctuations and, as a consequence, sensor measurement variations. Alternatively, the current lowing in the LEDs can be fixed by using a controlled current supply, with a minimal additional electronic circuit. Another aspect to take into account is the thermal inertia of the LED: due to this phenomenon, it is necessary to

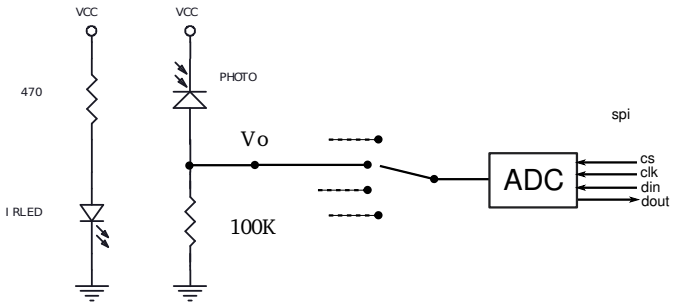

FIGURE 4.13: Measuring circuit for the sensors based on optoelectronic components.

wait a couple of minutes after the system power is on to reach a stable value of the device current and then a reliable response of the sensor. The electronics of the DEXMART Hand is based on Surface Mount Devices (SMD) both to reduce the dimensions of the boards and to allow automating the assembly of the electronics. Moreover, the DEXMART Hand electronics, as well as the hand mechanics, have been conceived to be modular and easy to mount on the mechanical structure of the hand. The DEXMART Hand has not been conceived for mass production nor for prostheses but is a test-bench for the evaluation of suitable solutions toward the next generation of robotic hands. Therefore, no particular investigation has been performed about the robustness of the wiring between the boards. Rather, standard miniaturized cables for digital data and digital communications for all the data that flow through the system have been adopted to reduce the risks of stability in electrical interfaces. This result has been achieved by simplifying the electronics as much as possible, thanks to the use of sensors based on optoelectronic components as shown in Fig. 4.13, and by digitalizing the data as closely as possible to the sensors in such a way as to interconnect all the sensors (as well as the actuators) to the control system by means of digital buses. As in the case of the hand mechanics, the adopted solution has been inspired by simplicity in assembling and by low cost. On the basis of our experience, the solutions adopted for the DEXMART Hand electronics do not require long to be assembled on the hand compared to the other manufacturing and assembly steps required for the hand production. They also do not detract anything nor negatively influence the evaluation of the solutions adopted for the DEXMART Hand, and in particular for the mechanical components. In the remainder of this section, a brief description of the developed sensors is reported with reference to the related literature. The location of all sensors in the finger of the DEXMART Hand can be clearly identified from Fig. 4.11, while the details about each sensor are reported in the following subsections. The description of the motor position sensors is not reported in this paper since they are simple, custom made optical encoders.

4.4.1 The Motor Force Sensor

The motor module force sensor exploits LED and PhotoDetector (PD) couples with a narrow angle of view to measure the small deformations imposed by the tendon force to the motor module itself. As schematized in Fig. 4.14(a), the compliant beams implemented in themotor module produce a translation Δx of the upper part of the structure under the effect of the transmission force F. The linearized deformation behavior of the beam with translation constraints at both its ends, highlighted by the red dashed rectangle in Fig. 4.14(a), is given by the contribution of the two compliant beams as

$$\Delta x = \frac{1}{2}\frac{F\,L^3}{12\,E\,I_b} = \frac{F\,L^3}{24\,E\,I_b} \tag{4.14}$$

where

$$I_b = \frac{h^3\,b}{12}$$

is the moment of inertia of the beam sectional area, L is the beamlength, E is the Young modulus of the material and h and b are the height and the thickness of the beams, respectively. The displacement Δx causes a variation of both the light angle and the distance between the LED and the PD, allowing an indirect measurement of the force F through the change in the PD photocurrent caused by the deformation of the motor module structure. Figure 4.14(b) shows a LED and a PD positioned symmetrically to each other, similarly as they are mounted on the compliant frame. In this symmetrical configuration, β represents the angle between the LED (or the PD) mechanical axis and the segment that indicates the distance d from the tip of the PD to the tip of the LED. In this state a certain amount of light emitted by the LED reaches the PD and is proportionally converted into a photocurrent $I(\beta)$. When the relative position x of the optoelectronic components experience a variation Δx compared to its initial value due to the deformation of the compliant frame, also the viewing angle β between the optoelectronic components varies and a different amount of light will be sensed by the PD and converted into a variation of the photocurrent $I(\beta - \Delta\beta)$. This happens because both the radiation pattern value of the LED and the responsivity pattern value of the PD vary with the viewing angle β, and the distance d between the two components varies with the relative position. Recalling the theory on LED radiation patterns [98], it is possible to model the system in order to optimize the selection and the positioning of the optoelectronic components. In particular, if the distance d is large enough to assume the far-field approximation valid, the LED and the PD could be regarded as a point source and a point receiver respectively. In this case the photocurrent $I(\beta)$ can be expressed as

$$I(\beta) = K\frac{\mathcal{I}(\beta)\mathcal{R}(\beta)}{d^2(\beta)} \tag{4.15}$$

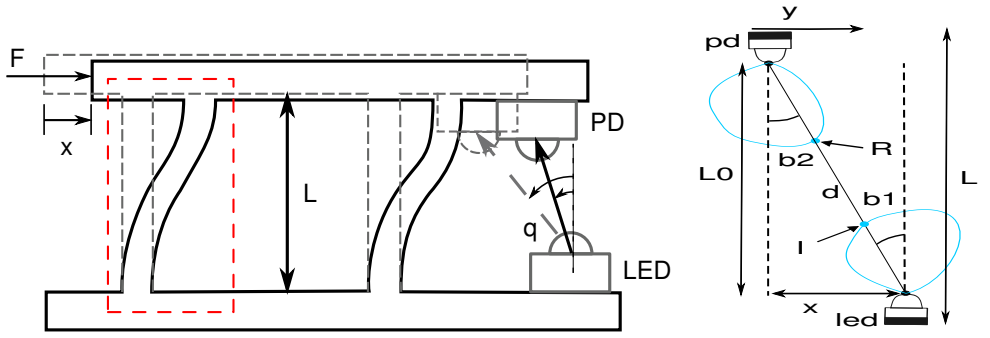

(a) Scheme of the force sensors based on optoelectronic components.

(b) Working principle of the proposed force sensor.

FIGURE 4.14: Schematic representation of the force sensor implemented in the actuation module.

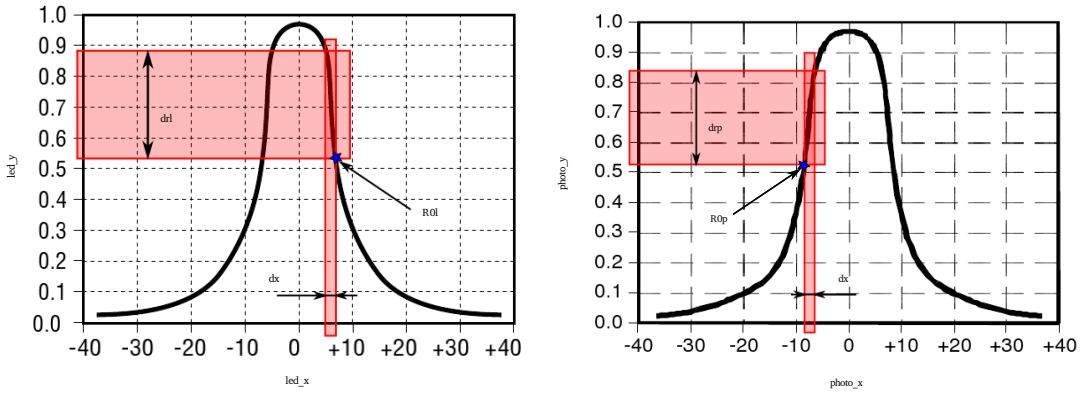

(a) Normalized LED radiant intensity pattern Vs. angular displacement.

(b) Normalized PD responsivity pattern Vs. angular displacement.

FIGURE 4.15: Characteristics (from datasheets) of the optoelectronic components used in the force sensors, SEP8736 (LED) and SDP8436 (PD), both from Honeywell .

where K is a dimensional multiplicative constant, $\mathcal{I}(\beta)$ is the radiant intensity pattern of the LED, $\mathcal{R}(\beta)$ is the responsivity pattern of the PD and d is the distance between the components. This model explains that the sensor characteristics, in terms of sensitivity, full-scale and SNR, depend on how the responsivity and radiation patterns of the optoelectronic components are sensitive to β variations. In Fig. 4.15(a) and 4.15(b) the characteristics of the LED and of the PD are reported and the large variation of radiant intensity pattern $\Delta\mathcal{I}$ and responsivity pattern $\Delta\mathcal{R}$ over a very limited variation of the angular displacement in a suitably selected region has been highlighted.

On the basis of the radiant intensity pattern of the LED and the responsivity pattern of the PD reported in Fig. 4.15, by exploiting eq. (4.16) the following optimization problem can be solved to choose the relative initial positioning (i.e., β) of the optoelectronic

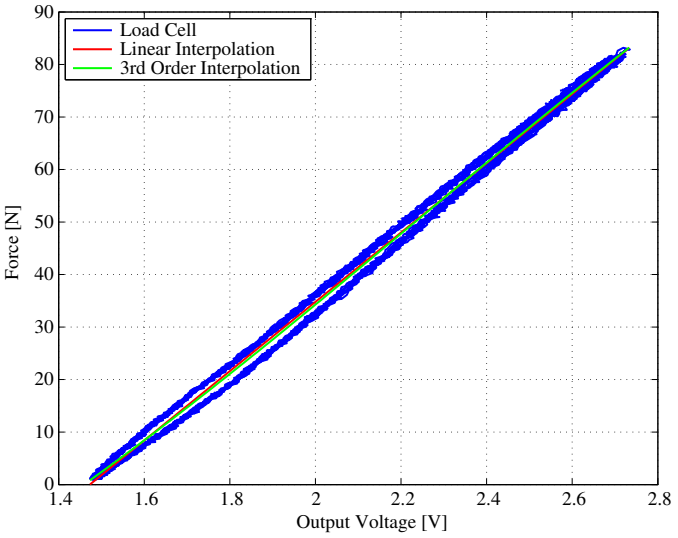

FIGURE 4.16: Calibration curve of the tendon load cell based on optoelectronic components.

components that maximize the sensor sensitivity:

$$\max_{\beta} J(\beta) = \max_{\beta} \left| \frac{I(\beta - \Delta\beta) - I(\beta)}{I(\beta - \Delta\beta)} \right| 100. \tag{4.16}$$

The details of this optimization procedure can be found in Palli and Pirozzi [78], from which the optimized value β =7.15 deg has been determined and then implemented in the sensor prototypes.

4.4.1.1 Sensor Calibration

The calibration curve of the proposed sensor has been derived using a strain-gauge load cell as reference sensor and applying a continuously varying load to the motor module up to the maximum desired value (80 N). The calibration curve of the proposed sensor is reported in Fig. 4.16: in this plot several pulling and release phases are reported to show both the limited hysteresis, given mainly by the properties of the plastic material of the flexible beams, and the repeatability of the sensor. Moreover, the experimental data have been interpolated by means of both a linear function and a 3rd-order polynomial to show simple methods to reconstruct the force information: even though the linear function gives a quite good estimation of the effective force in all the conditions, the use of a 3rd-order interpolation function results in a maximum estimation error of about 2 N, which is compatible with the tendon-driven robotic system.

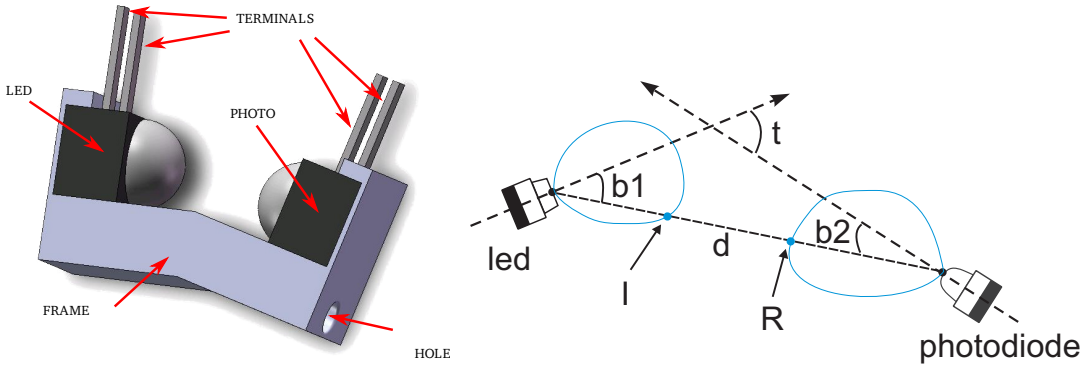

(a) (b)

FIGURE 4.17: Overall view of the force sensor (a) and working principle (b).

4.4.2 The Tendon Force Sensor

The tendon force sensor exploits the same optoelectronic components of the previously described sensor to measure the small deformations imposed by the tendon tension on a suitably designed deformable structure, also referred to as "compliant frame". For a detailed description of the sensor optimization both for the compliant frame and the optoelectronic components positioning, together with a complete characterization of the sensor, the reader is referred to Palli and Pirozzi [78]. A CAD model of the whole sensor, constituted by the compliant frame and the optoelectronic components, is depicted in Fig. 4.17, while Fig. 4.17(b) illustrates the interaction between the LED and the PD, assuming that the LED and the PD are positioned with an initial relative angle between their mechanical axes $\gamma = \beta_1 + \beta_2$. In Fig. 4.17(b), β_1 represents the angle between the LED mechanical axis and the segment that indicates the distance d from the tip of the PD to the tip of the LED, and β_2 representing the angle between the PD mechanical axis and the same segment. In this state a certain amount of light emitted by the LED reaches the PD and is proportionally converted into an electrical current I_γ.

When the angle γ experiences a variation compared to its initial value a different amount of light will be sensed by the PD and converted into a current different from I_γ. This happens because the radiation pattern of the LED varies with the angle β_1, see Fig. 4.15(a), so that the receiver detects different values of radiant flux for different values of β_1. At the same time, also the way the PD weights received light varies according to the variations of its responsivity pattern with β_2, see Fig. 4.15(b). The combination of these two effects leads to the observed variations of the photocurrent. The compliant frame is a monolithic element suitably designed to obtain an angular displacement of the optical axes of the optoelectronic components linearly proportional to the tension force applied to the tendon. Compared to previous solutions, the particular characteristic of the designed sensor is that it can be mounted in any position along the tendon and

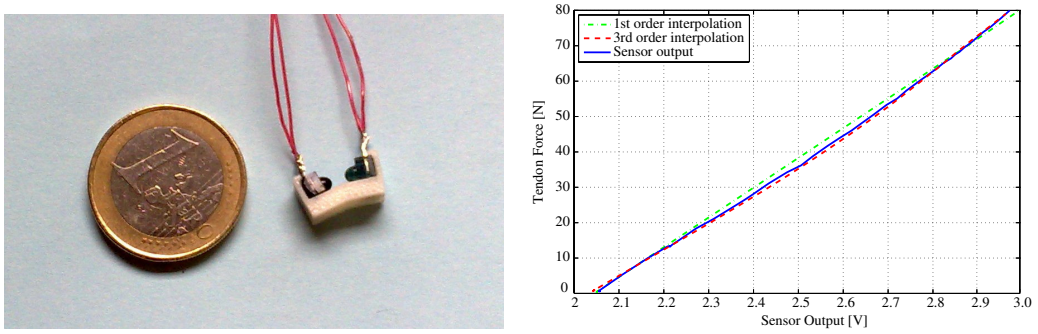

(a) (b)

FIGURE 4.18: Prototype of the tendon force sensor based on optoelectronic components (a) and its calibration curve (b).

needs not to be designed as a structural element, i.e. it can be designed independently of the other components of the robot. This is possible thanks to the V-shaped channel that traverses the length of the compliant frame through which the tendon passes: the surface friction ensures that a minimal tendon tension prevents the frame from slipping along the tendon, while the shape of the channel allows the frame to be inflected because of the reaction forces exerted by the tendon on the channel as the effect of its tension. The compliant frame can then be modeled as a flexible beam with concentrated load at its middle point and constrained at its ends. This simplified modeling allows designing the compliant frame starting from the maximum tendon tension and the corresponding desired optical displacement of the optoelectronic components.

Figure 4.18(a) reports a picture of a sensor prototype, while Fig. 4.18(b) shows a typical calibration curve. It is noteworthy that the voltage variations of this sensor output allow direct digitalization by means of the ADC without any additional amplification/filtering stage and as a consequence a direct connection to the DEXMART Hand control electronics through the SPI digital bus.

4.4.3 The Tactile Sensor

The tactile sensor developed for the DEXMART Hand is based on commercial SMD optoelectronic components and is capable of providing a tactile image of the contact area, a measurement of the contact force and torque components and an estimation of the position and orientation of the contact plane, which is assumed to be the surface of the object in contact with the sensor. Also this sensor integrates an ADC with an SPI digital interface to allow the direct connection with the robotic hand control electronics. The details on the sensor technology and its functionality can be found in D'Amore et al. [99]. Here a short description is reported for the sake of completeness.

4.4.3.1 Working Principle

The tactile sensor is constituted by a deformable elastic layer with an hemispherical shape positioned above a matrix of sensitive points, called "taxels", realized with LED/hototransistor couples. The optoelectronic component couples are organized in a 4×4 matrix structure. For each couple, the LED illuminates the reflecting surface which coincides with the bottom facet of the deformable layer. In practice, the deformable layer transduces an external force and/or torque into a deformation of its bottom facet through its stiffness. An external force applied to the deformable layer produces local variations of the bottom surface of the elastic material and the optoelectronic couples measure the deformations in a discrete number of points. These deformations produce a variation of the reflected light intensity and, accordingly, of the photo-current flowing into the photo-detector. The photo-current variations are finally transduced into voltage signals by using standard resistors. The deformable layer is realized with black silicone in order to avoid optical cross-talk between taxels and ambient light disturbances. Only the surface which faces each sensitive point is white to increase the sensor sensitivity.
The top of the deformable layer is a section of a sphere with a radius of 11.4 mm. With the silicone choice, according to the numerical simulations reported in D'Amore et al. [99], the expected measurement range of the sensor prototype is $[0, 4]$ N, the sensitivity is about 0.1 N and 1 Nmm for forces and torques, respectively. The selected tactile sensor measurement range is suitable for most of the common manipulation tasks, as shown in Palli et al. [70]. Instead, during grasping tasks which involve larger forces, the measurements of the tendon force (whose full scale is 80 N), can be used to control the task execution. The silicone rubber adopted for the implementation of the tactile sensor described in this paper presents shore hardness 9A. The working range of the tactile sensor can be changed by selecting a silicone rubber with different shore hardness for the implementation of the deformable layer. In particular, as detailed in D'Amore et al. [99], the relation between the sensor full scale and the silicone hardness is quite linear, e.g., by using a silicone with a hardness two times higher, also the sensor full scale is practically doubled. Each taxel of the sensor is composed of an infrared LED (code SFH480), and a silicon NPN phototransistor (code SFH3010). The digital interface has been implemented by means of the AD7490, which is a 12-bit high-speed, low-power, 16-channel, successive-approximation ADC with a maximum sample rate of 1 MHz. It also presents versatile serial input/output ports, supporting several communication protocols (SPI/QSPI/MICROWIRE), including the one (SPI) used in the DEXMART Hand. The overall power consumption of the tactile sensor is about 100 mW, and the estimated cost is much lower than any commercial 6-axis F/T sensor.

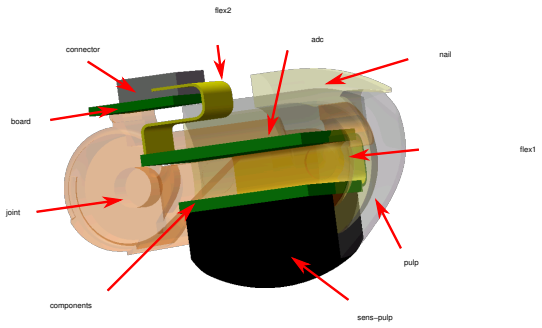

(a) Section of the fingertip with integrated tactile sensor.

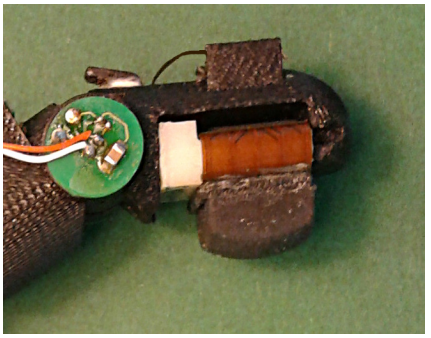

(b) Integration of the tactile sensor in the fingertip.

FIGURE 4.19: CAD drawing (a) and picture (b) of the tactile sensor integrated into the fingertip.

4.4.3.2 Sensor Calibration

Aiming at using it as a six-axes force/torque sensor, the proposed approach for the calibration of the tactile sensor is based on the use of a neural network used to model the relationship between the applied forces and torques and the phototransistors measurement. The sensor has been mounted on a six-axes load cell used as reference sensor, i.e., FTD-Nano-17 manufactured by ATI. An operator carried out various experiments, using a stiff plane, applying different external forces and torques and simultaneously acquiring all the voltage variations on the phototransistors and all the forces and torques components measured by the reference load cell. These data, acquired at a sample rate of 100 Hz, have been organized in a training set and a validation set to be used as input data (voltage variations) and target data (forces and torques components) of the neural network. A standard two-layer feed-forward neural network f_{NN} trained with the Levenberg-Marquardt method has been used to fit training data. Figure. 4.20 shows the accuracy of the tactile sensor in reconstructing the force and torque components. The reader can refer to De Maria et al. [79] for details about tactile sensor characterization.

4.4.4 The Angular Sensor

Each joint of the DEXMART Hand integrates a miniaturized angular position sensor based on commercial optoelectronic components [77]. The angular measurement takes place by modulation of the radiation light power that goes from a LED to a PD by means of a variably shaped channel that moves together with the joint. The main advantage of this solution is that the light path is entirely enclosed within the joint itself, so the sensor is insensitive to disturbances caused by adjacent sensors or external infrared sources.

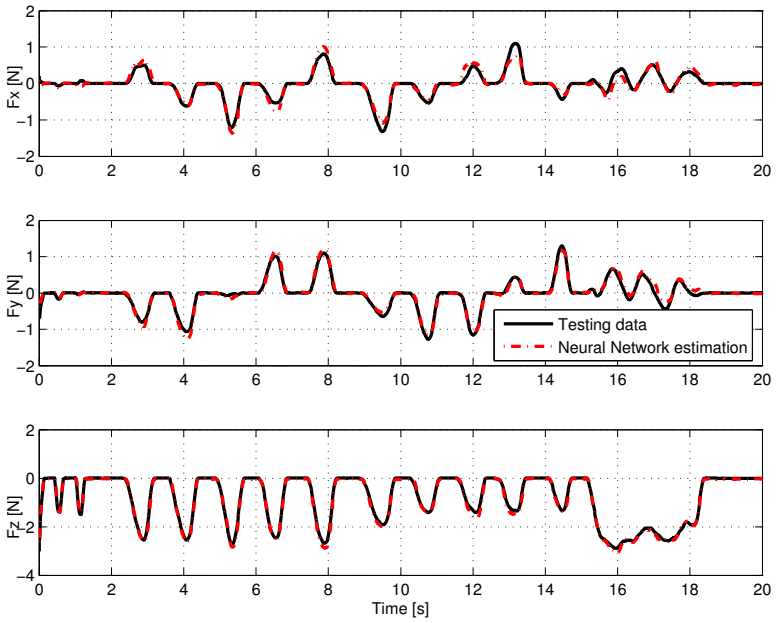

(a) Force Reconstruction.

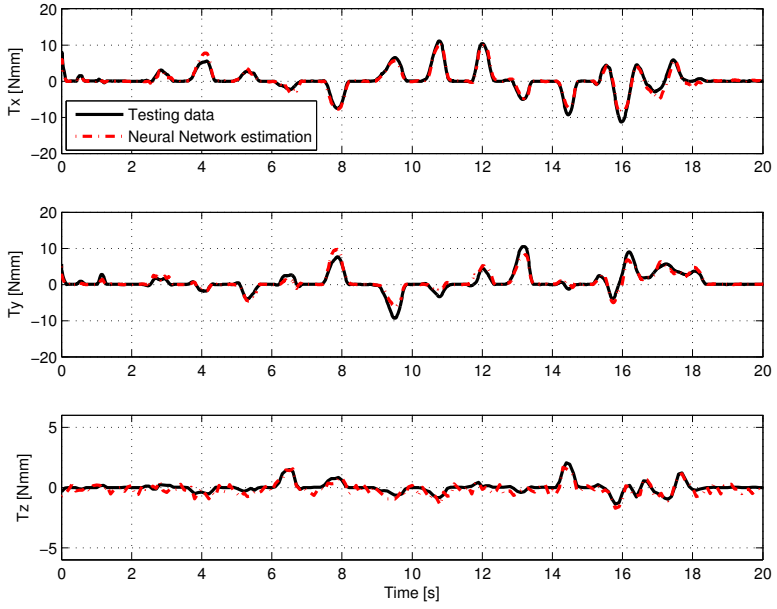

(b) Torque Reconstruction.

FIGURE 4.20: Reconstruction of the force and torque components by means of the tactile sensor.

4.4.4.1 Working Principle

To describe the working principle of the angular sensor, the interaction between the LED and the PD has been schematized in Fig. 4.21. In particular, according to Kasap [98]: the LED is approximated as a point source positioned at a point A that generates light in all directions with an intensity that depends on the emission angle according to the LED radiation pattern; the PD is modeled as a finite surface $\overline{CD}$, whose midpoint is

indicated with B, with a sensitivity that varies with the receiving angle according to the responsivity pattern of the PD. Due to the axial symmetry of the optical components and their corresponding radiation and responsivity patterns, the dependence of the model on the spherical coordinate ϕ can be omitted. As a consequence, the design of the sensor can be addressed using a 2D coordinate system instead of a 3D system without loss of generality. The optoelectronic components are mounted at a fixed relative position with the optical axes aligned to maximize the signal level.

In the initial condition, i.e. without any occlusion as reported in Fig. 4.21(a), the PD measures an optical power P_1. If a mechanical component is partially positioned between the two optical devices, see Fig. 4.21(b), a certain amount of the light emitted by the LED is occluded and, as a consequence, the PD measures an optical power P_2 smaller than P_1. With reference to Fig. 4.21(a) where the case of no occlusion is shown, the distance between the emitter and the midpoint of the receiver is defined as d_0, the segments $\overline{AC}$ and $\overline{AD}$ delimit the light flux impacting on the PD and γ_0 is the angle between these segments.

Figure 4.21(b) shows a generic case with partial occlusion, where the occlusion is defined as a variable δ that assumes values between 0 (no occlusion) and 1 (total occlusion). Note that the occlusion is assumed to be symmetric with respect to the optical axes of the optoelectronic components to maintain the symmetry of the system. The LED emits light in all directions but, due the occlusion, the PD receives only the amount of light with an emitting angle $\gamma < \gamma_0$. A proper mechanical design allows to obtain an occlusion δ of the light flux proportional to the physical variable to be measured: the angular position of the robotic joint.

4.4.4.2 Sensor Design and Calibration

Each joint is composed of a first link on which the LED and the PD are mounted and a second link where a variable width channel is implemented. On the first link two sockets for the optoelectronic components are realized so that the two devices are mounted face to face with the optical axes aligned and the light beam is entirely enclosed inside the joint itself (see Fig. 4.22(a)). The channel in the second link is designed in order to obtain a variable occlusion for the light emitted by the LED and received by the PD according to the working principle presented above. The dimensions of the channel are fixed so that the relationship between the occlusion and the joint angle is linear for the entire range of angle variations (see Fig. 4.22(b)).

For each finger of the DEXMART Hand three identical sensors (from the mechanical point of view) have been used for the DIP joint, the PIP joint and the second axis of

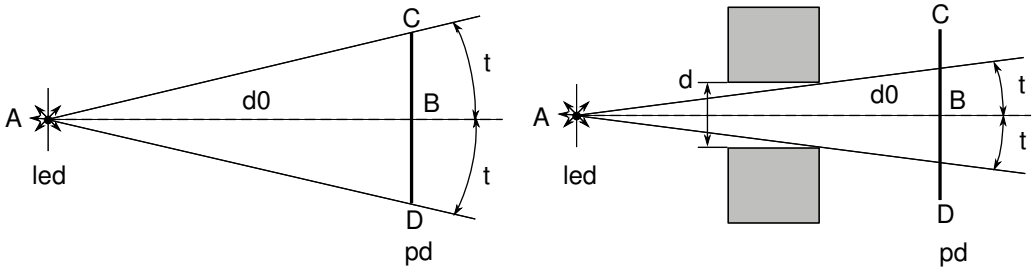

(a) (b)

FIGURE 4.21: Sketch of the interaction between the LED and the PD for the angular sensor: (a) interaction in the case of no occlusion and (b) in the case of occlusion.

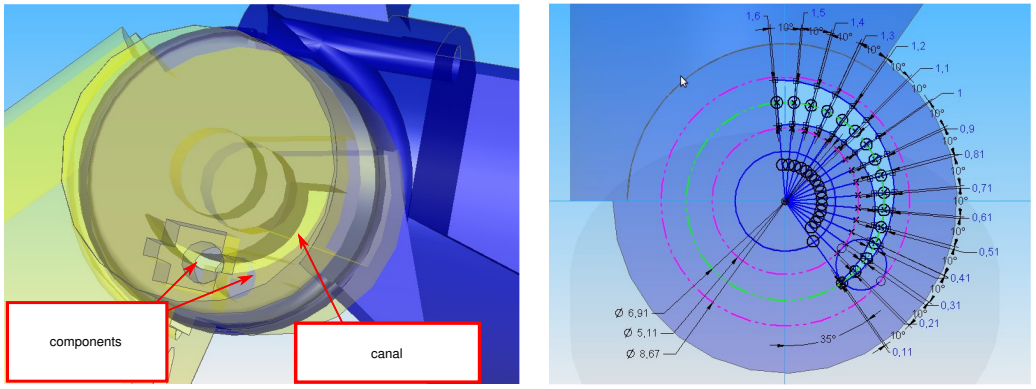

(a) Detailed view of the variable-width channel. (b) Dimensions of the channel (in mm).

FIGURE 4.22: Details of the robotic joint: (a) detail of the optoelectronic component sockets and (b) detail of the variable-width channel.

the MC joint. The same sensor is used also in the MP and IP joints of the thumb. For these joints, compatible with their size, the distance between the optoelectronic components has been selected to $d_0 = 7\,\text{mm}$. These three joints differ only by the angle ranges of the variable-width channel, which are $[0, 110]$ deg, $[0, 90]$ deg and $[0, 80]$ deg for the medial joint, the proximal joint and the distal joint, respectively. Suitable PCBs (Printed Circuit Boards) have been designed and optimized to be integrated into the finger joints. For the first axis of the MC joint and the two axes of the CMC joint of the thumb, a different joint implementation has been adopted because of the different implementation of these joints due to the higher mechanical strength required. In these cases, the joint dimensions are greater than the previous ones and, as a consequence, the distance between the optoelectronic components has been selected $d_0 = 9\,\text{mm}$. A different PCB has been designed to integrate the same position sensor concept in this joint. Figures 4.23(a) and 4.23(b) show two pictures where the two different implementations of the sensor for the two axes of the MC joint can be appreciated. These figures show the details of the different variable-width channel used for the corresponding axis and how the PCBs are assembled with the mechanical structure of the finger.

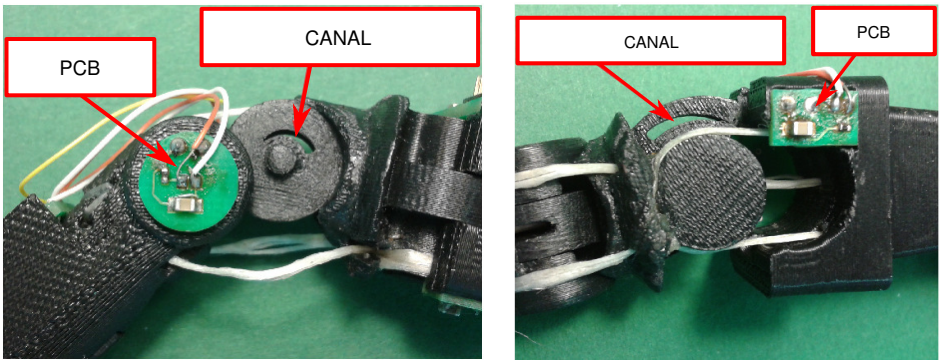

(a) (b)

FIGURE 4.23: Detailed picture of the second (a) and first (b) axis of the MC joint with the corresponding channel and PCB.

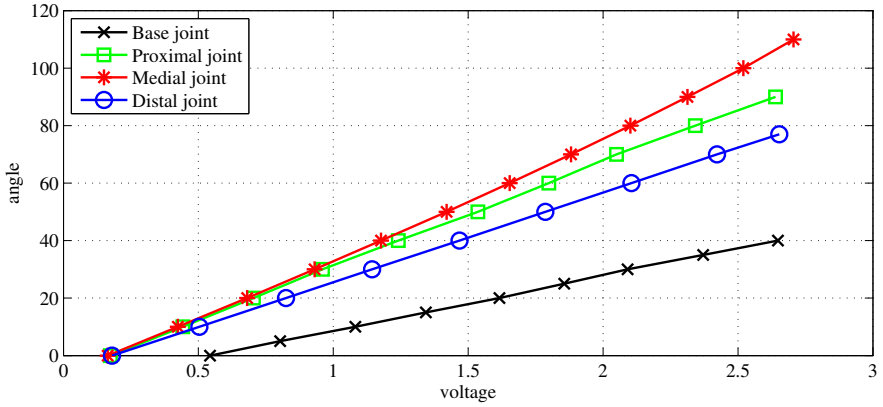

FIGURE 4.24: Calibration curve of the finger angular position sensor.

The typical calibration curves for the 4 sensors of a robotic finger are reported in Fig. 4.24. This characteristic is fundamental for a position sensor since it becomes attractive for the integration in complex systems such as anthropomorphic robotic hands. In fact, the linearity allows calibrating the whole system in a single step by estimating the calibration constant of each sensor on the basis of its output measured in two known positions only, e.g., the stroke limits of the joint angular motion, instead of having a long calibration phase different for each joint and always based on the use of a reference sensor. Also in this case, the sensor output variations as shown in Fig. 4.24 are large enough to allow a direct digitalization of the measurement signals, without any additional amplification/filtering stage. As a consequence, the sensor signals are directly connected to the ADC on the finger embedded electronics and transmitted to the DEXMART Hand controller through the SPI bus. Another important feature of this sensor is that, in case of joint dislocation, the output signal of the position sensor will likely reach a value very close to zero, which means full occlusion, or close to the power supply voltage (3.3 V), which means no occlusion at all. Since these values are outside the working range of a properly assembled sensor (and joint), as can be seen

from Fig. 4.24, they can be used by the hand control logic to detect joint dislocation and then react in a proper way, e.g., by stopping the system to allow reassembly of the joint before restarting the task.

The use of FDM for the manufacturing of the variable-width channel of the position sensors imposes several tests and design adjustments, a suitable selection of the printing directions and the separate manufacturing of some parts constituting the position sensors, in particular for the thumb and the wrist, to achieve the linear sensor response shown in Fig. 4.24. Finally, the polishing of the channel surfaces allows the measurement noise to be reduced. Probably the adoption of a different and more precise manufacturing method may simplify these operations, but will probably increase the sensor prototyping and the robotic hand production costs.

Chapter 5

Design of an Underwater multi-fingered Gripper

In the next future, a rapid increase in underwater applications is expected for exploration, industrial activities and scientific purposes. Even if robots are already intensively used for undersea operations, actually they are remotely controlled by a human operator and they require a (usually big) surface vessel, making their usage very expensive. In this context, the availability of autonomous robotic platforms equipped with manipulation devices for the execution of grasping and manipulation activities will improve significantly the affordability of underwater robotic missions. In any case, for underwater robots intended to manipulate objects, the end-effectors are going to play an important role, as it is already the case in other contexts like industrial or space applications. The devices currently available on the market usually present a quite simple kinematics, a reduced dexterity, often limited to only one degree of freedom, and very limited or even absent sensorial equipment [100, 101]. Indeed, the limited variety of tasks to be executed so far in submarine activities did not really require a very "dexterous" device. On the other hand, the expected developments in the field, e.g. the introduction of automatic systems for assembly, inspection and intervention, will need more versatile end-effectors able to grasp and manipulate different objects in a very diversified way. In literature, few robotic end-effectors for underwater applications have been presented. The devices described in [102], [103], [104], [105] are among the few examples of systems for undersea grasping and manipulation purposes. Remarkable examples of grippers for underwater applications equipped with tactile sensors can be found in [106, 107]

In this chapter, a three-fingered robotic gripper for underwater applications is presented. The main characteristics of this device are: 1) the transmission system based on cables routed through sheaths, allowing the arrangement of the actuators around the wrist

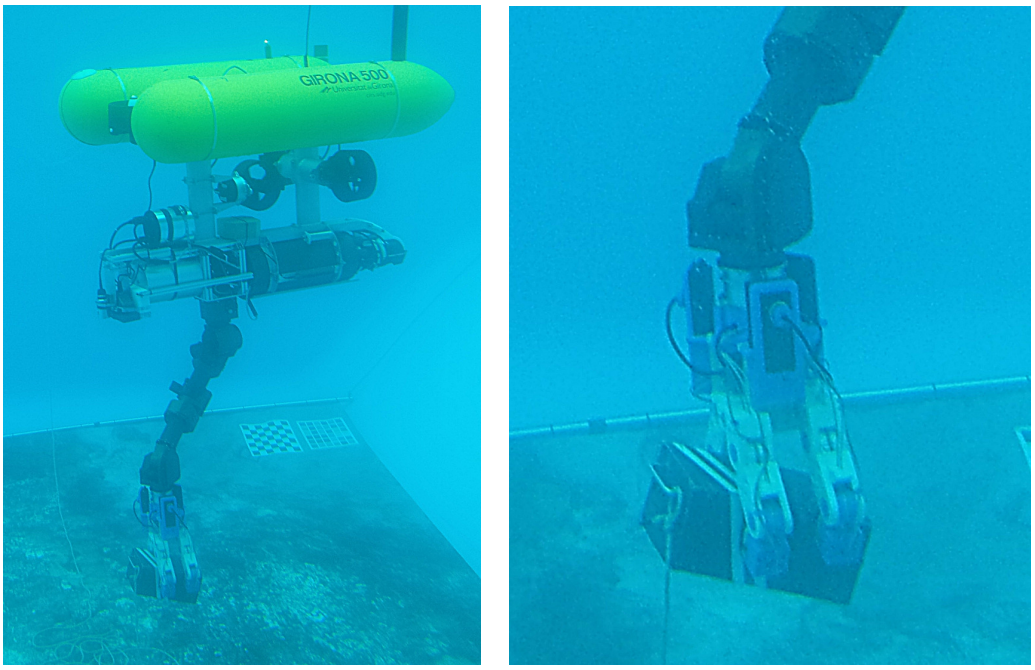

FIGURE 5.1: The Girona 500 AUV platform with the redundant arm and the gripper operating in the CIRS (Centre d'Investigació en Robòtica Submarina of the University of Girona) pool: a dummy black box is recovered from the pool floor.

both for reducing the distance between the palm and the wrist itself and for a better weight distribution; 2) the ability of grasping objects with very different shapes and dimensions with both parallel and precision grasp (fingers opposition); 3) the availability of force/torque sensors on the fingertip. This work has been developed as a part of the TRIDENT project, a research program supported by the European Commission and aiming at developing an autonomous system for submarine intervention activities, [108, 109]. The paper briefly reports also the results of the experimental evaluation of the autonomous underwater vehicle (AUV), developed within this project and equipped with a redundant arm and the gripper, see Fig. 5.1, as a demonstration of the effectiveness of the proposed device.

5.1 General Design Specifications

During typical missions foreseen in the TRIDENT project, the AUV will autonomously explore wide underwater areas searching for a specified object to be recovered. Then, the intervention actions will be planned for retrieving the object(s), and non trivial manipulation activities will be performed. For these purposes, the currently available grippers have some limitations, deriving from the limited workspace, the limited type of achievable grasps (usually only parallel or enveloping grasps) and limited (or absent) sensory equipment, making it very difficult to achieve real autonomy in task execution. Therefore, a more versatile gripper has been designed within the TRIDENT project in

order to provide the AUV with a more "dexterous" device, in such a way to ease the autonomous execution of (possibly) complex tasks. The main functional specification for the gripper are the following:

- the hand must be able to grasp objects with dimensions (diameter) in the range 5 ÷ 200 mm;
- the foreseen operating depth of the final project demonstration is about 25 m;
- the hand must be able to apply both force and form closure grasps with irreversible constraints;
- two- or three-finger precision, parallel and power grasps are desirable;
- local compliance on finger surfaces and/or actuation compliance is desirable in order to adapt to object shape irregularities, dimension uncertainties and stabilize the grasp;
- the sensory equipment of the hand should consider tactile sensors;
- the dimension should be kept as limited as possible, in order to have a low encumbrance of the arm/hand system during navigation.

In order to increase the manipulation capabilities of the AUV, the hand is installed on a 7 DoF, redundant arm. The arm has been designed with a modular approach, and is actuated by electric motors. For this reason, electric actuation is used also for the gripper. The communication between the control system, the motors and the sensors of both the arm and the gripper is implemented through a 2-wire CAN bus.

5.2 Design of the Gripper

According to the general specifications briefly summarized in Sec. 5.1, the typology, in terms of size and shape, of objects to be grasped by the gripper may be quite large. On the other hand, it is not strictly required any internal manipulation capability, but rather the capability to firmly grasp an object. For these reasons, a solution composed by a mechanism with three fingers capable of a large workspace has been adopted. Moreover, almost all the mechanical parts are manufactured in ABS plastic for reducing the weight and increase the buoyancy, whereas anodized aluminum has been adopted for the metallic parts to prevent corrosion. The overall weight of the gripper is about 4.5 daN in air, while in water it is about 1 daN, that can be easily compensated by adding proper floats.

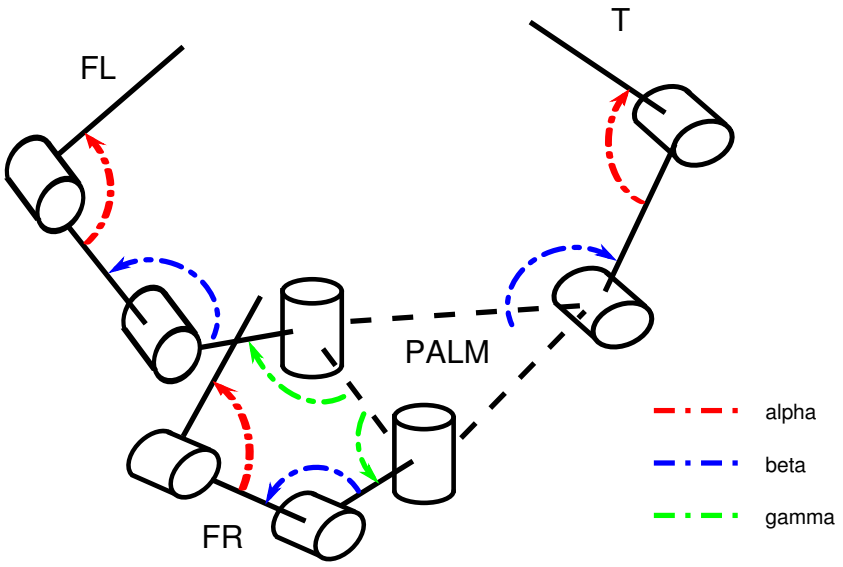

FIGURE 5.2: Kinematic structure of the gripper.

5.2.1 Kinematics

In Fig. 5.2 a schematic view of the gripper kinematics is reported. All the joints are of revolute type with PTFE bushings to reduce friction and prevent corrosion in marine environment. The gripper has three fingers: one named T (which can be intended as an opposable thumb), and two identical fingers named FR and FL (right and left finger respectively). This kinematic configuration is clearly inspired by the well known Barret Hand [32], that represents a suitable trade-off between hand functionality and design simplicity. The thumb has two links only: the proximal link, connected to the palm by a revolute joint (proximal joint) with a rotational axes parallel to the palm plane, and a distal link connected to the proximal link by a revolute joint (distal joint) whose rotational axes is also parallel to the palm plane. The FR and FL fingers differ from the thumb by the connection of the finger to the palm: in this case, an additional joint (palm joint) with rotational axis perpendicular to the palm plane is introduced between the palm and the proximal link, allowing the rotation of the whole finger with respect to the palm axis. This arrangement allows performing both parallel grasps as well as precision grasps, by means of opposition of the fingertips.

In total, the gripper has 8 joints, each one driven by an independent closed-loop cable actuation. On the basis of an analysis of the required gripper capabilities, and in order to reduce the overall weight, only 3 (identical) motors are used for the actuation. Obviously, couplings among the joints is present: these couplings are implemented in a very simple way by connecting in parallel the cable driving system of the three joint groups (i.e. distal, proximal and palm joints) to the same motor. With reference to Fig. 5.2, the angle $\alpha \in [90,\ 240]$ deg (distal joint angle) is actuated by a single motor for the three fingers at once, and the same applies to the angle $\beta \in [30,\ 180]$ deg (proximal joint

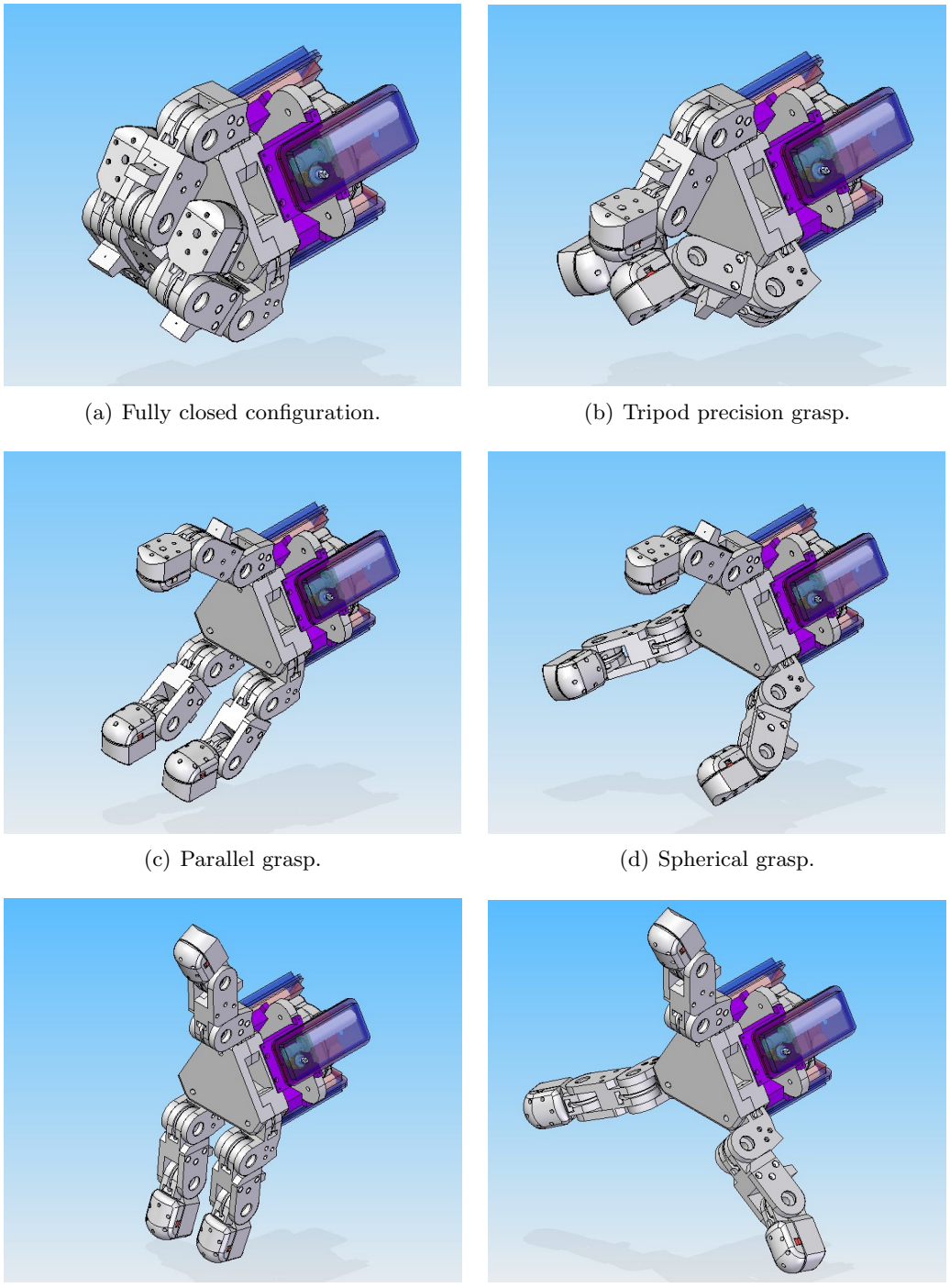

(a) Fully closed configuration.

(b) Tripod precision grasp.

(c) Parallel grasp.

(d) Spherical grasp.

(e) Parallel opened configuration.

(f) Fully opened configuration.

FIGURE 5.3: CAD view of the gripper design and kinematic configurations.

angle) and the angle $\gamma \in [90,\ 150]$ deg (palm joint angle). The consequence is that, although only three motors are used, different configurations can be achieved, allowing a potential of many types of grasps on a great variety of objects, both in force and in form closure. Some significant finger postures and grasp configurations are reported in Fig. 5.3.

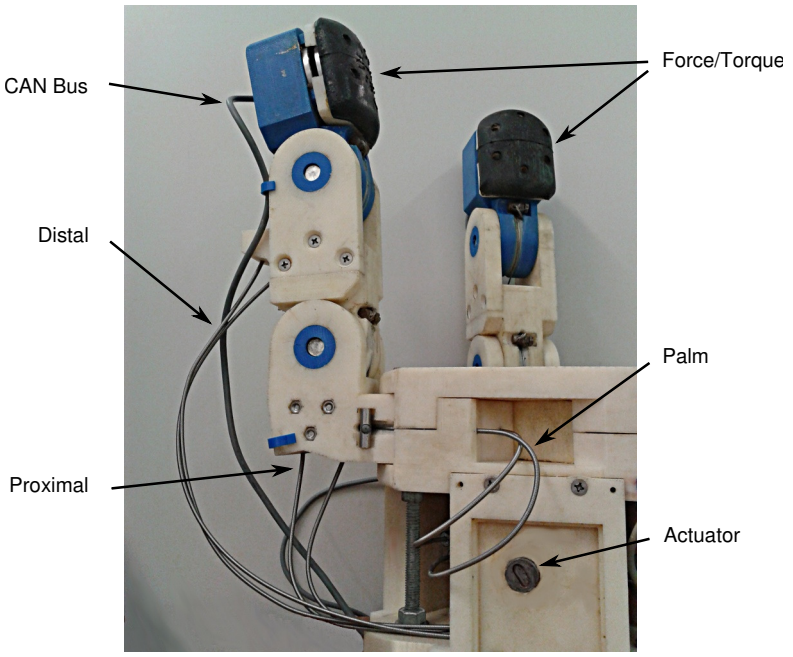

FIGURE 5.4: Detailed view of the cable transmission system.

5.2.2 Actuation

The actuation system of the gripper is based on the Faulhaber 12 W brushless DC motor EN 2250 BX4 CCD with integrated motion controller and CAN interface, provided with a 14:1 gearbox, guaranteeing a maximum torque of 1 Nm in continuous operation and of 1.54 Nm in intermittent operation. An additional worm gear 20:1 speed reducer is connected to the motor output shaft in order to obtain a proper torque/speed ratio between the motor and the load axis together with a more suitable arrangement of the motor for reducing the actuation encumbrance. Moreover, a reduction ratio of 4.6:1 is achieved by means of the different radii of the driving and the joint pulleys adopted in the cable transmission. Due to the gripper design, the main contribution to the normal fingertip force is given by the base joint. To compute the maximum fingertip normal force, we assume: 1) an equal distribution of the actuator torque between the base joints of the three fingers; 2) a distance between the finger base joint and the center of the fingertip of 170 mm; 3) a 20% torque loss due to friction along the cable transmission. It results that the maximum normal force applicable by each finger in continuous operation is about 150 N, which can be considered satisfactory for the typical operations of the TRIDENT project. Moreover, thanks to the introduction of the worm gear reducer, the actuators are non-backdrivable, a fact that allows holding the desired gripper configuration without further supplying power to the motors also during a grasp. The closed-loop cable transmission of the gripper, whose details are visible in Fig. 5.4, implements a double-acting actuator [110]. This transmission system has been adopted for several reasons:

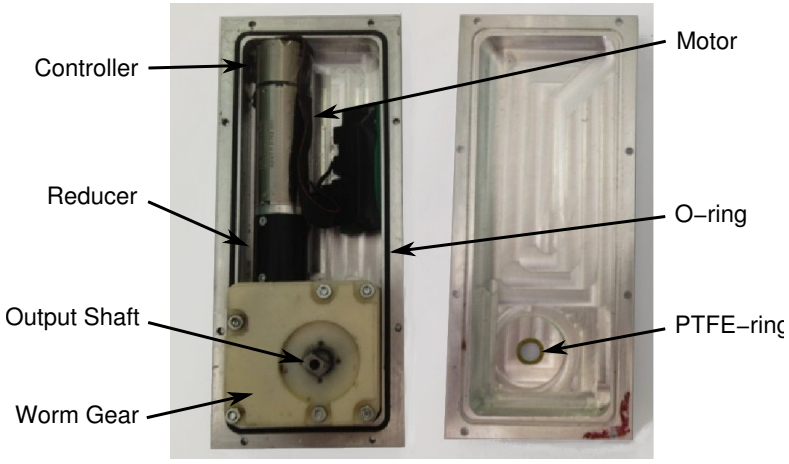

FIGURE 5.5: Detail of the actuator and sealing parts.

- it allows to optimize the allocation of the motors in terms of required space and weight distribution;
- it represents a simple and convenient way to couple several joints to a single motor in a fixed way, so that the effective number of degrees of freedom is equal to the number of motors;
- it simplifies the transmission chain;
- the sheath-based routing introduces a small compliance in the transmission, allowing to prevent damages to actuators and speed reducers due to unexpected overloads.

The cable loop can be adjusted and preloaded by means of a suitable pretension mechanism (similar to the mechanism used in the bicycle brakes). The motor output shaft is connect to the cable driving pulley by means of a prismatic coupling, is such a way that the motor box can be detached from the cable transmission system (and the gripper structure) for repairing or maintenance without disassembling the cable transmission itself. The sealing system adopted for the actuators is very simple: each actuator, including the gear worm reducer, is enclosed in an aluminum box composed by two shells sealed by an o-ring, see Fig. 5.5, whereas the output shaft of the gear worm reducer is sealed by a couple of PTFE-rings for reducing the friction loss. Finally, a 4-wire cable carrying the 24 V power supply and the CAN bus is sealed by means of an epoxy resin for marine applications.

5.2.3 Fingertip Force/Torque Sensor

Specific force/torque sensors have been designed and implemented on each finger, see Fig. 5.6. In particular, the fingertip structure includes the sensitive parts of the sensor

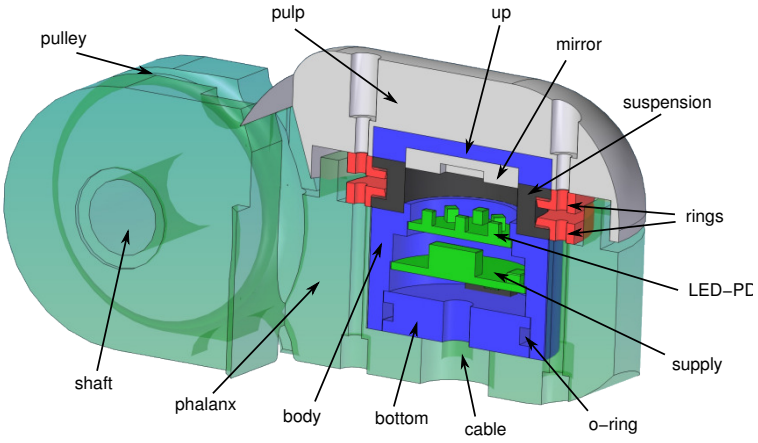

(a) Internal view of the fingertip force/torque sensor.

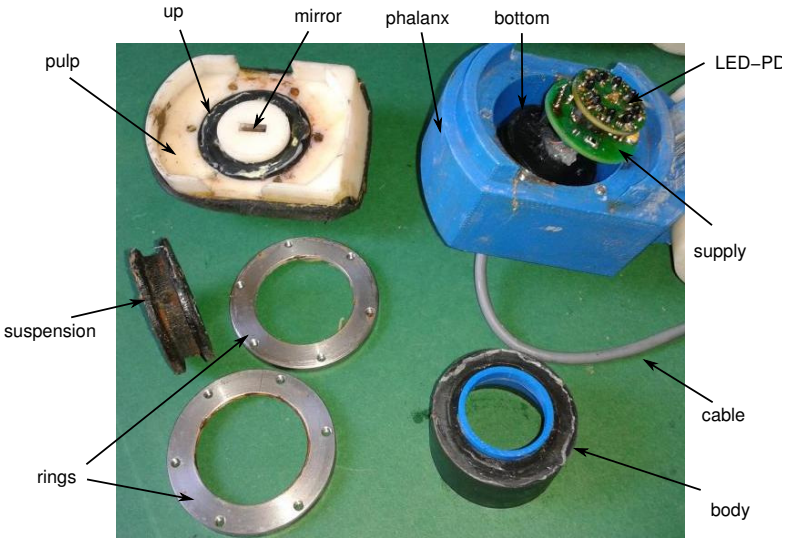

(b) The components of the fingertip force/torque sensor.

FIGURE 5.6: Detailed view of the fingertip force/torque sensor.

and its conditioning electronics, the data acquisition system and the CAN communication interface. The data acquisition and communication system has been implemented by means of a microcontroller that provides also filtering, scaling and conversion of the acquired data. Moreover, a rubber mold acts as a soft skin for the fingertip, increasing also the contact friction and the stability of the grasp [81]. The sensor is entirely enclosed in a plastic housing ensuring the sealing of the electronics. The working principle of the sensor adopted in the gripper is quite simple and has been already successfully adopted for other robotic applications, such as for the force and tactile sensors of the UB Hand IV anthropomorphic robot hand [79, 111]. The sensor is composed by 8 PhotoDetectors (PDs) mounted on a printed circuit board (PCB) and circularly arranged around an infrared light source (LED), and by a rectangular mirror facing the PCB and the optoelectronic components. The PCB is rigidly connected to the distal phalanx structure, whereas the mirror is connected to the fingertip contact surface. A deformable sealing ring, see Fig. 5.6(a), connects these two parts, allowing the relative motion of

the fingertip contact surface with respect to the distal phalanx structure. The measurement principle of the sensor is based on the modulation of the current flowing through a PD generated by the variation of the relative position of the LED, and in particular of the angle of view between the optoelectronic components and the length of the optical path [98]. By means of this simple principle it is possible to detect the small changes of position/orientation of the rectangular mirror in any direction. The pose of the mirror can be then associated to the contact force/torque components applied to the fingertip surface by means of a suitable calibration procedure. In Fig. 5.7(a) and 5.7(b) a comparison of the forces/torques measured by the sensor and by a reference sensor (ATI Gamma SI-130-10) are respectively reported. The details about the model and the working principle of this sensor are not reported here for brevity, the interested reader can refer to [78, 112, 113] for a more detailed description of the sensing principle. It is important to note that the water pressure causes an offset on the force normal to the fingertip surface: this offset can be measured when the AUV reaches the desired working depth (before a contact occurs at the fingertips), registered by the control system and then subtracted from the measurement for a correct force estimation. In Fig. 5.6(b) the components of the fingertip force/torque sensors are shown in details.

5.3 The Arm-Gripper Control System

All the motors and the sensors of both the arm and the gripper share the same power supply and are interconnected via a standard CAN bus. A hierarchical structure has been adopted for the control of the whole system, composed by the AUV, the arm and the gripper. For both the arm and the gripper the low-level velocity/position control is directly implemented in the Faulhaber motor controllers. The Faulhaber motion controllers are commanded using the OpenCAN protocol [114] that allows basic functions such as monitoring of temperature and currents, velocity/position control, customization of the controller parameters and so on. The gripper force/torque sensors exploit the same CAN interface and protocol for data communication.

A middle-level controller is devoted to the coordination of the arm/gripper system with the AUV and is implemented, under the RTAI-Linux realtime operating system running on a PC-104 hosted on the vehicle, by means of a realtime task running at 100 hz. This controller communicates with the arm/gripper motors and sensors through the CAN interface (at 1 Mb/s) and calculates the set-point velocities of each joint in order to stabilize and hold the grasp at the desired shape on the basis of the kinematic model of the gripper and the force/torque fingertip sensors information. The middle-level

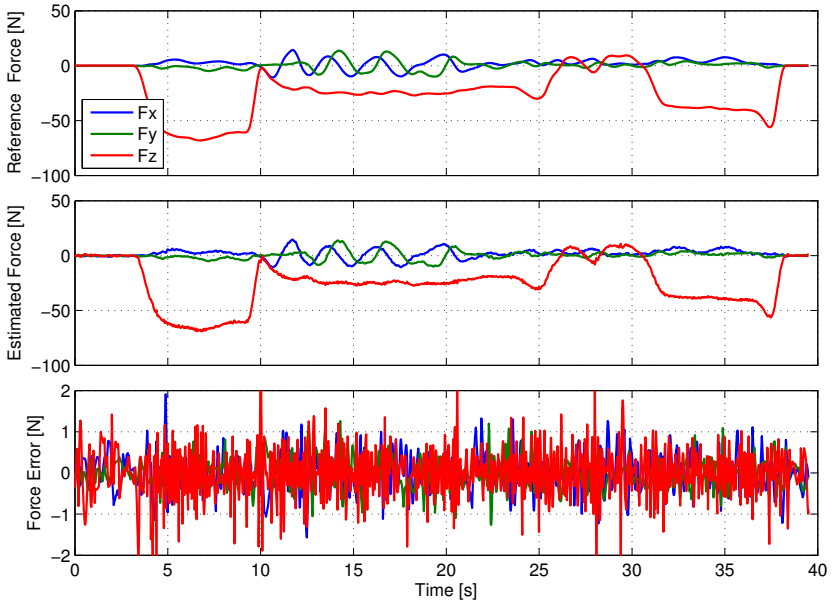

(a) Comparison of the estimated force with the reference sensor.

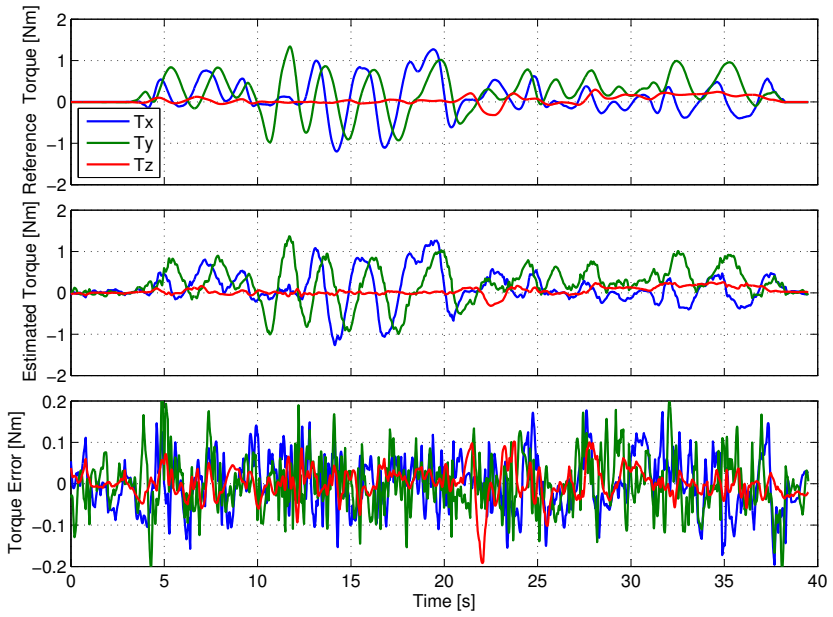

(b) Comparison of the estimated torque with the reference sensor.

FIGURE 5.7: Forces/torques given by means of the fingertip sensor.

controller receives also the commands from the high-level mission controller through an Ethernet connection.

5.4 Experimental results

Preliminary experiments have been carried out in the laboratory to test the capabilities of the gripper. In Fig. 5.8 several grasps executed by the gripper are shown. The gripper is able to perform power grasps, see Fig. 5.8(a), to grasp different objects both in

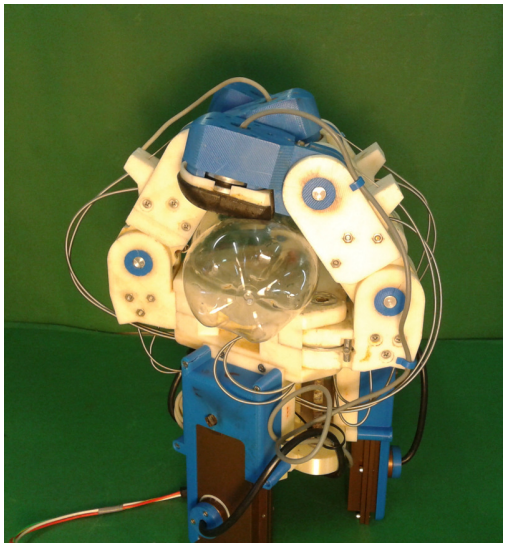

(a) Power grasp.

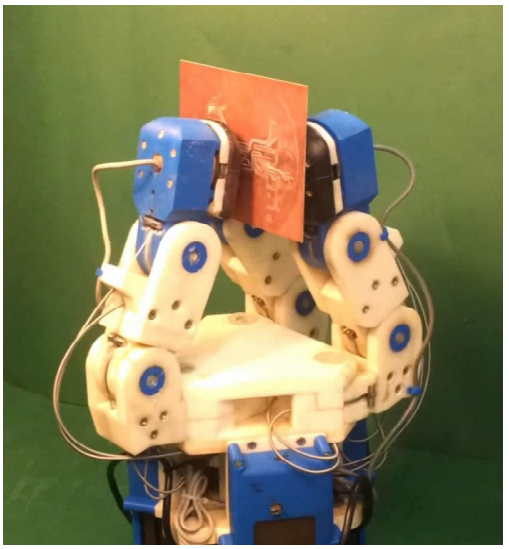

(b) Parallel grasp on a thin object.

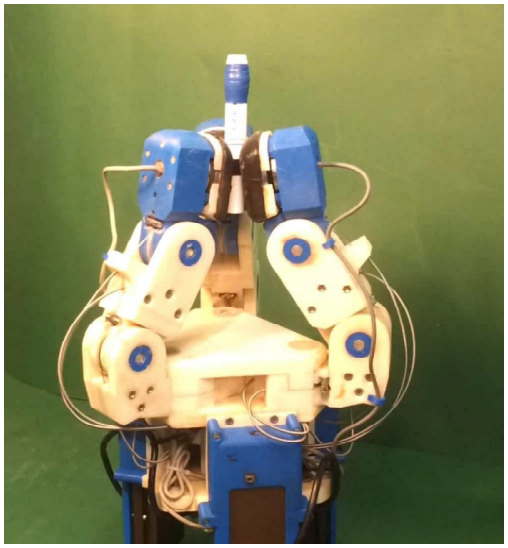

(c) Pen tripod grasp.

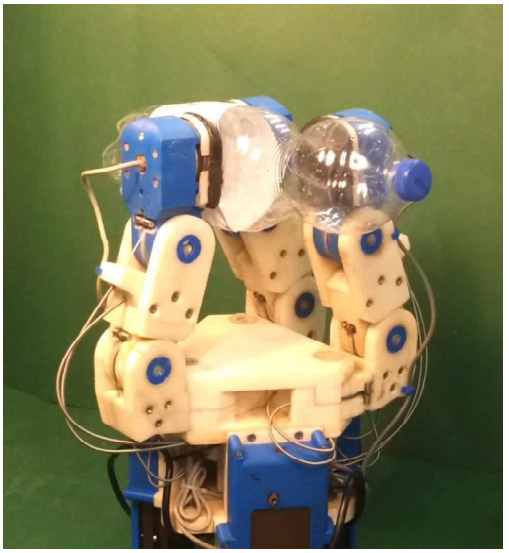

(d) Parallel grasp on a plastic bottle.

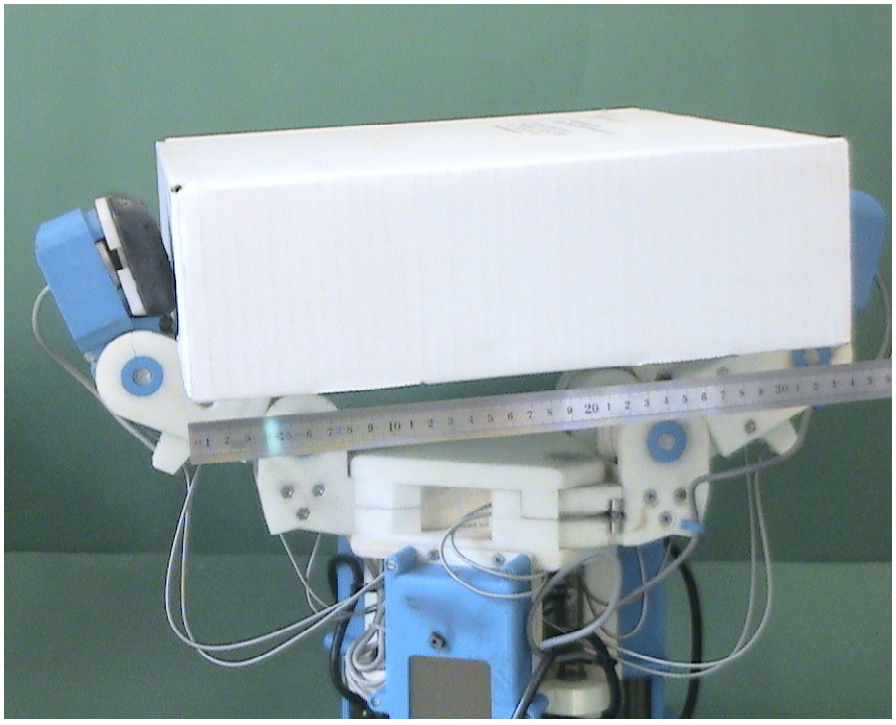

(e) The gripper grasping a 340 mm width box.

tripod configuration, as shown in Fig. 6.9, and in parallel configuration, see Fig. 5.8(b) and Fig. 5.8(d). In particular, Fig. 5.8(e) shows the ability of the gripper of grasping objects up to 340 mm width, whereas Fig. 5.8(b) shows the ability of grasping very thin objects. The whole integrated system composed by the gripper, the arm and the Girona 500 AUV [115, 116] has been then tested first in a pool available at CIRS (Centre d'Investigació en Robòtica Submarina of the University of Girona) as shown in Fig. 5.1. As a demonstration of more complex tasks, an experimental test in real undersea operations have been executed, according to the goals of the TRIDENT project. The AUV integrated with the arm/gripper system has been tested in the harbor at Port de Soller, Spain, operating at a working depth of about 25 m. Autonomous operations of the overall system have been successfully executed, as shown in Fig. 5.9 and in the video attached to this paper. The complete video showing the final experiments of the TRIDENT project is available at *http://www.irs.uji.es/2nd-i-auv/videos/E3-Autonomous-Intervention/TRIDENT-Final-Exp.mp4*. In particular, after getting the seafloor mosaic (generated on the survey phase), the AUV performed autonomous detection of the dummy black box to be recovered, and the grasp was specified by the human operator using a purposely designed user interface. Then, with the aid of the AUV vision system, the black box recovery stage was autonomously initiated by the system, as detailed in Fig. 5.9(d). For that purpose, a robust vision system has been implemented on the AUV by using both a 2D camera and a 3D vision system. Once the black box has been autonomously grasped by the gripper, the AUV brought it to the surface. The success of the experiment was observed thanks to the images provided by the onboard cameras of the AUV, and with the help of divers that recorded the experiment from outside, as shown in Fig. 5.9(b) and 5.9(c).

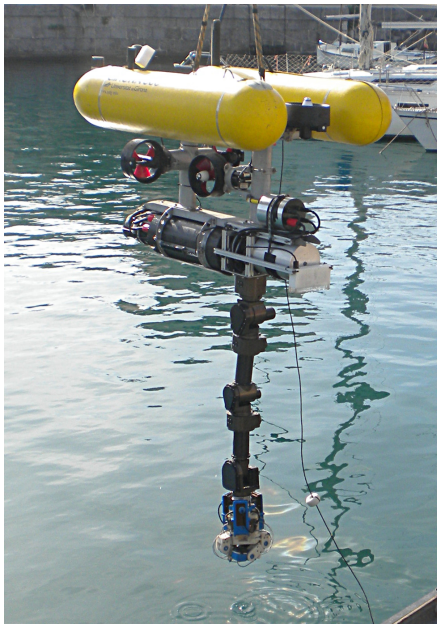

(a) AUV deployment.

(b) AUV approaching the black box.

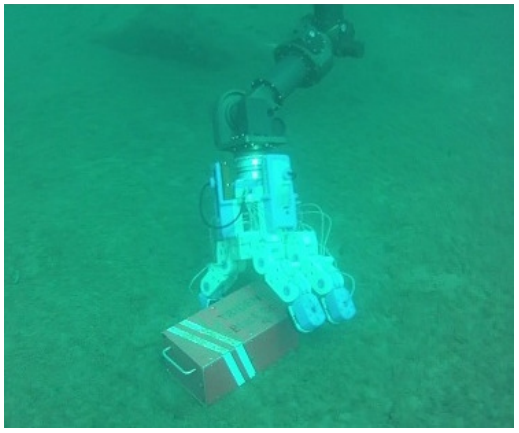

(c) The black box is approached.

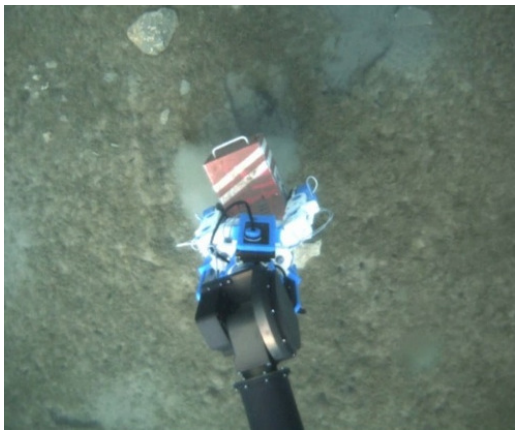

(d) Grasp execution seen from the AUV camera.

FIGURE 5.9: The AUV with integrated arm and gripper during the experimental tests at Port de Soller, Spain.

Chapter 6

Arm Hand Coordination

In this chapter, we deal with the problem of planning a manipulation task for a robotic system composed of at least one dexterous arm and a dexterous multi-fingered hand. The goal of the local planner is to include both, the arm and the hand, in the execution of the task in a coordinated way. This is achieved by using the workspace of the hand which is computed offline. During the online planning, the current in-hand manipulation capability is evaluated taking advantage of the dimensions of the hand workspace and considering the task itself. Dynamic weights enable the computation of the instantaneous contributions of the two subsystems on the motion of the manipulated object. The method is evaluated in simulation as well as in several experiments on the real robot.

6.1 The problem of coordination in literature

Several anthropomorphic robot arms and hands have been developed in the last decades and, due to the high complexity, they have been often conceived as separate devices. As a consequence, researchers have been investigating methods to plan object manipulation separately for arm and hand. Nowadays technology is enabling us to develop integrated robotic systems in which it is possible to synchronously control the degrees of freedom of the arm and the hand with a comparable precision and reliability. That allows to design planners in which the contribution of the two subsystems can be involved in a coordinated way.

The importance of coordinating the arm and the hand for object manipulation was e.g. demonstrated by Khatib in 1990 [57]. He showed that, in a robotic chain resulting from a serial combination of two manipulators, the inertia seen from the load is upper bounded by the inertia of the mini-manipulator, i.e., the dexterous hand. As the inertias of the arm and of the fingers are largely different, the advantage of using the mini-manipulator

FIGURE 6.1: SpaceJustin executing a manipulation task

to accomplish the manipulation task becomes clear as an increased precision and speed as well as power saving [57]. In 2011, Ma and Dollar pointed out that the redundancy introduced by an articulated gripper enhances the dexterity of the whole manipulator especially close to singular configurations or in presence of obstacles [58]. Thus, the use of a mini-manipulator in combination with a macro-manipulator, i.e. a dexterous arm, increases the manipulation capabilities of the robotic system if they are used in a coordinated way. Nevertheless, the joined use of the dexterous manipulator poses several challenges due to, for example, the high number of degrees of freedom and the different workspaces of mini- and macro-manipulator.

Trying to achieve the coordination from the control point of view, Melchiorri and Salisbury published in 1990 a control scheme in which the arm and the hand systems reached together towards a goal position by using an extended Jacobian [117]. The results have been shown by means of simulations and experiments in which a robotic finger was mounted in series of an anthropomorphic arm. In 2001, Casalino et al. published work on a hierarchical control system for an arm-hand system which allowed the overall tracking of the object involving at the same time the mini- and macro-manipulators. To guarantee a stable grasp during the motion, an external force control loop has been added [118]. In 2007, Wimböck et al. showed a control strategy based on object-level impedance control in which both the grasp and the manipulation tasks were defined by means of virtual springs and the whole hand-arm system has been considered as a redundant robot [119]. These works give feasible solutions to the problem of hand-arm coordination, but leave some of the related problems uncovered. For example, Cartesian limits of the in-hand manipulation result from the specific grasp and the shape of the finger workspace and cannot be considered explicitly, as well as a priority strategy for the two subsystems.

From a planning perspective, a coordinated motion is typically achieved by planning (or optimizing) the motion taking all degrees of freedom of the robot into account [120]. As pointed out by Zacharias et al. [121], this high dimensional problem leads to heavy computational efforts to reach a feasible solution which makes planning not suitable for online execution. On the other hand, the planning can take into account e.g. obstacles and anthropomorphic resemblance of the motion in contrast to the control schemes.

This paper presents a planning strategy for coordinated manipulation involving the hand and the arm of a robotic system. The planner runs in realtime and allows to incorporate reactive behaviors, for example for obstacle avoidance. Instead of using the typical Jacobian based approach that gives local information on the manipulability of the system, we define an approach in which the potential object manipulation by the fingers is directly measured at every time step and used as a criterion for the decomposition of the task. We take advantage of a discrete representation to efficiently investigate the workspaces of the fingers.

6.2 Description of the Method

6.2.1 Grasp and Manipulation Planning

To manipulate an object, the task is usually described object-centered [62], that means that the task is completely defined in the object space. Therefore, we describe the task as a set of object poses (position and orientation) that the object has to reach, neglecting dynamics of the object.

A task is then described as a set of n object poses $\mathcal{O} : \{T_O(1), \ldots, T_O(n)\}$ in the world coordinate frame with the initial object pose $T_O(0)$. This object-centered formulation allows to be independent from the typology of the used robotic system. A dexterous hand-arm system has the capability of changing the object pose with respect to the world frame in three ways:

- using the arm: keeping the grasp configuration fixed (i.e. the relative pose between palm and object, as well as the finger joint angles) and only acting on the degrees of freedom of the arm;
- using the fingers of the hand: keeping the arm configuration fixed and varying the object hand relative pose trough coordinated finger motion;
- using a combination of both.

The first two scenarios have dual characteristics: the arm manipulation offers a wide range of motion due to the typically large workspace of the dexterous arm, but involves the motion of big inertia even if the mass of the object to be manipulated is low. The in-hand manipulation is characterized by a reduced workspace but has the advantage of low inertia (light fingers) that allows fast and accurate motions of the object. In the next section, we present a method to automatically vary the contribution of the arm resp. the hand to the movement of the object.

With regard to the manipulation planning, we use the following assumptions:

- the 3D shape of the object and its initial pose $T_O(0)$ in the world frame are considered known;
- the grasp is defined as:
  - a set of N contact points ${}^O\mathbf{p}_{CP_j}$ lying on the object surface, where the contacts between the object and the hand are restricted to the fingertips and are modeled as point contacts with friction;
  - a relative pose between the object and the hand ${}^OT_{H_{\text{grasp}}}$;
- the relative contact points between the fingertips and the object do not change (the rolling effects are neglected).

Under these assumptions, the object-hand system can be considered as parallel mechanism in which the palm is the fixed base, the object is the moving body, and the fingers are the links.

6.2.2 The Structure of the Planner

In order to plan the coordinated contribution of hand and arm to the motion of the object, we use a hierarchical structure as shown in Figure 6.2. The task descriptor outputs a consecutive pair of points from $\mathcal{O}$: T_{O_c} and T_{O_g}, where T_{O_c} is the current object pose and T_{O_g} is the next goal pose. In this way, our planner only depends on the next goal pose of the object and allows for a dynamic change of the task description, i.e. by reactive algorithms. The current and goal pose are interpolated, in this work a simple low pass filter is used but a more sophisticated motion generation can be easily integrated, that returns in every step i the difference $\Delta T_O(i)$ between the desired and the actual object pose. Since the homogeneous transformation representation does not allow for an easy interpolation of the rotational component, the axis-angle convention has been chosen to represent the change of orientation. Therefore, a generic change of

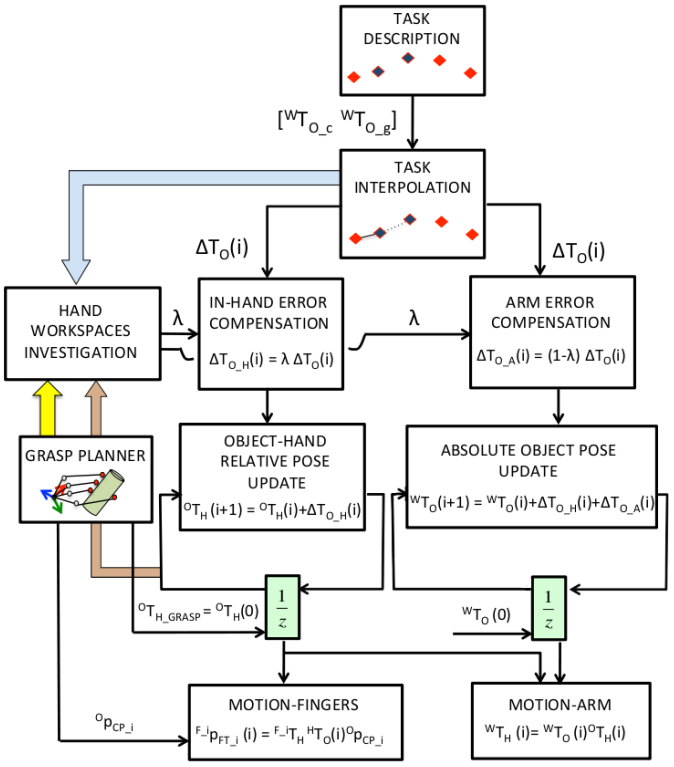

FIGURE 6.2: Structure of the planner for coordinated manipulation

reference system from A to B, usually represented with a homogeneous transformation ${}^{A}T_{B} = [{}^{A}R_{B},\ {}^{A}\mathbf{p}_{B}]$, becomes:

$$[\mathbf{a}, \theta] = \text{axis-angle}({}^{A}R_{B}) \tag{6.1}$$

$${}^{A}\mathbf{v}_{B} = [{}^{A}\mathbf{p}_{B}\ \mathbf{a}\ \theta], \tag{6.2}$$

where $\mathbf{a}$ represents the resulting rotation axis and θ the rotation angle. We assume that it is always possible to switch representation without any loss of information, thus, from here on we will refer either to one or the other notation to denote a frame displacement. $\Delta T_O(i)$ can be then represented by means of a vector containing $\mathbf{v}_O(i) = (d_t(i), \mathbf{a}_r, d_r(i))$, which are respectively the desired instantaneous translational displacement $d_t(i)$, the axis $\mathbf{a}_r$ along which the rotation has to be performed, and the angular displacements $d_r(i)$.

As we have mentioned in Section 6.2.1, $\Delta T_O(i)$ can be split in a desired motion of the hand and of the arm. We define a weight vector $\lambda \in \mathbb{R}^4$, $\lambda(k) \in [0; 1]$ that represents the contribution of the hand to the motion with respect to the arm. λ has four dimensions to allow an independent treatment of every axis of motion (three for every translational axis and one for the overall angle of rotation). Only one weight coefficient has been considered for the rotational component because of the non-commutative property of consecutive rotations. This problem is overcome using the axis-angle convention and

applying the weight coefficient only to the angle value. If $\lambda(k) = 1$, the motion is executed only by the hand and if $\lambda(k) = 0$, only the arm contributes to the motion of the object.

The contributions of the in-hand $T_{O_H}(i)$ and arm $T_{O_A}(i)$ to the overall motion $\Delta T_O(i)$ are calculated as:

$$\Delta T_O(i) = \Delta T_{O_H}(i) + \Delta T_{O_A}(i) \tag{6.3}$$

$$\Delta T_{O_H}(i) = \Delta T_O(i)\,\mathrm{diag}(\lambda(i)) \tag{6.4}$$

$$\Delta T_{O_A}(i) = \Delta T_O(i)\,\mathrm{diag}(1-\lambda(i)). \tag{6.5}$$

The in-hand component $\Delta T_{O_H}(i)$ of the object error compensation is added to the actual state of the relative pose between the hand and the object ${}^{O}T_H(i)$, leading to new positions of the desired contact points within the hand frame in which the motion of the fingers is computed:

$${}^{O}T_H(i+1) = {}^{O}T_H(i) + \Delta T_{O_H}(i). \tag{6.6}$$

The arm component is added to the object pose virtually reached by the in-hand contribution as:

$${}^{W}T_O(i+1) = {}^{W}T_O(i) + \Delta T_{O_H}(i) + \Delta T_{O_A}(i) \tag{6.7}$$

$$= {}^{W}T_O(i) + \Delta T_O(i). \tag{6.8}$$

Then, the reference pose for the arm can be calculated as:

$${}^{W}T_H(i+1) = {}^{W}T_O(i+1)\,{}^{O}T_H(i+1). \tag{6.9}$$

To execute the manipulation motion, both cartesian position or impedance controller can be used for the arm and the hand dependent on the requirements of the task.

6.2.3 Investigation in the Hand Workspace

The common approach to plan in-hand manipulation is based on the combined use of the hand Jacobian and the grasp matrix to iteratively compute joint displacements of the fingers that lead to the desired object motion. A weakness of this method lies in the impossibility to predict how much the object can be moved in a given direction, since neither the Jacobian nor the grasp matrix consider intrinsically the distance in the Cartesian space to the boundary of the reachable space, given by physical joint limits of the fingers. In addition, it is not sufficient to consider an independent adaptation of

the Jacobian of each finger (as we can see in [122] for a single serial chain), because the constraints of the fingers involved in the grasp need to be evaluated together. Indeed, reaching the joint limits of one finger restricts the capability of internal manipulation of the entire hand. In contrast, we propose a method to explore the manipulability of a dexterous end effector, given an actual grasp configuration (i.e. the current contact points ${}^{H}\mathbf{p}_{CP_j}$ for each finger j and the relative pose ${}^{O}T_{H}$) and a desired displacement to be executed within the object space $\Delta T_O(i)$. The approach is based on direct measures in the 3D workspaces of the fingers as linear and angular distances. The workspaces of the fingers Ψ_j are precomputed as they are only dependent on the (fixed) kinematics of the hand. They can be represented as a grid in the 6D space (position and orientation) where each cell has a binary value that indicates if it is reachable or not. For the computation, we use the hybrid approach proposed by [123] that combines forward and inverse kinematics. This method allows to obtain an accurate and structured description of the finger capabilities by setting the resolution r of the grid. The workspace of the robotic hand is then the combination of all finger workspaces: $\Psi = \cup_j \Psi_j$. With the assumption made in Section 6.2.1, we guarantee that a grasp planner (e.g. [124]) returns a grasp in which all the fingers actively involved have a desired contact point for the fingertip confined within their relative workspace, and we want to ensure that during the internal manipulation none of these constraints will be violated.

The computation of a manipulability score δ describing the current manipulation capability within the hand is summarized in Algorithm 1.

For each finger j involved in the manipulation, we calculate the intersections with the relative workspace of the rays emerging from the current contact point in the three directions of the axis of the current object frame, as schematically shown in Figure 6.3. In terms of rotation, we use the above mentioned axis-angle convention to compute the amount of rotation that the contact points can undergo before hitting the workspace boundary. At every iteration, the algorithm inputs:

- the current positions of the contact points in the hand frame;
- the actual relative pose between the object and the hand;
- the desired object displacement.

The parameters are the structures containing the fingers workspaces expressed in the hand frame and their resolution r. The search for the intersection with the workspace surface starts from the actual contact point of each finger. Then, the point is moved along the directions of the three axis of the object frame with steps of the same width as the granularity of the workspace discretization. The loop ends when the new calculated

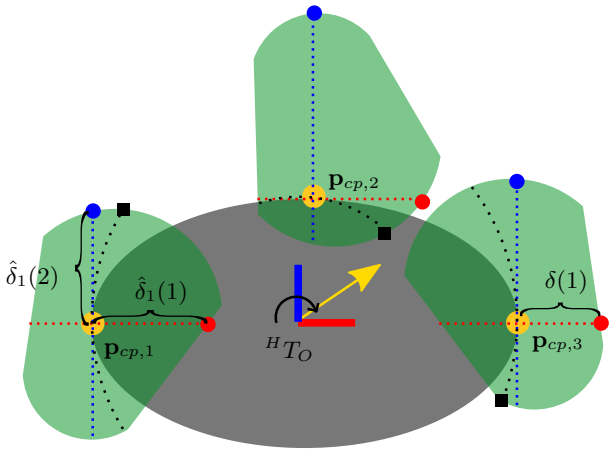

FIGURE 6.3: Schematic representation of the intersection algorithm

point is outside the workspace. Then, the distance $\hat{\delta}_j$ between this point and the initial value is saved. In a similar way, the rotational intersection is found moving the initial contact point along a circular path. The origin of the circle is in the object frame origin (here for simplicity we are considering that the axis of instantaneous rotation always crosses the origin of the object frame) and the axis of rotation is calculated using the axis-angle convention applied to the the rotation matrix of $\Delta T_O(i)$. Again, the loop returns when the point crosses the boundary and the distance is saved as the angle delimited by the arch. The manipulability score δ is then calculated finding the minimum values for each of the four distances for the fingers involved in the manipulation task: $\delta = \min(\hat{\delta})$. The vector δ gives an instantaneous picture of the manipulability capability of the actual grasp relative to the desired manipulation task.

6.2.4 Coordination Policy

This section shows the integration of the manipulability score δ in the control strategy and its conversion to λ which coordinates the hand/arm movements. A simple and effective solution consists in using the ratio between δ and $\Delta T_O(i) = \mathbf{v}_O = (d_t, d_r)$, that is the the fraction of the actual desired displacement of the object that can be compensated by internal manipulation:

$$\lambda(k) = \alpha \frac{\delta(k)}{\mathbf{v}_O(k)}, \tag{6.10}$$
$$\textbf{if } \lambda(k) \geq 1 \textbf{ then } \lambda(k) = 1.$$

If the resulting $\lambda(k)$ value is greater than 1, it is truncated to 1. This is the case when the internal capability exceeds the desired displacement. The coefficient α allows to influence the priority to the motion of the hand with respect to the arm. Two cases are

Algorithm 1 Compute the manipulability score δ

Require:

- current contact points ${}^{H}\mathbf{p}_{CP_j}$, $j \in [1, N]$;
- current hand object relative pose ${}^{H}T_O(i) = [{}^{H}R_O \; {}^{H}\mathbf{p}_O]$ and distance $\Delta T_O(i) = [d_t(i), d_r(i)]$;
- workspaces of the fingers $\Psi_1, \ldots, \Psi_n$ represented in the hand frame;
- resolution of the grid of the workspaces r.

Ensure: manipulability score δ

for all fingers $j \in [1, N]$ **do**
  $\mathbf{p} \leftarrow^{H} \mathbf{p}_{CP_j}$
  for all $k \in [1, 3]$ **do**
    while $\mathbf{p} \in \Psi$ **do**
      $\mathbf{p} = \mathbf{p} + \text{sign}(d_t(i)) \cdot \text{column}({}^{H}R_O, k) \cdot r$
    end while
    $\hat{\delta}_j(k) \leftarrow \mathbf{p} -^{H} \mathbf{p}_{CP_j}$
  end for
  $\mathbf{p} \leftarrow^{H} \mathbf{p}_{CP_j}$
  $\mathbf{a} \leftarrow$ rotation axis of ΔT_O (in the hand frame)
  $c = 0$;
  while $\mathbf{p} \in \Psi$ **do**
    $\mathbf{p} \leftarrow$ rotate $\mathbf{p}$ by r along the rotation axis $\mathbf{a}$
    $c = c + 1$
  end while
  $\hat{\delta}_j(4) \leftarrow c$
end for
for all k=1:4 **do** $\delta(k) = \min(\hat{\delta}_1(k), \ldots, \hat{\delta}_n(k))$
end for

particularly interesting. When α is set to 1, the planner gives priority to the hand and the arm is involved in the manipulation only when the internal manipulation capability is over. When alpha is set to 0.5, the planner equally distributes the task between the two subsystems until the in-hand manipulation capability is exceeded.

As a matter of fact, the in-hand capability for translation is very limited considered the overall workspace of the hand-arm system. Therefore, we want to avoid involving the in-hand manipulation when the next desired manipulation reference is clearly not reachable by translational internal manipulation. A simple trick to avoid this behavior is to compute a check every time a new pair of points are extracted from $\mathcal{O}$ and given to the interpolator (see Figure 6.2). The test consists in comparing the norm of the overall desired translational object displacement with a fixed threshold. In this work, we did not investigate in choosing the optimal value of this threshold. Instead, we consider a rule of thumb choosing it in relation with the size of the bounding box containing the 3D representation of the fingers workspace (in this study the threshold has been chosen equal to 0.12 m). When the required displacement is above the threshold, the translational distances in Algorithm 1 are not calculated and the first three elements of

λ are set to zero until the actual reference is not reached.

6.3 Simulations and Experimental results

6.3.1 Setup

Experiments are conducted using SpaceJustin which is a modified version of DLR's humanoid robot Justin [125], shown in Figure 6.1. SpaceJustin has 17 actuated degrees of freedom (DoF) for torso, head, and arms and interacts with the environment with two DLR-HIT Hands II [126]. The hands are five-fingered hands with modular fingers, each having three DoF. We modified the position of the thumb such that it opposes the middlefinger and widened the opening angle. This enables a larger workspace and thus more in-hand manipulation capability compared to the commercially available version.

The workspaces of the fingers have been represented as voxelized space with a resolution r of 0.001 m, a minimum bounding box of 0.122 m $\times$ 0.05 m $\times$ 0.094 m, and a total number of 573400 voxels. For each voxel inside the bounding box, an integer is stored: it is 1 if the voxel is reachable by the fingertip and 0 if it is unreachable. Trivial functions allow to check whether a Cartesian point is inside the bounding box or to transform it to the index of the relative voxel.

6.3.2 Computation Times

The planner has been implemented on a 64-bit Linux machine with processor Intel®Core™ i7-4790 CPU 3.60 GHz x 8. The measures of the execution time have been restricted to the hand investigation algorithm as it is the most time consuming section during the execution of the planner (described in Section 6.2.3).
The execution time depends on the actual distance of the contact point to the boundary of the workspace. The intersection, indeed, is computed iteratively checking which is the point along a ray that crosses the workspace. Therefore, during an in-hand motion, the execution time decreases as the the contact point approaches the boundary. Another important factor is the resolution r chosen to discretize and to investigate the workspace itself. With the same condition, the number of iterations needed to check the intersection is inversely proportional to r. It seems reasonable to chose r in relation with the dimension of the workspace of the considered robot and as a trade off between the execution time and accuracy requirements.

A grasp involving all the 5 fingers has been considered, and a set of meaningful movements (translational and rotational) have been tested. The result of the measures reveals

an execution time that is always bounded between 0.6 ms (when the manipulability is maximum) and 0.15 ms (when the hand is very close to the boundary of in-hand manipulation), which makes it suitable for the implementation in real-time. The simulated and practical experiments shown in the following sections are compliant with the computation times delivered.

6.3.3 Simulation Results

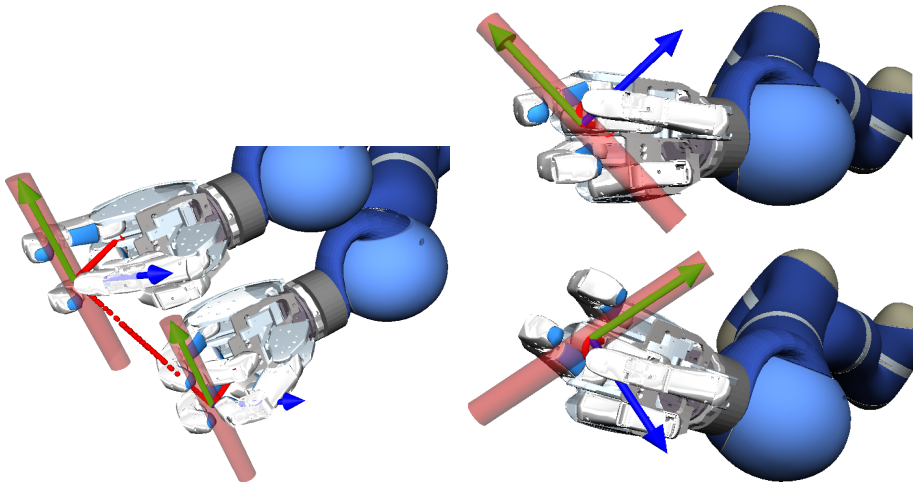

(a) Pure translational manipulation (b) Pure rotation manipulation

FIGURE 6.4: Coordinated manipulation

In this section, we show how the system evolves during a manipulation task by means of simulation examples. The first task is a pure translation of a cylindrical object grasped with three fingers. According to the notation introduced in Section 6.2.1, the task will be represented as a pair of object poses (given in [m] and []):

- the initial pose $T_O(0) = [[-1, 0.4, 0.3], [1, 0, 0, -90]]$;
- the final pose $T_O(1) = [[-1, 0.35, 0.4], [1, 0, 0, -90]]$, ${}^c\mathbf{v}_g = [0, -0.05, 0.1, 0]$;

In Figure 6.4(a), two screenshots of the simulation view are reported. One at the beginning and one at the end of the task. In Figure 6.5, the variables affected by the motion are shown. Especially the last three subplots are interesting, where $\delta_{y,z}$, and $\Delta T_O y, z$ and the resulting $\lambda_{y,z}$ are shown. When the new point is passed to the interpolator ($t = 0.1\,\text{s}$), there is a jump in δ reflecting the change of the direction of the object pose error. In this simulation, α has been set to 1 (Eq. (6.10)), therefore the contribution of the hand subsystem is prioritized with respect to the arm. Indeed, we can see how the in-hand manipulability is progressively consumed and the arm contribution in a specified

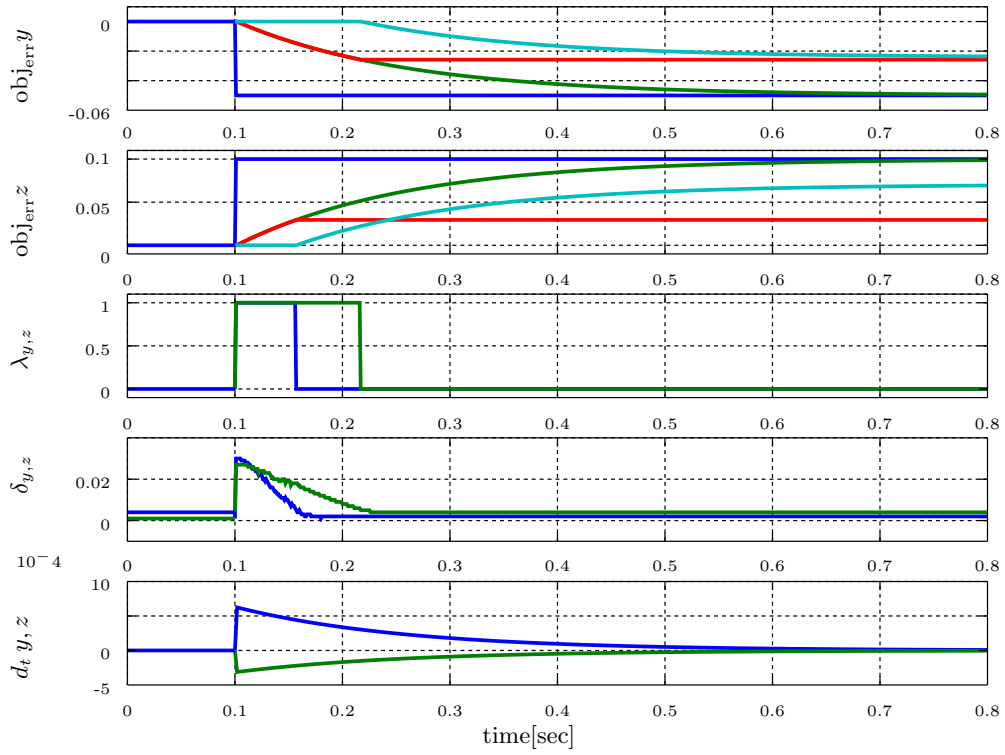

FIGURE 6.5: Evolution of the planner state during a pure translational manipulation

direction is not involved until the respective value of δ approaches zero. It is also worth to note how the different directions of the object error are independently treated and the activation and deactivation of the two subsystems can happen in different points in time. In this case, along the y-axis of the object 0.03 m of the 0.05 m required (60 %) are accomplished by the hand, while in the z-direction 0.03 m of the 0.1 m required (33 %).

The second task shows the evolution of the system against a pure rotation of a cylindrical object grasped with three fingers (Figure 6.4(b) and 6.6). Although similar considerations to the previous example can be done, it is important to underline how in-hand manipulation can be relevant especially with regard to rotations. In this case, indeed, the object is required to perform a rotation of 100 round its x-axis:

- the initial pose $T_O(0) = [[-1, 0.4, 0.4], [1, 0, 0, -145]]$;
- the final pose $T_O(1) = [[-1, 0.35, 0.3], [1, 0, 0, -45]]$, ${}^c\mathbf{v}_g = [0, 0, 0, 100]$;

From the plots we can see that 90 % of the motion are accomplished by the hand subsystem, which substantially enriches the reachable space of the object exclusively using the arm.

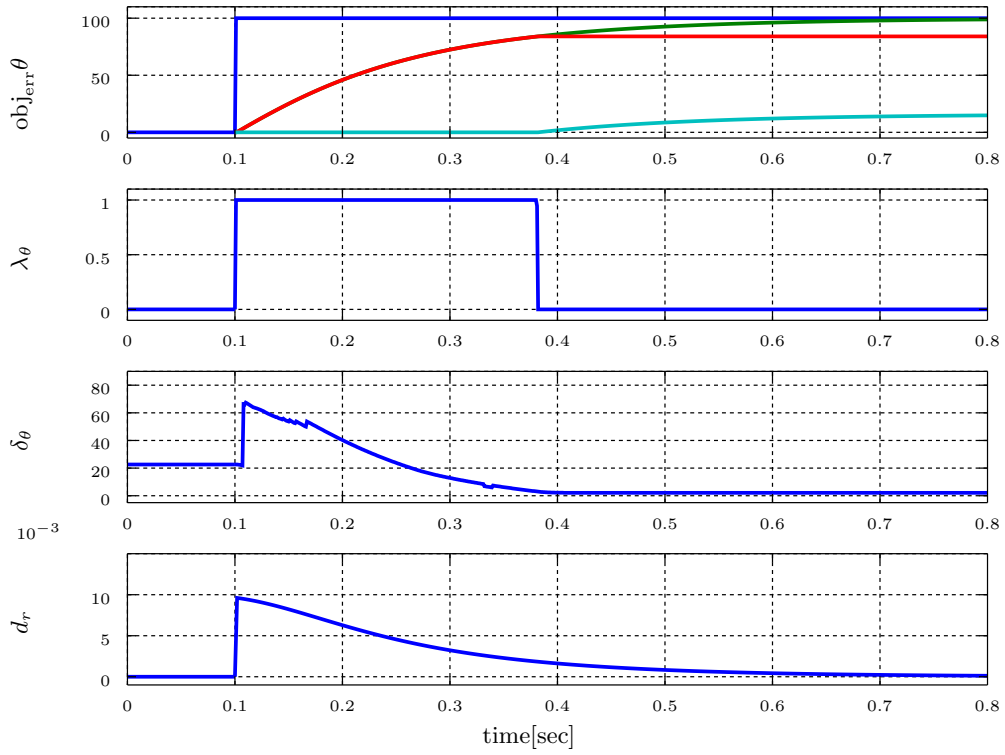

FIGURE 6.6: Evolution of the planner state during a pure rotation manipulation

6.3.4 Experimental Results

We performed several experiments on the real system to prove the performance of the planner. They can all be seen in the video attachment of the paper [127]. The computational time required by the algorithm allows an implementation in real time. It keeps the update rate of SpaceJustin's interface at 1 ms.

We exploited the embedded inertial sensor of a smart phone to measure the horizon angle and therefore evaluating the accuracy and reliability of the manipulation execution as shown in Figure 6.7. The task was defined as an incremental rotation of the object by 10 The grasp resulted to be stable during the in-hand manipulation and we did not experience loss of performance when the coordination scheme was active and when only the arm was involved in the execution of the task. Same positive results are shown in

Figure 6.8, where SpaceJustin places a cylindrical object on a surface first only using the arm and then using both subsystems. Finally, we show in Figure 6.9 a close view of the hand during an internal manipulation task.

6.4 Conclusion and Future Works

We described a method to evaluate in-hand manipulability based on a direct investigation of the 3D workspace of the dexterous hand. We use this score as a weight function to plan the execution of a manipulation task defined in the object space with a coordinate contribution of the arm and hand system. The computational time required by the algorithm is very low and allows an implementation in real time. Future works will include the use of this approach in a telemanipulation application in which the user will be able to feedback the actual distance from hand manipulation boundary and freely explore the in-hand manipulation subspace by means of some kind of joystick (e.g. a space mouse or the HUG system developed by the DLR [128]). We also want to investigate deeper the null space motion of the object available using the coordination of the arm and the hand. In addition, we foresee to extend these result in the field of grasp planning, adapting the initial grasp configuration when the pose of the object to grasp requires the arm manipulator to work close to singularities, joint limits or obstacles.

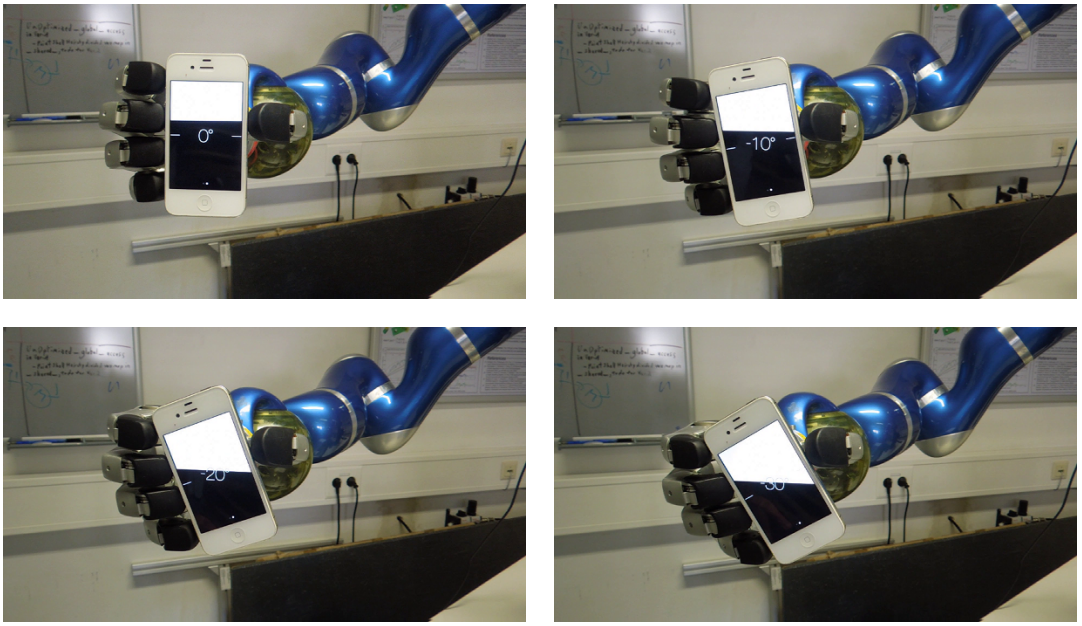

FIGURE 6.7: SpaceJustin manipulating a smartphone

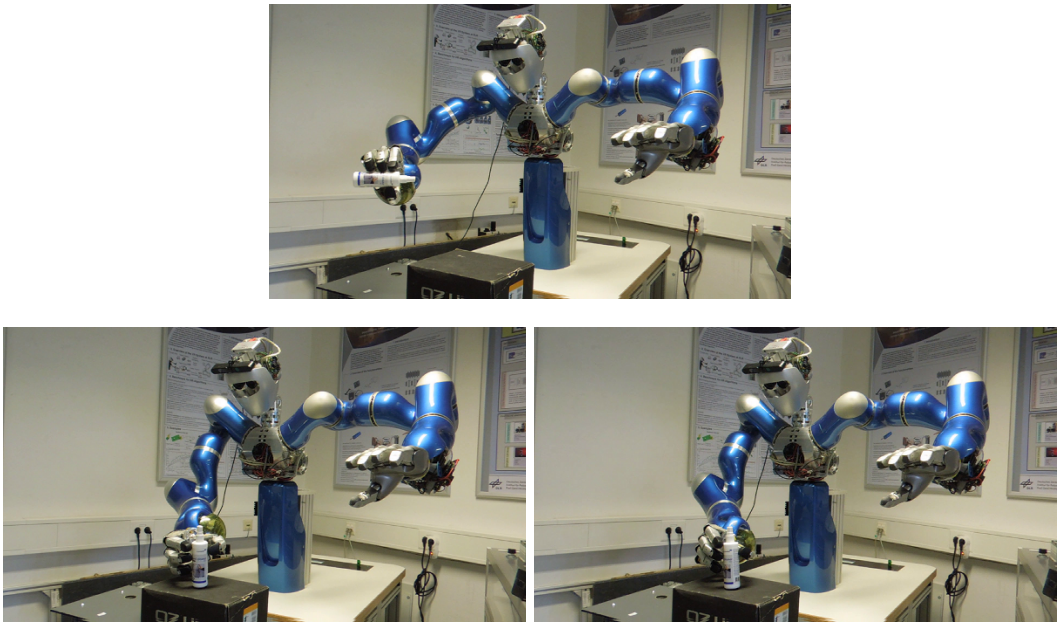

FIGURE 6.8: SpaceJustin placing a spray bottle on a surface with and without the coordination of the two subsystems

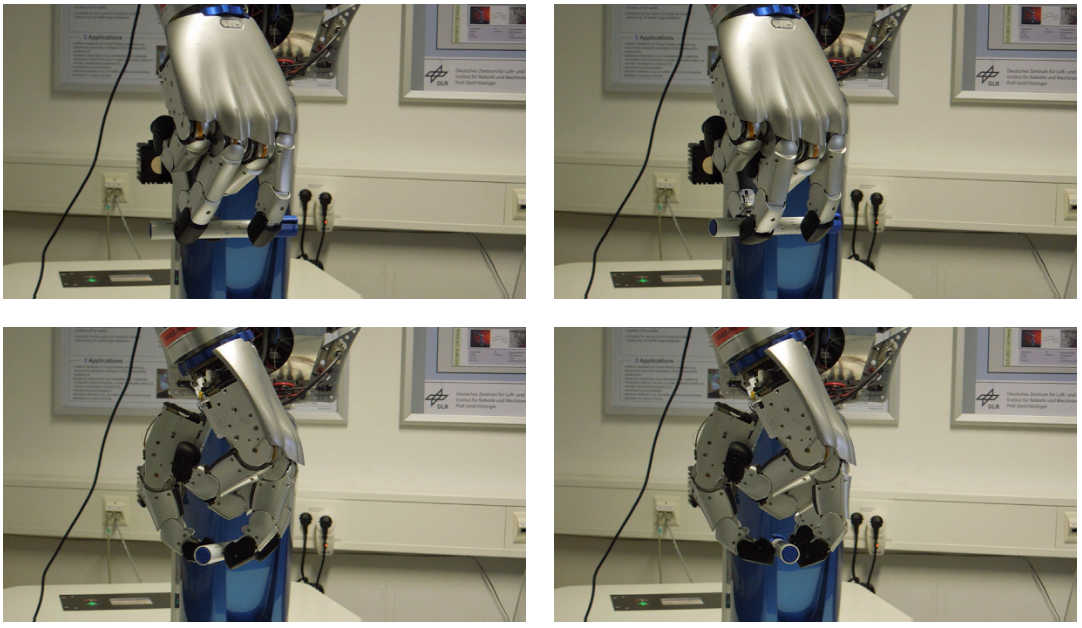

FIGURE 6.9: SpaceJustin manipulating a pen

Chapter 7

Conclusions

7.1 Conclusion

The field of science that attempts to reproduce human prehensile and manipulation ability is very fascinating and attractive. Thousands of researchers all over the world are exploring different directions in order to discover what is at the basis of human dexterity and how it can be efficiently reproduced with a machine. The topic cover many technological and methodological issues and, nowadays, more then ever seems to be a promising future market.

The work done for this thesis can be divided in three stages: observation, design and prototyping, and benchmark.

During the observation, in order to get familiar with the problem, the review of the state of the art has been accompanied by the use of empirical and mathematical instruments. For example during the design process of the UB-Hand IV, in which one of the main requirements was to have the highest level of anthropomorphism, it has been very helpful to directly observe and get measures on my hand. Through a computer-aided-design program it has been possible to traduce the observed features with constraints of the robotic hand design and predict and check its kinematic behavior. The design framework also allowed to keep the kinematic of the hand as a variable of the project. Hence, we did not design a robotic hand, but a family of devices that can be generated

varying the kinematic variables of the mechanical structure (location of the joints, length of the phalanxes). In this way we are able to manufacture hands for different type of application and specification.
Regarding the design and prototyping stage, the main goal of simplification can be considered achieved. We exploited completely original solutions that ease the mechanical structure, the manufacturing process and the assembly. We believe that the conception of smart sensors and actuators, cheap and enough reliable to accomplish their purpose, is the key factor of the reduction of complexity of such robotic challenge.
Some of the solutions adopted, for example the manufacturing of the joints of the UB Hand as sliding parts without bearing and the the lack of pulleys and sheaths to route the tendons, gain simplicity at the expense of the generation of friction. To ensure great performance of the hand this side effect has to be considered in the control. The friction has been modeled and compensated by force control.
In the prototyping of the underwater gripper, the same design approach has been employed. The rapid prototyping has been used in combination with traditional manufacturing processes. Smart solutions have been found to deal with the sealing of the actuators and the sensors. In this project, at the beginning, we payed the inexperience in the field of Submarine Robotics, as many are challenges arising in the design of mechanisms that have to work immersed in salted water. The risks for the device caused by the contact with sea water are mainly two:

- the oxidation: the choice of material is very important in terms of resistance to oxidation and corrosion. To this end, inox steel represents a good option, even if its specific weight is very high compared to other metal such as the aluminum or titanium. Plastic materials with low liquid absorption like the PVC seem to be also suitable, offering less mechanical resistance and gaining in lightness. If aluminum alloys need to be used, the parts can be post-processed with anti-oxidation superficial treatments. In the design these options were carefully evaluated and chosen on the basis of the particular requirement of the single parts. For example for the axis shafts of the joints inox steel has been used in order to be able to resist without bending to the forces arising during the grip. The sealed boxes containing the motors instead have been manufactured milling an aluminum block afterwards

treated superficially with anodization. The bearings have been realized with teflon bushings, instead of using classic ball bearings.

- shortcut: the sea water, differently from mineral water is conductive. It means that as soon as two points of a circuit are immersed in sea water they generate a short circuit. The consequence of such event in an autonomous or tele-manipulated underwater robot can also be disastrous. Then it is required to conceive solutions which are extremely robust to this risk. Our approach is to use classic o-rings and to chose conservative ways of integration at the expense of a laborious assembly. The motor boxes are sealed with an o-ring mounted between two parallel flat surfaces, tightened by a matrix of screws. Closing and opening the box is quite time consuming, but the solution guarantee a safe and reliable sealing. The output shaft of the motor, that needs to rotate with respect to the box, is sealed by means of combined gasket, consisting of an o-ring with and teflon containing ring. The cables and the connectors, instead are realized by molding with synthetic resin.

In both cases, the resulting devices have been tested with benchmark applications.
The UB Hand IV has been used under different scenarios:

- the test of synergy based control strategies. The synergies have been extracted through a database of grasp configurations performed by human users, recorded by means of a Kinect vision system. The configurations found are analyzed by principal component analysis and a base of the synergy space with reduced dimension is extracted. The reduced dimension, allow to lighten the complexity of the control during the grasp and the manipulation. In this case the UB Hand controlled with a simple position control revealed the advantages coming by its intrinsic compliance, compensating safely the error introduced by the consideration of different hand kinematics and of reproduction of the grasp projected in the synergy space.
- the use of the hand in a robotic system conceived for the execution of industrial like operations, in which the repeatability and the speed of execution play a crucial role. An industrial manipulator has been equipped with a simplified version of the UB Hand IV, with a reduced sensing apparatus. In the forearm has been

mounted a single eye camera to retrieve information about objects. Simple tracking algorithms have been used to retrieve visual informations. Benchmark tasks have been implemented, like pouring from a bottle into glasses located on a table, revealing a great repeatability in the execution of the operation.

- the use of the hand to test internal manipulation control strategies: the target tasks are characterized by light objects that need to be manipulated only by means of the fingers. We are interested to prove that for objects, which inertia is negligible, even a simple Cartesian position control of the fingers can be suitable to accomplish the task. Basically the contact points need to follow rigidly the desired motion of the object. The result are quite promising, revealing good tracking of the fingers to Cartesian trajectories.

Also the underwater gripper has been tested in real applications to prove its usability. In particular it has been mounted on an AUV (Autonomous Underwater Vehicle) provided with a 7DoF arm. The AUV has been commanded to scan the sea bottom within a certain area and look for a known object, in this case a black box of a ship or of an airplane. Once the object is found the AUV and the arm move the gripper toward the target in such way the grasp becomes feasible. When the vehicle is stable the fingers closure is commanded and the fingertip sensors give a feedback of the force applied to the object. When the grasp is stable, the AUV and the arm move the retrieved object to the human. During these tests the gripper responded positively to the sealing even against unexpected collisions with the sea bottom. The control resulted in firm grasps with low power consumption. This is possible thanks to an high transmission ratio, that makes the fingers almost not back drivable.

During the period of research a great effort has been spent also to get confident with the problem related to the coordination of a robotic system composed of an arm and a dexterous gripper, while manipulating an object. First of all we tried to understand why such ability differentiates so deeply a manipulation system with a gripper with few DoFs with one in which the hand is able of internal manipulation. The literature provides

extensive analysis on this problem that have been summarized in the Introduction and in Chapter 6. However, studying the problem we have found that there are some lacks in the theoretical and experimental investigation. In particular, the common approach based on an extended Jacobian, given by the Jacobian of the arm, of the fingers and the Grasp Matrix, does not consider that the available internal manipulation in a given direction is very limited and therefore need to be evaluated in the planning of the manipulation in order to exploit it at most and never violate its boundary. As a matter of fact, the workspace reachable by in-hand manipulation, fixed the kinematic of the hand, varies in relation at the shape of grasp. We consider that the relative position of the contact points with respect to the object does not change during the motion of the object, and then the grasp can be seen as a rigid body connected to the object. A feasible grasp consists in a set of contact points on the object reachable by the fingertips (i.e. that are inside the workspace of the fingers). When the object is moved by internal manipulation every contact points (i.e. fingertips), remain always inside the workspace of the relative finger. When one of the fingertip hits the boundary the entire ability of the hand to move the object in that direction is suppressed.

The idea behind our approach is to find an index that is able to give an instantaneous picture of the residual in-hand mobility in the direction of the current object desired velocity. Therefore, more than checking the distances of each finger joints from their joint limits, we want to measure the distance in the Cartesian space between the current contact point and the intersection of the ray emerging from the contact point in the direction of the object velocity with the Cartesian finger workspace. Since we would like to implement an online planner, the computation of the manipulability index should be as fast as possible. To this end, it appeared convenient to take advantage of a discrete representation of the workspace of the finger, computed offline and use very simple geometric functions to compute the index.

The algorithm has been implemented on a complex system, the robot SpaceJustin developed by the DLR. The introduction of the planner has kept the update time of the system within 1 ms. The results shown in Chapter 6 are very promising. The community also seems to be interested in this approach as confirmed by the comments of the reviewers that have accepted the paper for ICRA 2015.

7.2 Future Works and Vision

I feel quite confident to say that the results collected during the last four years of activity of the Laboratory of Automation and Robotics were brilliant. First of all we built a great team. Today the group is numerous and it is composed of people that make their work with passion. There is a hierarchy, but the atmosphere is first of all friendly. The participation to important international projects pushed us to collaborate, finding our role in a spontaneous way. This is the environment where best ideas come to life.
Personally, I am satisfied of my work as I always got positive feedback in different occasions. We had the chance to participate to a public Robotic exhibition in London hosted by the Science Museum, and thousands of visitors were excited and surprisingly thankful of our work. We participated to a national hardware challenge promoted by Altera, a programmable logic devices producer, and we won the first prize with our project. I have been invited to give a public speech in Munich to talk about Robotics and future trends. Many were the publications accepted to international conference and journals with positive comments. In my perspective these are extremely positive signs that should address us to keep working together and widen our ambitions.
For the future, I think the first goal would be to open a communication channel with industries and end-users and try to focus more the research on real problems. Considering realistic constraints will be the key to improve the devices and possibly give solutions ready to be applied. One possible environment would be the prosthetics in which our knowledge as roboticists and hardware developers at the same time could give relevant insights in the improvement of the state of the art. Also the industrial scenario has to be evaluated. A great move would be to interview as many companies hypothetically interested in our research, for example the ones involved with food. The exchange of ideas with the industry might give important cues to understand how to address our research.
Another objective is to get updated on the the directions of research that the European community is pushing and find out how we can give our contribution.
With regard to the design of the UB Hand, new improvements are behind the corner. The results obtained with the DEXMART project were surprising in term of prototype, but still a lot of work has to be done to make the device more integrated and robust.

Based on the experience gained, we want to redesign the hand optimizing the twisted string motor module and its relative sensing apparatus. Also investigating other field of application of such actuators and sensors would be definitely interesting.
To this end we believe that is worth to push the integration of research groups specialized in different disciplines like Artificial Vision, Embedded System or Biomechanics.

Bibliography

[1] A. Bicchi. Hands for dexterous manipulation and robust grasping: a difficult road toward simplicity. *Robotics and Automation, IEEE Transactions on*, 16(6): 652–662, Dec 2000.

[2] L. Biagiotti, F. Lotti, C. Melchiorri, and G. Vassura. How far is the human hand? A review on anthropomorphic robotic end-effectors. 2004.

[3] M. C. Carrozza, C. Suppo, F. Sebastiani, B. Massa, F. Vecchi, R. Lazzarini, M. R. Cutkosky, and P. Dario. The spring hand: Development of a self-adaptive prosthesis for restoring natural grasping. *Auton. Robots*, 16:125–141, March 2004.

[4] M. C. Carrozza, G. Cappiello, S. Micera, B. Edin, L. Beccai, and C. Cipriani. Design of a cybernetic hand for perception and action. *Biological Cybernetics*, 95: 629–644, 2006.

[5] H. Huang, L. Jiang, Y. Liu, L. Hou, H. Cai, and H. Liu. The mechanical design and experiments of HIT/DLR prosthetic hand. In *Proc. Int. Conf. on Robotics and Biomimetics*, pages 896 –901, Kunming, China, dec. 2006.

[6] M. S. Johannes, J. D. Bigelow, J. M. Burck, S. D. Harshbarger, M. V. Kozlowski, and T. van Doren. An overview of the developmental process for the modular prosthetic limb. *Johns Hopkins APL Technical Digest*, 30(3):207–216, 2011.

[7] S.A. Dalley, T.E. Wiste, T.J. Withrow, and M. Goldfarb. Design of a Multifunctional Anthropomorphic Prosthetic Hand With Extrinsic Actuation. *IEEE/ASME Trans. on Mechatronics*, 14(6):699–706, December 2009.

[8] K. Hertkorn, M.A. Roa, M. Brucker, P. Kremer, and C. Borst. Virtual reality support for teleoperation using online grasp planning. In *Intelligent Robots and Systems (IROS), 2013 IEEE/RSJ International Conference on*, pages 2074–2074, Nov 2013.

[9] B. Pitzer, M. Styer, Christian Bersch, C. DuHadway, and J. Becker. Towards perceptual shared autonomy for robotic mobile manipulation. In *Robotics and Automation (ICRA), 2011 IEEE International Conference on*, pages 6245–6251, May 2011.

[10] Johannes Englsberger, Alexander Werner, Christian Ott, Bernd Henze, Maximo A. Roa, Gianluca Garofalo, Robert Burger, Alexander Beyer, Oliver Eiberger, Korbinian Schmid, and Alin Albu-Schaffer. Overview of the torque-controlled humanoid robot toro. In *Humanoid Robots (Humanoids), 2014 14th IEEE-RAS International Conference on*, pages 916–923, Nov 2014.

[11] Matthew T. Mason and J. Kenneth Salisbury, Jr. *Robot Hands and the Mechanics of Manipulation*. MIT Press, Cambridge, MA, USA, 1985.

[12] F. Ficuciello, G. Palli, C. Melchiorri, and B. Siciliano. A model-based strategy for mapping human grasps to robotic hands using synergies. In *Advanced Intelligent Mechatronics (AIM), 2013 IEEE/ASME International Conference on*, pages 1737–1742, July 2013.

[13] L. Birglen and C. Gosselin. On the force capability of underactuated fingers. In *Proc. IEEE Int. Conf. on Robotics and Automation*, pages 1139–1145, 2003.

[14] Oussama Khatib, Vijay Kumar, and George Pappas, editors. *Underactuated Robotic Hands*, volume 40 of *Springer Tracts in Advanced Robotics*. Springer Berlin / Heidelberg, 2008.

[15] L.U. Odhner and A.M. Dollar. Dexterous manipulation with underactuated elastic hands. In *Proc IEEE Int. Conf. on Robotics and Automation*, pages 5254–5260, 2011.

[16] J. E. Huber, N. A. Fleck, and M. F. Ashby. The selection of mechanical actuators based on performance indices. *Proceedings of the Royal Society of London A: Mathematical, Physical and Engineering Sciences*, 453(1965):2185–2205, 1997.

[17] G. Udupa, P. Sreedharan, and K. Aditya. Robotic gripper driven by flexible microactuator based on an innovative technique. In *Advanced Robotics and its Social Impacts (ARSO), 2010 IEEE Workshop on*, pages 111–116, Oct 2010.

[18] K. Andrianesis and A. Tzes. Design of an anthropomorphic prosthetic hand driven by shape memory alloy actuators. In *Biomedical Robotics and Biomechatronics, 2008. BioRob 2008. 2nd IEEE RAS EMBS International Conference on*, pages 517–522, Oct 2008.

[19] R. Kurtz and V. Hayward. Dexterity measure for tendon actuated parallel mechanisms. In *Advanced Robotics, 1991. 'Robots in Unstructured Environments', 91 ICAR., Fifth International Conference on*, pages 1141–1146 vol.2, June 1991.

[20] K.S. Salisbury and B. Roth. Kinematics and force analysis of articulated mechanical hands. In *Journal of Mechanims, Transmissions and Actuation in Design*, pages 35–41, 1983.

[21] C. Melchiorri and G. Vassura. Mechanical and control issues for integration of an arm-hand robotic system. In *Experimental Robotics II*, volume 190, pages 136–152. Springer Berlin / Heidelberg, 1993.

[22] L. Biagiotti, F. Lotti, C. Melchiorri, G. Palli, P. Tiezzi, and G. Vassura. Development of UB Hand 3: Early results. In *Proc. IEEE Int. Conf. on Robotics and Automation*, pages 4488–4493, Barcelona, Spain, 2005.

[23] A. Caffaz, G. Cannata, G. Panin, and E. Massucco. The DIST-hand, an anthropomorphic, fully sensorized dextrous gripper. In *In First IEEE-RAS Int. Conf. on Humanoid Robots*, 2000.

[24] G. Berselli, G. Borghesan, M. Brandi, C. Melchiorri, C. Natale, G. Palli, S. Pirozzi, and G. Vassura. Integrated mechatronic design for a new generation of robotic hands. In *Proc. IFAC Symp. on Robot Control*, volume 9, Part 1, pages 105–110, Gifu, Japan, 2009.

[25] S. C. Jacobsen, J. E. Wood, D. F. Knutti, and K. B. Biggers. The UTAH/M.I.T. dextrous hand: Work in progress. *The Int. Journal of Robotics Research*, 3(4): 21–50, 1984.

[26] M. T. Mason and J. K. Salisbury. *Robot Hands and the Mechanics of Manipulation.* MIT Press, Cambridge, MA, 1985.

[27] M. Grebenstein and P. van der Smagt. Antagonism for a highly anthropomorphic hand-arm system. *Advanced Robotics*, 22(1):39–55, 2008.

[28] M. Grebenstein, M. Chalon, W. Friedl, S. Haddadin, T. Wimböck, G. Hirzinger, and R. Siegwart. The hand of the DLR hand arm system: Designed for interaction. *The Int. Journal of Robotic Research*, 31(13):1531–1555, 2012.

[29] Shadow Robot Company. Design of a Dextrous Hand for advanced CLAWAR applications. In *Climbing and Walking Robots and the Supporting Technologies for Mobile Machines*, pages 691–698, Catania, Italy, 2003.

[30] J. Butterfass, M. Grebenstein, H. Liu, and G. Hirzinger. DLR-Hand II: Next generation of a dextrous robot hand. In *Proc. IEEE Int. Conf. on Robotics and Automation*, 2001.

[31] H. Kawasaki, T. Komatsu, and K. Uchiyama. Dexterous anthropomorphic robot hand with distributed tactile sensor: Gifu hand II. *IEEE/ASME Trans. on Mechatronics*, 7(3):296–303, 2002.

[32] W.T. Townsend. The barrett hand grasper - programmably flexible part handling and assembly. *Industrial Robot*, 27(3):181–188, 2000.

[33] C.S. Lovchik and M.A. Diftler. The robonaut hand: a dexterous robot hand for space. In *Proc. IEEE Int. Conf. on Robotics and Automation*, 1999.

[34] N. Fukaya, S. Toyama, T. Asfour, and R. Dillmann. Design of the TUAT/Karlsruhe humanoid hand. In *Proc. IEEE/RSJ Int. Conf. on Intelligent Robots and Systems*, pages 13–19, 2000.

[35] L.B. Bridgwater, C.A. Ihrke, M.A. Diftler, M.E. Abdallah, N.A. Radford, J.M. Rogers, S. Yayathi, R.S. Askew, and D.M. Linn. The robonaut 2 hand - designed to

do work with tools. In *Robotics and Automation (ICRA), 2012 IEEE International Conference on*, pages 3425–3430, May 2012.

[36] H. Liu, K. Wu, P. Meusel, N. Seitz, G. Hirzinger, M.H. Jin, Y.W. Liu, S.W. Fan, T. Lan, and Z.P. Chen. Multisensory five-finger dexterous hand: The dlr/hit hand ii. In *Intelligent Robots and Systems, 2008. IROS 2008. IEEE/RSJ International Conference on*, pages 3692–3697, Sept 2008.

[37] R.B. Katragadda and Yong Xu. A novel intelligent textile technology based on silicon flexible skins. In *Micro Electro Mechanical Systems, 2007. MEMS. IEEE 20th International Conference on*, pages 301–304, Jan 2007.

[38] J. Rossiter and T. Mukai. An led-based tactile sensor for multi-sensing over large areas. In *Sensors, 2006. 5th IEEE Conference on*, pages 835–838, Oct 2006.

[39] Giorgio Cannata, M. Maggiali, G. Metta, and G. Sandini. An embedded artificial skin for humanoid robots. In *Multisensor Fusion and Integration for Intelligent Systems, 2008. MFI 2008. IEEE International Conference on*, pages 434–438, Aug 2008.

[40] G. Berselli, M. Piccinini, G. Palli, and G. Vassura. Engineering design of fluid-filled soft covers for robotic contact interfaces: Guidelines, nonlinear modeling, and experimental validation. *Robotics, IEEE Transactions on*, 27(3):436–449, June 2011.

[41] Zhe Xu, B. Dellon, and Y. Matsuoka. Design of artificial skin with integrated tactile sensors for anthropomorphic robotic hands. In *Robotics and Biomimetics (ROBIO), 2011 IEEE International Conference on*, pages 2919–2924, Dec 2011.

[42] A. Eusebi, C. Fantuzzi, C. Melchiorri, M. Sandri, and A. Tonielli. The ub hand ii control system: design features and experimental results. In *Industrial Electronics, Control and Instrumentation, 1994. IECON '94., 20th International Conference on*, volume 2, pages 782–787 vol.2, Sep 1994.

[43] A. Bicchi and P. Dario. Intrinsic tactile sensing for artificial hands. In *Proceedings of the 4th International Symposium on Robotics Research*, pages 83–90, Cambridge, MA, USA, 1988. MIT Press.

[44] Maximo A. Roa and Raul Suarez. Grasp quality measures: review and performance. *Autonomous Robots*, 38(1):65–88, 2015.

[45] Yun-Hui Liu. Qualitative test and force optimization of 3-d frictional form-closure grasps using linear programming. *Robotics and Automation, IEEE Transactions on*, 15(1):163–173, Feb 1999.

[46] J.C. Trinkle. A quantitative test for form closure grasps. In *Intelligent Robots and Systems, 1992., Proceedings of the 1992 lEEE/RSJ International Conference on*, volume 3, pages 1670–1677, Jul 1992. doi: 10.1109/IROS.1992.594246.

[47] Antonio Bicchi. On the closure properties of robotic grasping. *International Journal of Robotics Research*, 14:319–334, 1995.

[48] S. El-Khoury and A. Sahbani. A sufficient condition for computing n-finger force-closure grasps of 3d objects. In *Robotics, Automation and Mechatronics, 2008 IEEE Conference on*, pages 791–796, Sept 2008. doi: 10.1109/RAMECH.2008.4681451.

[49] Yu Zheng, M.C. Lin, and D. Manocha. A fast n-dimensional ray-shooting algorithm for grasping force optimization. In *Robotics and Automation (ICRA), 2010 IEEE International Conference on*, pages 1300–1305, May 2010.

[50] Yun-Hui Liu, Miu ling Lam, and Dan Ding. A complete and efficient algorithm for searching 3-d form-closure grasps in the discrete domain. *Robotics, IEEE Transactions on*, 20(5):805–816, Oct 2004.

[51] Yun-Hui Liu. Qualitative test and force optimization of 3-d frictional form-closure grasps using linear programming. *Robotics and Automation, IEEE Transactions on*, 15(1):163–173, Feb 1999.

[52] Yu Zheng and Chee-Meng Chew. A numerical solution to the ray-shooting problem and its applications in robotic grasping. In *Robotics and Automation, 2009. ICRA '09. IEEE International Conference on*, pages 2080–2085, May 2009.

[53] XiangYang Zhu, Han Ding, and M.Y. Wang. A numerical test for the closure properties of 3-d grasps. *Robotics and Automation, IEEE Transactions on*, 20(3): 543–549, June 2004.

[54] C. Natale, B. Siciliano, and L. Villani. Robust hybrid force/position control with experiments on an industrial robot. In *Advanced Intelligent Mechatronics, 1999. Proceedings. 1999 IEEE/ASME International Conference on*, pages 956–960, 1999.

[55] S. Stramigioli, Claudio Melchiorri, and S. Andreotti. A passivity-based control scheme for robotic grasping and manipulation. In *Decision and Control, 1999. Proceedings of the 38th IEEE Conference on*, volume 3, pages 2951–2956 vol.3, 1999.

[56] T. Wimbock, C. Ott, and G. Hirzinger. Analysis and experimental evaluation of the intrinsically passive controller (ipc) for multifingered hands. In *Robotics and Automation, 2008. ICRA 2008. IEEE International Conference on*, pages 278–284, May 2008.

[57] O. Khatib. Object level manipulation. In *Intelligent Motion Control, 1990. Proceedings of the IEEE International Workshop on*, volume 2, pages 497–502, Aug 1990.

[58] R.R. Ma and AM. Dollar. On dexterity and dexterous manipulation. In *Advanced Robotics (ICAR), 2011 15th International Conference on*, pages 1–7, June 2011.

[59] N.C. Dafle, A. Rodriguez, R. Paolini, Bowei Tang, S.S. Srinivasa, M. Erdmann, M.T. Mason, I. Lundberg, H. Staab, and T. Fuhlbrigge. Extrinsic dexterity: In-hand manipulation with external forces. In *Robotics and Automation (ICRA), 2014 IEEE International Conference on*, pages 1578–1585, May 2014.

[60] S.J. Mousavi and E. Masehian. A new taxonomy of robotic regrasp planning approaches and methods. In *Robotics and Mechatronics (ICRoM), 2013 First RSI/ISM International Conference on*, pages 90–95, Feb 2013.

[61] Igor Mordatch, Emanuel Todorov, and Zoran Popović. Discovery of complex behaviors through contact-invariant optimization. *ACM Trans. Graph.*, 31(4), July 2012. URL http://doi.acm.org/10.1145/2185520.2185539.

[62] A.M. Okamura, N. Smaby, and M.R. Cutkosky. An overview of dexterous manipulation. In *Proc. IEEE Int. Conf. on Robotics and Automation*, pages 255–262, 2000.

[63] M. Santello, M. Flanders, and J. F. Soechting. Postural hand synergies for tool use. *Journal of Neuroscience*, 18(23):10105–10115, 1998.

[64] G. Gioioso, G. Salvietti, M. Malvezzi, and D. Prattichizzo. Mapping synergies from human to robotic hands with dissimilar kinematics: An object based approach. 2011.

[65] T. Geng, M. Lee, and M. Hulse. Transferring human grasping synergies to a robot. *Mechatronics*, 21(1):272–284, 2011.

[66] I. Oikonomidis, N. Kyriazis, and A. A. Argyros. Full dof tracking of a hand interacting with an object by modeling occlusions and physical constraints. In *Proc. 13th Int. Conf. on Computer Vision*, pages 1260–1264, Barcelona, 2011.

[67] V. Frati and D. Prattichizzo. Using kinect for hand tracking and rendering in wearable haptics. In *IEEE World Haptics Conference*, Istanbul, 2011.

[68] F. Ficuciello, G. Palli, C. Melchiorri, and B. Siciliano. Planning and control during reach to grasp using the three predominant UB Hand IV postural synergies. In *Proc. IEEE Int. Conf. Robotics and Automation*, pages 1775–1780, Saint Paul, MN, 2012.

[69] L. Villani, V. Lippiello, F. Ruggiero, F. Ficuciello, B. Siciliano, and G. Palli. *Advanced bimanual manipulation*, chapter Grasping and Control of Multifingered Hands, pages 219–266. Springer Tracts in Advanced Robotics (STAR). Springer, 2012.

[70] G. Palli, C. Melchiorri, G. Vassura, G. Berselli, S. Pirozzi, C. Natale, G. De Maria, and C. May. *Advanced bimanual manipulation*, chapter Innovative Technologies for the Next Generation of Robotic Hands, pages 173–218. Springer Tracts in Advanced Robotics (STAR). Springer, 2012.

[71] F. Ficuciello, G. Palli, C. Melchiorri, and B. Siciliano. Postural synergies and neural network for autonomous grasping: a tool for dextrous prosthetic and robotic hands. In *Proc. Int. Conf. on NeuroRehabilitation*, Toledo, Spain, November 2012.

[72] G. Palli, C. Natale, C. May, C. Melchiorri, and T. Würtz. Modeling and control of the twisted string actuation system. *IEEE/ASME Trans. on Mechatronics*, 18 (2):664–673, 2013.

[73] G. Berselli, M. Piccinini, and G. Vassura. Comparative evaluation of the selective compliance in elastic joints for robotic structures. In *Proc. IEEE Int. Conf. on Robotics and Automation*, pages 4626 –4631, Shanghai, China, 2011.

[74] G. Borghesan, G. Palli, and C. Melchiorri. Design of tendon-driven robotic fingers: Modeling and control issues. In *Proc. IEEE Int. Conf. on Robotics and Automation*, pages 793–798, Anchorage, AK, 2010.

[75] G. Palli, G. Borghesan, and C. Melchiorri. Modeling, identification and control of tendon-based actuation systems. *IEEE Trans. on Robotics*, 28(2):277–290, 2012.

[76] T. Würtz, C. May, B. Holz, C. Natale, G. Palli, and C. Melchiorri. The twisted string actuation system: Modeling and control. In *Proc. Int. Conf. on Advanced Intelligent Mechatronics*, pages 1215–1220, Montreal, Canada, 2010.

[77] G. Palli and S. Pirozzi. Optical sensor for angular position measurements embedded in robotic finger joints. *Advanced Robotics*, 27(15):1209–1220, 2013.

[78] G. Palli and S. Pirozzi. A miniaturized optical force sensor for tendon-driven mechatronic systems: Design and experimental evaluation. *Mechatronics*, 22(8): 1097–1111, 2012.

[79] G. De Maria, C. Natale, and S. Pirozzi. Force/tactile sensor for robotic applications. *Sensors and Actuators A: Physical*, 175:60–72, 2012.

[80] M. Piccinini, G. Berselli, A. Zucchelli, and G. Vassura. Predicting the compliance of soft fingertips with differentiated layer design: A numerical and experimental investigation. In *Proc. Int. Conf. on Advanced Robotics*, pages 1–6, Munich, Germany, 2009.

[81] G. Berselli, M. Piccinini, G. Palli, and G. Vassura. Engineering Design of Fluid-Filled Soft Covers for Robotic Contact Interfaces: Guidelines, Nonlinear Modeling, and Experimental Validation. *IEEE Trans. on Robotics*, 27(3):436–449, 2011.

[82] G. Borghesan, G. Palli, and C. Melchiorri. Friction compensation and virtual force sensing for robotic hands. In *Proc. IEEE Int. Conf. on Robotics and Automation*, pages 4756–4761, Shanghai, China, 2011.

[83] J.R. Napier and R. Tuttle. *Hands*. Princeton Science Library. Princeton University Press, 1993. ISBN 9780691025476. URL http://books.google.it/books?id=mNQM4jvG7hgC.

[84] Markus Grebenstein, Maxime Chalon, Gerd Hirzinger, and Roland Siegwart. A method for hand kinematics designers 7 billion perfect hands. In *Proc. of 1st Int. Conf. on Applied Bionics and Biomechanics*, Venice, Italy, 2010.

[85] R. Tubiana, J.M. Thomine, and E.J. Mackin. *Examination of the Hand and Wrist*. Martin Dunitz, 1998. ISBN 9781853175442. URL http://books.google.it/books?id=G1gWHR1_J9UC.

[86] M. Kaneko, M. Wada, H. Maekawa, and K. Tanie. A new consideration on tendon-tension control system of robot hands. In *Proc. IEEE Int. Conf. on Robotics and Automation*, volume 2, pages 1028–1033, Sacramento, CA, 1991.

[87] G. Palli and C. Melchiorri. Optimal control of tendon-sheath transmission systems. In *Proc. IFAC Symp. on Robot Control*, volume 8, pages 73–78, Bologna, Italy, 2006.

[88] H. Liu, P. Meusel, G. Hirzinger, M. Jin, Y. Liu, and Z. Xie. The modular multisensory DLR-HIT-Hand: Hardware and software architecture. *IEEE/ASME Trans. on Mechatronics*, 13(4):461–469, 2008.

[89] P. C. Chou and B. Hannaford. Measurement and modeling of McKibben pneumatic artificial muscles. *IEEE Trans. on Robotics and Automation*, 12(1):90–102, February 1996.

[90] S. C. Jacobsen, R. B. Jerrard, D. Knutti, and J. Carruth. The ladd actuator as a prosthetic muscle. In *Proc. of 5th Int. Symp. on External Control of Human Extremities*, Dubrovnik, Yugoslavia, Aug 1975.

[91] K. L. Pottebaum and J. J. Beaman. A dynamic model of a concentric ladd actuator. *Journal of Dynamic Systems, Measurement, and Control*, 105(3):157–164, 1983.

[92] G. Mennitto and M. Buehler. Ladd transmissions: Design, manufacture, and new compliance models. *Journal of Mechanical Design*, 119(2):197–203, 1997.

[93] M. Shoham. Twisting wire actuator. *Journal of Mechanical Design*, 127(3):441–445, 2005.

[94] T. Sonoda and I. Godler. Multi-fingered robotic hand employing strings transmission named "Twist Drive". In *Proc. IEEE/RSJ Int. Conf. on Intelligent Robots and Systems*, pages 2733–2738, Taipei, Taiwan, 2010.

[95] T. Sonoda and I. Godler. A five fingered robotic hand prototype by using twist drive. In *Proc. Int. Symp. on Robotics*, pages 594–599, Munich, Germany, 2010.

[96] Y. J. Shin, H. J. Lee, K-.S. Kim, and S. Kim. A robot finger design using a dual-mode twisting mechanism to achieve high-speed motion and large grasping force. *IEEE Trans. on Robotics*, 28(6):1398 –1405, dec. 2012. ISSN 1552-3098. doi: 10.1109/TRO.2012.2206870.

[97] A. Bicchi, G. Tonietti, M. Bavaro, and M. Piccigallo. Variable Stiffness Actuators for Fast and Safe Motion Control. In Paolo Dario and Raja Chatila, editors, *In Robotics Research*, volume 15 of *Springer Tracts in Advanced Robotics*, pages 527–536. Springer Berlin / Heidelberg, 2005.

[98] S.O. Kasap. *Optoelectronics and Photonics: Principles and Practices*. Prentice Hall, Englewood Cliffs, NJ, 2001.

[99] Alberto D'Amore, Giuseppe De Maria, Luigi Grassia, Ciro Natale, and Salvatore Pirozzi. Silicone-rubber-based tactile sensors for the measurement of normal and tangential components of the contact force. *Journal of Applied Polymer Science*, 122(6):3757–3769, 2011.

[100] Sarobotics, UK. June 2012. URL http://www.sarobotics.co.uk/.

[101] Schilling Robotics, USA. 2012. URL http://www.schilling.com/.

[102] D.M. Lane, G. Bartolini, G. Cannata, G. Casalino, J.B.C. Davies, G. Veruggio, M. Canals, and C. Smith. Advanced manipulation for deep underwater sampling: the amadeus research project. In *Proc. IEEE Int. Conf. on Control Applications*, volume 2, pages 1068–1073, 1998.

[103] R.S. Gad, G.M. Naik, and N. Aralgedad. A design of 2-dof gripper circuit for deep-sea objects. In *MTTS/IEEE TECHNO-OCEAN*, volume 3, pages 1402–1409, 2004.

[104] Qingxin Meng, Hua Wang, Ping Li, Liquan Wang, and Ze He. Dexterous underwater robot hand: HEU Hand II. In *Proc. IEEE Int. Conf. on Mechatronics and Automation*, pages 1477–1482, 2006.

[105] Peng Jia, Qingxin Meng, and Liquan Wang. Dynamic analysis on fingers of the underwater multi-fingered robot hand. In *Proc. IEEE Int. Conf. on Mechatronics and Automation*, pages 757 –762, 2007.

[106] D.M. Lane, J.B.C. Davies, G. Casalino, G. Bartolini, G. Cannata, G. Veruggio, M. Canals, C. Smith, D.J. O'Brien, M. Pickett, G. Robinson, D. Jones, E. Scott, A. Ferrara, D. Angelleti, M. Coccoli, R. Bono, P. Virgili, R. Pallas, and E. Gracia. AMADEUS: advanced manipulation for deep underwater sampling. *IEEE Robotics Automation Magazine*, 4(4):34–45, 1997.

[107] D.J. O'Brien and D.M. Lane. Force and slip sensing for a dextrous underwater gripper. In *Proc. IEEE Int. Conf. on Robotics and Automation*, volume 2, pages 1057–1062, 1998.

[108] M. Prats, J.C. Garcia, S. Wirth, D. Ribas, P.J. Sanz, P. Ridao, N. Gracias, and G. Oliver. Multipurpose autonomous underwater intervention: A systems integration perspective. In *Mediterranean Conf. on Control Automation,*, pages 1379–1384, 2012.

[109] G. De Novi, C. Melchiorri, J.C. Garcìa, P.J. Sanz, P. Ridao, and G. Oliver. New approach for a reconfigurable autonomous underwater vehicle for intervention. *IEEE Aerospace and Electronic Systems Magazine*, 25(11):32–36, 2010.

[110] C. Melchiorri and M. Kaneko. Robot hands. In B. Siciliano and O. Khatib, editors, *Springer Handbook of Robotics*, pages 345–360. Springer, 2008.

[111] G. Palli, C. Melchiorri, G. Vassura, G. Berselli, S. Pirozzi, C. Natale, G. De Maria, and C. May. Innovative technologies for the next generation of robotic hands. In *Advanced Bimanual Manipulation*, pages 173–218, B. Siciliano (Ed.), Springer Tracts in Advanced Robotics, vol. 80, Springer, 2012.

[112] G. Palli and S. Pirozzi. Force sensor based on discrete optoelectronic components and compliant frames. *Sensors and Actuators A: Physical*, 165:239–249, 2011.

[113] G. Palli and S. Pirozzi. Optical force sensor for the DEXMART Hand twisted string actuation system. *Sensors & Transducers*, 148(1):28–32, 2013.

[114] CIA. CAN in Automation, 2012. URL http://www.can-cia.org/.

[115] D. Ribas, N. Palomeras, P. Ridao, M. Carreras, and A. Mallios. Girona 500 auv: From survey to intervention. *IEEE/ASME Trans. on Mechatronics*, 17(1):46–53, 2012.

[116] M. Prats, D. Ribas, N. Palomeras, J. C. García, V. Nannen, S. Wirth, J. J. Fernández, J. P. Beltrán, R. Campos, P. Ridao, P. J. Sanz, G. Oliver, M. Carreras, N. Gracias, R. Marín, and A. Ortiz. Reconfigurable AUV for intervention missions: A case study on underwater object recovery. *Journal of Intelligent Service Robotics*, 5(1):19–31, January 2012.

[117] Claudio Melchiorri and J.K. Salisbury. An algorithm for the control of a hand-arm robotic system. In *Advanced Robotics, 1991. 'Robots in Unstructured Environments', 91 ICAR., Fifth International Conference on*, pages 471–476, June 1991.

[118] G. Casalino, Giorgio Cannata, G. Panin, and A Caffaz. On a two-level hierarchical structure for the dynamic control of multifingered manipulation. In *Proc. IEEE Int. Conf. on Robotics and Automation*, volume 1, pages 77–84, 2001.

[119] T. Wimbock, C. Ott, and G. Hirzinger. Impedance behaviors for two-handed manipulation: Design and experiments. In *Proc. IEEE Int. Conf. on Robotics and Automation*, pages 4182–4189, April 2007.

[120] Hyejin Han, Jaemin Lee, and Jaeheung Park. A continuous task transition algorithm for operational space control framework. In *Ubiquitous Robots and Ambient Intelligence (URAI), 2012 9th International Conference on*, pages 148–152, Nov 2012.

[121] F. Zacharias, D. Leidner, F. Schmidt, C. Borst, and G. Hirzinger. Exploiting structure in two-armed manipulation tasks for humanoid robots. In *Proc. IEEE/RSJ Int. Conf. on Intelligent Robots and Systems*, pages 5446–5452, Oct 2010.

[122] Tan Fung Chan and R.V. Dubey. A weighted least-norm solution based scheme for avoiding joint limits for redundant joint manipulators. *Robotics and Automation, IEEE Transactions on*, 11(2):286–292, Apr 1995.

[123] O. Porges, T. Stouraitis, C. Borst, and M. A. Roa. Reachability and capability analysis for manipulation tasks. In M. Armada, A. Sanfeliu, and M. Ferre, editors, *ROBOT2013: First Iberian Robotics Conference*, Advances in Intelligent Systems and Computing 253, pages 703–718. Springer, 2014.

[124] K. Hertkorn, M.A Roa, and C. Borst. Planning in-hand object manipulation with multifingered hands considering task constraints. In *Proc. IEEE Int. Conf. on Robotics and Automation*, pages 617–624, May 2013.

[125] C. Borst, C. Ott, T. Wimböck, B. Brunner, F. Zacharias, B. Bauml, U. Hillenbrand, S. Haddadin, A. Albu-Schäffer, and G. Hirzinger. A humanoid upper body system for two-handed manipulation. In *Proc. IEEE Int. Conf. on Robotics and Automation*, pages 2766–2767, 2007.

[126] H. Liu, K. Wu, P. Meusel, N. Seitz, G. Hirzinger, M.H. Jin, Y.W. Liu, S.W. Fan, T. Lan, and Z.P. Chen. Multisensory five-finger dexterous hand: The DLR/HIT hand II. In *Proc. IEEE/RSJ Int. Conf. on Intelligent Robots and Systems*, pages 3692–3697, 2008.

[127] Local online planning of coordinated manipulation motion. Youtube, 2015. URL https://www.youtube.com/watch?v=6CQm9GQV5kA.

[128] T. Hulin, K. Hertkorn, P. Kremer, S. Schätzle, J. Artigas, M. Sagardia, F. Zacharias, and C. Preusche. The DLR bimanual haptic device with optimized

workspace. In *Proc. IEEE Int. Conf. on Robotics and Automation*, pages 3441–3442, 2011.